COMPUTER SIMULATION OF MACROSEGREGATION IN ESR INGOTS

by

ROBERT JOSEPH FURLONG, Jr.

S.B., University of Vermont
1974

Submitted in partial fulfillment of the requirements

for the degree of

MASTER OF SCIENCE

at the

Massachusetts Institute of Technology

February, 1977

Signature redacted

Signature of Author .....
Department of Materials Science and Engineering
January 21, 1977

Signature redacted

Certified by ... .
Thesis Supervisor

Signature redacted

Accepted by .....
Chairman, Departmental Committee on Graduate Students

ABSTRACT

COMPUTER SIMULATION OF MACROSEGREGATION IN ESR INGOTS

by

ROBERT JOSEPH FURLONG, Jr.

Submitted to the Department of Materials Science and Engineering on January 21, 1977, in partial fulfillment of the requirements for the degree of Master of Science.

Macrosegregation in ingots made by the electroslag remelting process (ESR) in small-scale laboratory molds at M.I.T. is compared with simulated composition profiles generated by an IBM 370 digital computer. Since adverse effects of macrosegregation upon ingot structure and mechanical properties are well documented, the ability to accurately predict macrosegregation ingots and castings is therefore practical. Feedback from computer-experiment interactions should expedite control of alloy composition leading to ingots and castings of more uniform and improved mechanical properties.

A macrosegregation model based upon the Local Solute Redistribution Equation and the application of D'Arcy's law to the mushy region in cylindrical coordinates is used as the basis of the computer program.

The pressure field within the mushy zone is determined by a relaxation technique. Interdendritic velocity and fraction liquid are subsequently computed. Updates of fraction liquid are recycled until deviations between successive cycles are insignificant. This final relaxed pressure field yields the appropriate values of interdendritic velocity and fraction liquid utilized in the approximate integral form of the Local Solute Redistribution Equation for generating into composition profiles.

An auxiliary heat balance routine for determining temperature distributions within the mushy zone is not attempted. Thermal data including temperature distributions must be determined by experimental measurements.

The specific permeability, K, is the process variable which is key to the investigation of interdendritic fluid flow. Two models are discussed. A new model directly linking specific permeability to the process variable known as cooling rate, ε, is explored. The Karman Kozeny relationship is also focused upon as an alternative method of describing the specific permeability.

Surface to center compositional variations (composition profiles) of five Al-4% Cu ingots are computer simulated on an IBM 370. Considering the large number of variables involved, calculations agreed remarkably well with experiments. The program predicted modest surface to center compositional variations for four ingots and no segregation for the fifth which solidified unidirectionally.

Severe-localized segregates, as sometimes found in large commercial ingots, are not pronounced using Al-4% Cu cast in the small-scale ESR molds (6.8 cm diameter). "Shrinkage induced" convection predominates due to a high cooling rate, and computer outputs correctly indicates that the rate ratio, $\vec{v}\nabla T/\varepsilon$, is positive throughout the mushy zone.

In order to study a wider range of segregation problems encountered in ESR ingots, calculations were compared to the macrosegregation in a Sn-15% Pb alloy. Simulation results gave a substantial range for the rate ratio: $-2 < \vec{v}\nabla T/\varepsilon < 0.8$, with values of $\vec{v}\nabla T/\varepsilon < -1$ occur between radius of 1.3 Cu and the center. Freckling is therefore predicted by the computer simulation which agrees with the actual structure of the ingot. It is evident that "gravitational induced" convection predominates in this ingot. The accuracy of simulated predictions to experimental measurements in both cases of Al-4% Cu and Sn-15% Pb alloys infers correctness of the underlying macrosegregation theory.

Finally, continuously cast ingot (30 cm in diameter of composition Al-4.5% Cu) is simulated using the same program. Radial increment spacings are varied. Mushy zone shape and other pertinent data are selected from the literature. A composition profile, which upon comparison to literature findings shows indisputable similarity, is generated.

Thesis Supervisor: Merton C. Flemings
Title: Ford Professor of Engineering

TABLE OF CONTENTS

LIST OF ILLUSTRATIONS

ACKNOWLEDGMENTS

I thank Professor Merton Flemings for his patience and encouragement during this course of the ESR program here at M.I.T.

Professor David Poirier is thanked for his assistance and suggestions. Many stimulating encounters have culminated in fruitful simulation investigations on the computer. His patience and encouragement are also recognized.

My lab partner, Sindo Kou, deserves special thanks for his key role in the investigation both theoretical and experimental.

I extend my thanks to Ms. Linda Sayegh for a fine job of typing this thesis.

I. INTRODUCTION

The phenomenon of macrosegregation and its subsequent problems have been with man for thousands of years. Only within the last few decades has there been analytical work on macrosegregation; prior to about 1960, the work reported on macrosegregation in alloys was empirical. The more recent research on the microstructure of metallic crystals and the effects of heat flow and fluid flow within the mushy zone and other fundamental investigations have led us closer to better definition of this problem.

Macrosegregation has many forms such as the "V" and "A" segregates in large, killed, steel ingots[1]. Transverse and even longitudinal segregation is often observed in industrial ingots. It seems that with so many forms that numerous mechanisms must be involved; yet, today the better informed researcher and theorist are beginning to evince similarities between the types. A common mechanism or a joint coupling of mechanisms may be detected in the future.

Industry never waits for detailed philosophies to develop but continues to plunge ahead seeking processes which appear qualified to do the job. One such process is the electroslag remelting (ESR) process which is commercially used for the "specialty" alloys. The main advantages are the refining capabilities derived from melting through a slag of controlled composition and the superior solidification structures obtained. Finer dendritic arm spacings and less porosity along with the reduction of nonmetallic inclusions result in a product with less segregation and better mechanical properties. The ESR process is not however, the panacea to the production of large alloy ingots. Segregation does occur and even

significantly.

This thesis deals with macrosegreation in ESR ingots in a quantitative manner. This new process, ESR, is examined using the analytical approach set forth by Flemings and Nereo[2] and later refined by Mehrabian, Keane, and Flemings[3]. A model is constructed from basic principles of fluid flow and next solved by numerical methods on a computer. The computer simulation yields solute composition distributions of the ingot. This distribution is then compared with actual distributions resulting from ESR castings solidified under controlled laboratory conditions. The ultimate aim is to establish control of solute redistribution in "large-scale" commercial ingots. This will lead to ingots of "optimum" homogeneity and therefore uniformity of mechanical structure.

Ingot structure substantially affects the properties of a cast material. This structure depends mainly on the heat flow pattern within the mushy zone during solidification. Fluid flow within the interdendritic region is a consequence of this heat flow pattern.

The experimental work concerns small laboratory ingots of 3 to 4 inches in diameter of both the Al-4.4% Cu and Sn-15% binaries whereas there are commercial ingots approaching two meters in diameter produced in Germany. Scale-up is not considered at this stage. Compositional variations are examined for various profiles of the solid-liquid region of the ingot.

II. LITERATURE REVIEW

In this chapter literature on macrosegregation and related topics are presented. Of interest are:

A. dendrite morphology,

B. permeability of dendritic networks,

C. macrosegregation in alloy ingots,

D. segregation types,

E. effects of macrosegregation on mechanical properties, and the

F. electroslag remelting process.

Of chief interest are the mechanisms of macrosegregation in alloy ingots. Some mechanisms are emphasized while others are in the process of being discounted or modified. It appears that several types of macrosegregation may to a large extent be governed by a single dominant mechanism which is the flow of interdendritic liquid. Solute is rejected from solidifying dendrites and is carried away by the liquid seeping through the dendritic arrays.

A. Morphology of Dendrites and Grains

During alloy solidification three zones distinguished by their grain morphologies, frequently occur. Coarse equiaxed grains often occur within the central ingot region while fine equiaxed grains are found at the mold wall. In between these zones is the columnar structure. All three zones are not always seen within the same ingot or casting. The grains, themselves, are made up of dendrites whether or not they are equiaxed or columnar. We are concerned with the morphology of dendrites because, as related to macrosegregation, the permeability of the dendritic network is a control-

ling factor of the convection within the mushy zone which leads to macrosegregation.

The primary and secondary dendrite arm spacings are related to temperature gradients of the liquid at the liquidus, G_L, and the growth velocity of the dendrite tips, R. The primary dendrite arm spacing, λ_1, has the following empirical relationship:[4]

$$\lambda_1 = k_1 \, G_L^{-a} \, R^{-b} \tag{1}$$

where k_1, a, and b are constants. The secondary dendrite arm spacing, λ_2, is proportional to the time spent within the liquid-solid zone, θ, such that

$$\lambda_2 = k_2 \, \theta^{n} \tag{2}$$

where k_2 and n are constants. Often Eq. (2) is written in terms of average cooling rate, ε, so that

$$\lambda_2 = k_2 \, \varepsilon^{-n} \tag{3}$$

For aluminum copper alloys Bower et al.[5] determined that the exponent n is approximately 0.39 whereas more recently Young and Kirkwood have established a value of 0.33.

Dendritic spacings have been related to ripening kinetics, and the coarsening of dendrites has been explained by considering the reduction of surface area and curvature of the solid-liquid dendritic interface. Coalescence, according to Chien and Kattamis[6] is the fusion of impinging dendrite arms. It is the final act of the coarsening phenomena. Again surface free energy diminishes. Alloy concentration also affects the coarsening or ripening of dendrites. Chien[6] and Young[4] agree that the

effect of increasing the composition is to increase the width of liquid grooves reducing the curvature at the dendrite roots. The ultimate result is that dendrites in dilute alloys coarsen faster for a given cooling rate than do concentrated alloys. The arms become dendritic cells.

Jacobi and Schwerdtfeger[7] and Tadayoshi and Hagiwara[8] have observed interesting alignments of dendrites in carbon steels. The experimental work of Jacobi and Schwerdtfeger[7] on 0.59 and 1.48% C steels show two arrays of primary dendrites. One is the aligned primary dendritic array. The other is the closer packed staggered arrangement.

B. Permeability of Dendritic Networks

In the mid 1960's Piwonka and Flemings[9] determined that the specific permeability within the two phase zone is proportional to the fraction liquid raised to a power. Their work was on Al-4.5% Cu alloy. With fraction liquid less than 0.3, the specific permeability, K, is

$$K = \gamma\, g_L^{\,2} \qquad (4)$$

where γ is a constant and g_L is fraction liquid. With greater amounts of liquid, the permeability was found to vary as

$$K \propto g_L^{\,9.4} \qquad (5)$$

Since most of the mushy zone has a fraction liquid less than 0.3 for this particular alloy, Eq. (4) was applied in a study of macrosegregation[3].

Flemings and Piwonka[9] and Apelian, Mehrabian, and Flemings[10] demonstrated that D'Arcy's Law is applicable to flow through the dendritic zone since it is a porous network. Therefore, the interdendritic velocity is directly proportional to the pressure gradient at any liquid position

within this region. This has been seconded by Streat and Weinberg[11] in their studies on Pb-Sn alloys. Agreed upon by both groups is the specific form of the permeability expression after modifications are taken into account. The equation is:

$$K = \frac{g_L^2}{8\pi\, n\, \tau^3} \tag{5}$$

where:

n = number of flow channels per unit area, cm^{-2},

τ = tortuosity factor, and

g_L = volume fraction liquid

The specific permeability is assumed to be isotropic. Streat and Weinberg show that the specific permeability is proportional to the square of the primary dendrite spacing. Thus

$$K = \frac{\lambda_1^2\, g_L^2}{8\pi\, \tau^3} \tag{6}$$

with

$$n = \lambda_1^{-2} \tag{7}$$

if the capillary model is used to describe flow through the interdendritic array. In experiments using Pb-20wt% Sn alloy Streat and Weinberg determined a value of 4.6 for the tortuosity[11].

Apelian and Flemings[10] speculate that the Karman-Kozeny relationship may be a possible method of investigation for future work. The implicit influence of dendrite surface resistance is clearly suggested by the S_o^{-2} term of the Karman-Kozeny Equation stated as:

$$K = \frac{g_L^3}{c\,(1-g_L)^2\,S_o^2} \tag{8}$$

where:

S_o = surface area of the porous medium exposed to the fluid divided by volume of the solid in the medium, and

$c = 4.2$.

Since

$$S_o = \hat{c} \cdot \frac{1}{\lambda_2} \tag{9}$$

Eq. (8) may be written as:

$$K = \frac{\lambda_2^2 \cdot g_L^3}{c \cdot \hat{c}^2 (1-g_L)^2} \tag{10}$$

Equation (10) is derived in Appendix B, Der. (1). The constant $c \cdot \hat{c}^2$ of Equation (10) is $\pi/4 \cdot 150/\phi_s^2$ in Eq. (1.8) of Appendix B. Since $\hat{c} \tilde{=} 4$ then $\hat{c}$ is approximately $\sqrt{\pi \cdot 150}/\phi_s$.

C. Macrosegregation in Alloy Ingots

Many theories have been proposed to explain macrosegregation. Four of the most prominent mechanisms are:

1. mixing or flow of the diffusion layer ahead of the growth interface into the bulk liquid,

2. precipitation of a solid phase from the bulk liquid,

3. fluid flow within the semisolid region due to volume contraction, and 4. natural convection within the dendritic zone.

The first mechanism of mixing of the diffusion layer into the bulk liquid[12] has met with considerable opposition in recent years. The characteristic distance is the thickness of the boundary layer ahead of an

advancing solidification front. Since it is only about 10^{-3} cm, many researchers have argued that very little solute is contributed to the bulk liquid by mixing with the turbulent currents within the bulk[2]. The characteristic thickness is simply D/U where D is a liquid diffusion coefficient and U is dendrite tip velocity. The mechanism has less validity if the growth front is not planar but rather cellular or dendritic. Most researchers, however, agree that this mechanism is likely for segregation in single crystal growth, (e.g., normal freezing).

The second mechanism of precipitation of the solid in the bulk liquid is based upon the recent theory of Jackson, et al.[13]. Turbulent currents within the bulk liquid produce temperature fluctuations at the dendrite tips causing them to melt from the main dendrite tree and be swept into the bulk liquid to nucleate solid grains. Heterogeneous nucleation occurs with the result of a "raining action" whereby the solid particles precipitate into the central region of the mushy zone resulting in the equiaxed structure and these grains settle to the bottom of the ingot or casting. If the partition ratio is less than unity a region depleted of solute composition forms the so-called "negative cone of segregation."

The contraction mechanism was discussed in the late fifties by Kirkaldy and Youdelis[14]. Volume contraction of the alloy causes "flow-back" of enriched fluid within dendritic channels, and this was used to explain inverse segregation. A decade later a more general model was constructed by Flemings and Nereo[2]. Use of a differential element (large enough to include both solid and liquid phases such that the fraction solid is at all times the local average) they modified the earlier analysis of

Kirkaldy and Youdelis and derived the "local solute redistribution equation." Both shrinkage terms and interdendritic velocity are considered making the analysis more general. Nereo and Flemings also pointed out the importance of the dimensionless group $\vec{v}\cdot\nabla T/\varepsilon$ where $\vec{v}$ is the velocity of the interdendritic liquid, ∇T is the temperature gradient and ε is the cooling rate.

Later work by Mehrabian et al.[3] showed how to apply the local solute redistribution equation to even more situations. Specifically, their main contribution was to combine D'Arcy's law for flow through porous media (with gravity acting as a body force on the interdendritic liquid) with the local solute redistribution equation. With this approach, a two-dimensional flow field was solved and the authors demonstrated how in some situations (depending upon the value of $\vec{v}\cdot\nabla T/\varepsilon$) there is flow of interdendritic liquid from colder to hotter regions within the mushy zone. In fact, if $\vec{v}\cdot\nabla T/\varepsilon < -1$ Mehrabian et al.[3] explain the formation of "freckles."

Briefly then the model of Kirkaldy and Youdelis[14] could be used to explain inverse segregation whereas the model of Flemings and co-workers[2,3,15] was derived to define all segregation types which could be explained by interdendritic fluid flow. They do not, however, "couple" the bulk liquid convection with that of the two phase zone.

Of the four mechanisms the most popular to date is gravity flow primarily dependent upon density differences of the liquid within the two phase zone. Based upon experiments, McDonald and Hunt[16] inaugurated the idea of continuous convective loops which sweep from the bulk liquid, through the mushy zone. Hebditch and Hunt[17] emphasized the influence of

the gravity effect while Fisher[18] maintains that the gravity flow occurs in castings of all nominal alloy compositions to roughly the same extent. The strongest effects of gravity occur small distances from the dendrite tips since this is the region of large liquid channels. For a Sn-5 wt% Pb is determined the distance to extend 0.4 cm. into the mushy zone. Szekely and Chen[19] formulated a model of flow based upon natural convection within the two phase zone. The unsteady state system convection within the two phase zone. The unsteady state system incorporates the equations of continuity and motion in the liquid portion of the two phase region and also the liquid pool. Stream function distributions are ultimately determined by the computer. Numerical values of the velocity are of the order of 10^{-3} cm/sec at the wall where velocities are found to be the highest. A more detailed analysis of this method is in Chen's Ph.D. thesis[20].

D. Segregation Types

Inverse "V" segregates ("A" segregates) have been studied by McDonald and Hunt[16]. Better channel formation results if the growth rate is low. Their system is ammonium chloride with a potassium permangate tracer for direct observational studies. Pipes or channels are formed only by ascending fluid and can be destroyed by mechanical mixing within the equiaxed region.

Narita and Mori[21] observed on "A" segregates in their studies on twenty ton ingots of steel statically frozen. Two important observations are:

1. there is a very close relationship among the freezing rate, its

distribution, and the solidification structure; and

2. "A" segregates appear in the region where the acceleration of the freezing rate is positive.

If condition two is satisfied it is observed that "A" segregates are likely to occur in the granular crystal region also. Acceleration of the freezing rate implies that rejected solute is not able to escape into the bulk liquid quickly enough to avoid being frozen into the local crystal structure. Freckles are extended trails of macrosegregation enriched in the normally segregated elements and depleted of the inversely segregated elements. Such well defined jets are the result of fluid instabilities. Flemings et al.[2] derived a dimensionless number $\vec{v}\cdot\nabla T/\varepsilon$ which defined the freckling behavior and quantitatively predicts its occurrence. A freckle should emerge if $\vec{v}\cdot\nabla T/\varepsilon<0$ with excessive melt back as this number approaches -1. A freckle is formed if the liquid jet erodes the dendrite forest by dissolution and dendrite dismemberment as enriched fluid traverses the mushy zone. However, it is not specified that a density inversion be required. Copley and Giamei[22] seconded the instability criteria by noting that suppression of both G and R "favors jet formation".

Copley and Giamei proposed that this suppression of G and R would occur longitudinally as the solidification front is displaced from the chill plate. Their research on the nonmetallic $30NH_4Cl$-H_2O system indicates that density inversion was the driving force for upward solute flow in unidirectional solidification. An interesting development is that the mushy zone orientation effected the critical radius where freckles appeared to congregate. A mushy zone which is convex upwards will have a concentric

ring of jet cross-sections towards the ingot center whereas a mushy zone concave upwards will have its jets at the mould wall periphery. This of course supports the density inversion mechanism.

Gould developed a hypothesis on segregation mechanisms[23]. As solutes are rejected during solidification, gases in the form of bubbles would also nucleate. These bubbles would migrate upwards leaving blowhole traces behind them. Upon migrating upwards, however, these bubbles would absorb CO. Thus, the gaseous phase migration would be a mechanism of segregation. This came from Gould's work on A-286 series steels. Burns and Beech[24] examined this hypothesis. From their work on iron base alloys containing CO gases they found:

1. the blowhole advances at the same rate as the dendritic solid/liquid interface. In their experiments they determined a value of 1.8×10^{-2} cm/sec for blowhole migration while the freezing rate was found to be 2.0×10^{-2} cm/sec;

2. the availability of oxygen is the controlling factor;

3. outward flow of solute from the bubble is small compared to influx; and

4. there is no evidence of solute flow in terms of macrosegregation in the ingot.

Oeters and Ruttiger[25] support Gould's hypothesis stating that new phases can form in the enriched layer in front of the solidification zone. This corresponds to statement one from Burns and Beech. The amount of precipitated new phases (bubbles of CO) depends upon the rate of solidification.

Another form of segregation is axial segregation. Some of the earliest works on segregation and its reduction are based upon the process of zone remelting studies. The main proponent of this work is Pfann[26] who calls it zone refining. The characteristic term found in zone refining expressions is the effective distribution coefficient, k_{eff}. Further work has been conducted by Fischer[27] and Graham[28].

Zone refining is fundamentally based on mechanism one. Oeters and Ruttiger[25] have quite recently described the method as being responsible for marked macrosegregation of the dissolved elements across horizontal ingot sections.

E. Effects of Macrosegregation on Mechanical Properties

In eliminating segregation, mechanical property variations with an alloy are greatly reduced. These aberrations are frequently responsible for high rejection rates during production. They also contribute to the failure of structural components throughout a broad spectrum of the alloy making and alloy fabrication industries. Heterogeneous distributions of chemical elements in solution along with nonmetallic inclusions are responsible for the transverse ductility of forgings being lower than longitudinal ductility.

Ductility is profoundly influenced by nonmetallic inclusions and small volume fractions of intermetallic compounds. Joy and Nutting[29] produced a series of experimental steels with all the EN39B specifications met with the exception of sulphur content. This was allowed to vary between 0.005 and 0.44%. Results of Izod impact tests determined that sulphur content influences the impact value of significantly. Little and Henderson[30]

also made a study of the effect of sulphur on the Charpy shelf energy (CSE) of steel. From Fig. (1), reduction of sulphur content from 0.026 to 0.007% results in a marked increase in both longitudinal and transverse CSE of about 86% and 103% respectively[29]. Fig. (2), illustrates the adverse effects of inclusions upon impact strength in En39B.

Variation of Charpy shelf energies throughout the ingot indicates variations of the sulphur content. If CSE is influenced predominantly by sulphur concentration then it is possible to determine the sulphur distribution within an ingot by testing for CSE distributions. This correlation of a physical property, CSE, to the impurity concentration (in this case sulphur) allows for direct identification of the segregation pattern of the ingot. Both Figures (1) and (2) show inverse relationships of Izod impact results to content of impurities. Weaker ingot sections correspond to greater than nominal concentration of impurity whether this is sulphur content or inclusion particles per unit area. If significant differences in physical properties occur within the ingot macrosegregation is the likely cause.

Thornton and Colangelo[31] examined the effects of forging reductions and the subsequent effects of carbon segregation upon the variation of mechanical properties of low alloy steel. The nominal compositions are approximately 0.35 to 0.4% carbon. They report that heterogeneous distribution of chemical elements in solution is responsible for the transverse ductility in forgings being lower than longitudinal ductility. Two ingots were examined. Longitudinal segregation of carbon in both ingots resulted in mechanical properties varying with position. Chemical tests

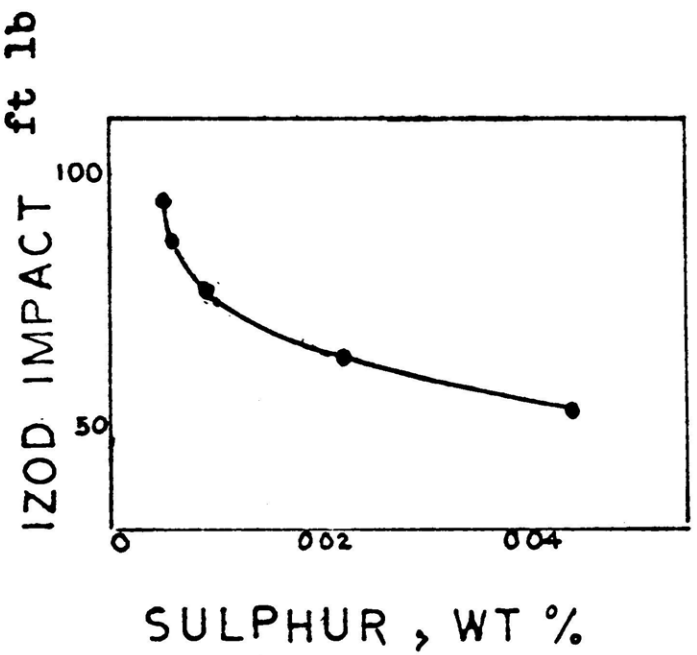

Fig. 1 - Variation of impact strength with sulphur content in En 39B steel. From Ref. 29.

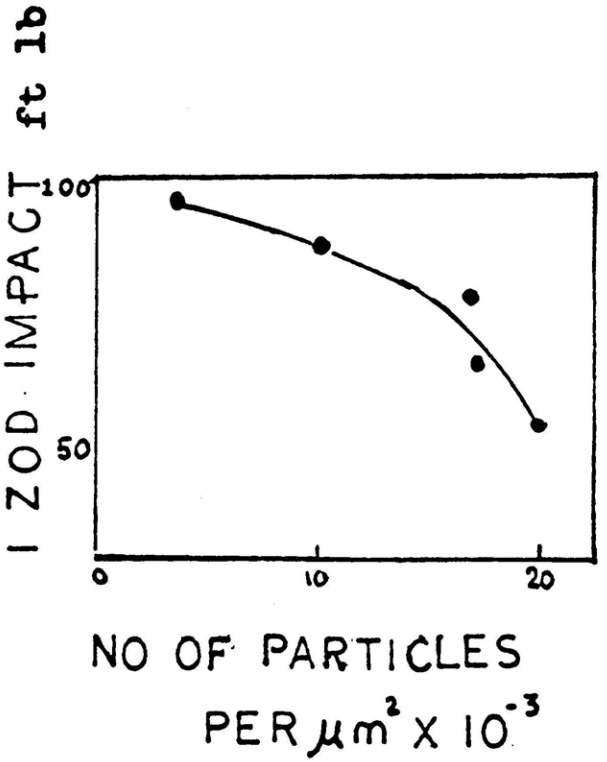

Fig. 2 - Variation of impact strength with number of inclusions per unit area in En 39B steel. From Ref. 29.

were used for the carbon analysis. They concluded that the upper ingot exhibited "noticeably different" mechanical behavior than the lower portion when forged to the same reduction (10:1).

Transverse carbon distributions are well documented by Thornton and Colangelo[31]. Chemical analysis at a total of seven radial test locations on 24 ingot disks were made. Prior to forging reductions the carbon distributions were generally concave upwards at the centerline and convex upward at the midradius. Upon mechanically working these ingot sections, it was found that the segregation profile was altered but that segregation was not eliminated.

Therefore, it is established that macrosegregation is a major contributor to mechanical property variation in steel and other alloy products of the metals industry. Chemical homogeneity in transverse sections is difficult if impossible to achieve even for large forging reductions (10:1) following ingot solidification. It is realized that the solution is that of modifying solidification mechanisms.

F. Electroslag Remelting Process

Electroslag remelting (ESR), is a secondary remelting of alloys. Current is carried along a consumable electrode to a slag bath. Within the slag an ohmic resistance is generated. Due to the effects of resistance slag temperatures several hundred degrees above the melting point of the alloy occur causing the electrode tip to melt. A thin film of molten metal forms a droplet at the tip of the electrode which is then detached by gravity forces. It drops through the slag layer to the metal pool beneath. Ingot formation is the result of the cooling effects of the water

cooled mold upon the metal pool.

The purpose of ESR is to produce materials which are more homogeneous. ESR is both a refining mechanism, and a casting technique. For steel, refining is carried-out at the electrode tip where sulphur, oxygen and nonmetallic impurities are preferentially dissolved at the slag/metal interface. As a casting process ESR offers unusually good control of the solidification process. Control of the melting rates and heat balances allows the metallurgist to "tailor-make" the solidification geometry of the two-phase zone. This affects the microstructure and ultimately the radial segregation profile of the ingot.

The thermodynamic aspect of nonmetallic inclusion dissolution in the slag has been studied by Kay et al.[32]. It was determined that synthetic inclusions are dissolved on the electrode tip. The section of electrode in contact with the slag, melts forming a thin film of molten metal at the tip of the electrode. The thickness of the film varies with melt rate, electrode size, and nominal alloy composition. It was demonstrated theoretically by Kluyev et al.[33] that film thickness decreases from 2500 μm in small lab furnaces to 30 μm in large industrial furnaces. Fredriksson and Jarleborg[34] also investigated the dissolution mechanisms of inclusions. Nonmetallic inclusions are rolled into "string like" structures upon formation of the electrode. Upon entering the molten zone they spheroidize. At the completely molten zone of the thin film they dissolve.

Another advantage of the ESR process is the control one has of the solidification zone of the ingot. It is well documented that the

inclination between the solidification front and the mold wall decreases with increasing melt rate[34]. Sun and Pridgeon[35] determined that the depth of the liquid pool is proportional to electrode melting rate. Several "disturbance" experiments were conducted by Medovar, Fredriksson[34] and others. Interruptions in electrode dipping, current flow, and electrode "change over" caused noticeable deviation of concentration profiles and crystal microstructures.

Since temperature gradients and cooling rates are more uniform in the transverse direction of ESR grown ingots than those of conventionally cast ingots similar of crystal morphology will exist transversely. This results in a reduction of anisotropy. Gulya and Swift[35] in their studies of 2.25% Cr, 1% Mo steel cast by the ESR process maintain that mechanical isotropy is greatly increased; especially, in the through-gage direction. Mechanical property data exhibited improvements in toughness and tensile properties in all conditions (annealed, normalized and tempered, quenched and tempered). Other improvements noted are superior fracture toughness as measured by K_{IC}, resistance to slow crack growth (da/dN), and resistance to bending fatigue. Heat resisting steel EI835 was melted by both the ESR process and the electric-arc melting technique in experiments by Maslenkov and Burova[37]. An equiaxed morphology occurs in ingots at the central zone when grown by the latter method while a continuous columnar morphology results from the ESR method. It was found that segregation of Mn changed more abruptly with increasing thickness of the crystallized layer in the electric arc ingot. At the columnar to equiaxed transition zone, the segregation profile changes sharply. This is seen in

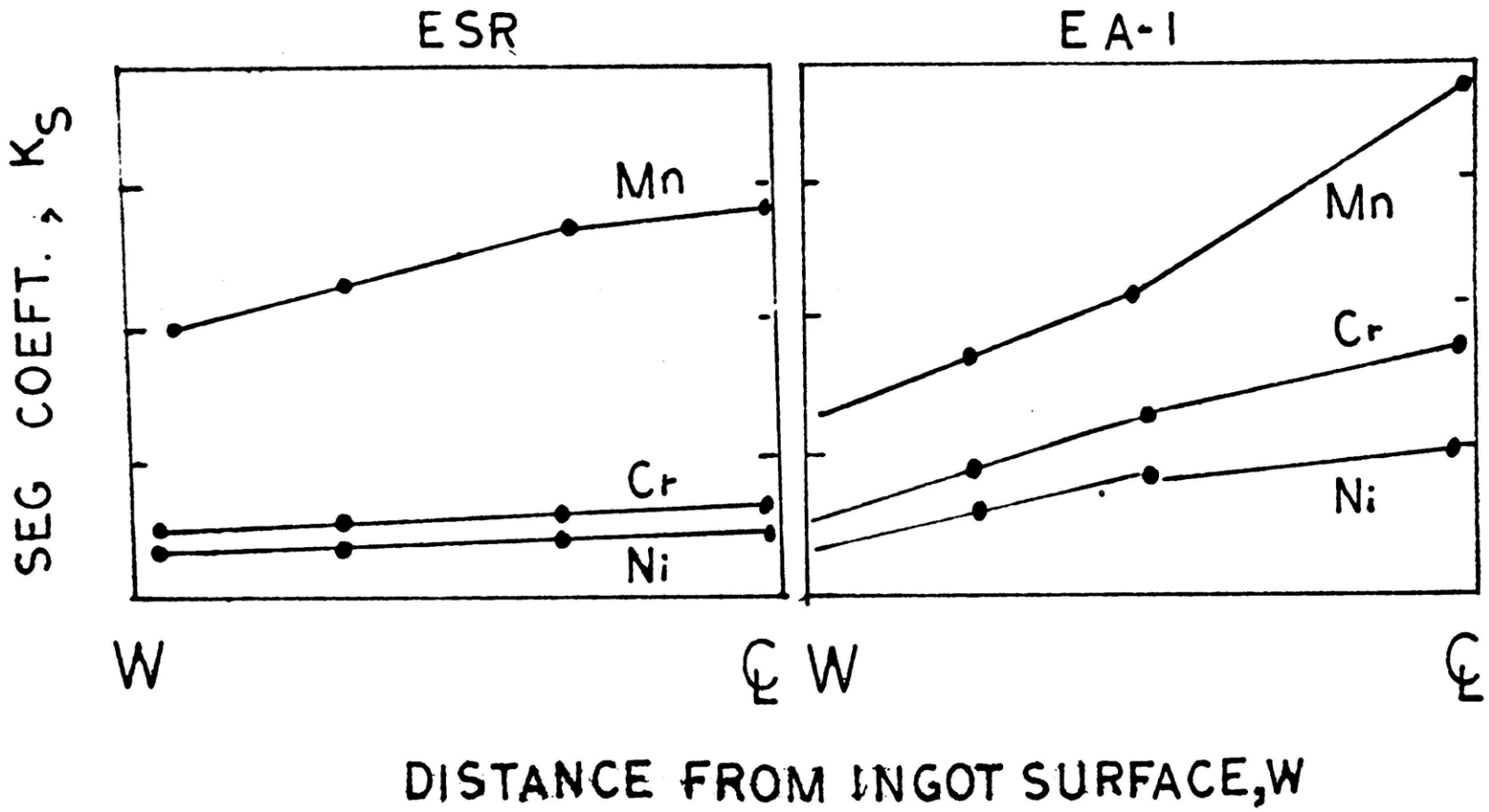

Fig. 3 - Profiles of the segregation coefficient, $K_s = C_s/C_o$ versus radius for EI 835 steel cast by both the ESR and electric-arc furnace (EA-1) methods. From Ref. 37.

Fig. (3). They concluded, statistically, that chemical heterogeneity of the rolled product is 25-30% higher in arc-furnace steel than in ESR steel. Due to this higher inclusion contents, arc-furnace steel shows twice as much property anisotropy as ESR steel. In Fig. (3) a plot of the "segregation coefficient", K_s, versus ingot radius is given. The segregation coefficient is the dimensionless ratio $\bar{C}_s/C_o$ where $\bar{C}_s$ is the composition at a given radius, r, and C_o is the nominal composition. It is evident from the Russian study on EI835 that:

a. the segregation coefficient is linear for a given crystal morphology, and

b. the slope of K_s/r for the ESR ingot is less than the slope for the arc-furnace grown ingot.

The segregates of concern are chromium, nickel and manganese.

In the axial direction some researchers treat the ESR process as a zone refining technique. The final concentration distribution is influenced by pool depth. Many researchers explicitly argue the case in terms of mechanism one. This is evident when they speak in terms of distribution coefficients. Mechanisms three and four, however, are more realistic. Edwards and Spittle[38] in their work on small Al-4.5% Cu ingots of 3.8 cm. diameter concluded that inverse segregation resulted at the ingot base for ESR grown ingots. Since columnar grains were maintained throughout the solidification process both mechanisms one and two were disqualified.

The literature contains good examples of solute profiles for transverse sections. Such transverse plots are found in the works of Fredriksson[34], Mèlberg[39], and Maslenkov[37]. Heterogeneity is augmented upon increasing

melt rates. If cooling rates as a function of radius are known it is possible to then define the dendrite morphology and size in a radial sense. Subsequent solute concentration profiles are then related to this morphology and size.

III. ANALYSIS OF MACROSEGREGATION

In this chapter the aspects of fluid flow within the mushy zone are dealt with analytically in cylindrical coordinates. The model is for steady state. Using the work of Flemings and Nereo[2] Kou derived the basic form of the partial differential equation (PDE), for the mushy zone interior[40]. This exact formulation is then transformed to the finite difference approximation in Section B; boundary conditions are also formulated in Section B. Section C elaborates upon the finite difference approximation of the local solute redistribution equation, LSRE, and the radial composition equation. Computer notations for the variables in these equations are found in Chapter IV, Section C and summarized in Appendix A.

A. Fluid Flow within the Interdendritic Region

In analyzing the flow within the mushy zone certain assumptions must be made. The general assumptions embodied in the Flemings Nereo model(1-3) along with other possibilities (4-5) are mentioned below.

1. The volume element within the mushy zone is large enough so that the fraction solid within it at any time is exactly the local average, but small enough that it can be treated as a differential element. The volume element has the coordinates (x, y, z, t).

2. Solute enters or leaves the element by liquid flow to feed shrinkage. Metal contraction induces solute flow.

3. Liquid composition and temperature within the element are uniform (within a differential amount) at any time.

4. Changes in convection affect thermal conditions in the liquid-solid region of a solidifying ingot.

5. Mass flow is also induced by the diffusion mechanism.

In the system presented in this work assumptions 4 and 5 are also neglected. Extra restrictions are presented.

a. Since the mold was a tube cylindrical coordinates were considered where:

$$r = (x^2 + y^2)^{\frac{1}{2}}$$

$$\theta = \tan^{-1}(y/x) \qquad \text{and}$$

$$z = z$$

b. Symmetry is also specified so that r = x resulting in y = 0. The final results $\theta = 0$ indicates that the coordinates are for a two-dimensional system (r, z).

c. The specific case of steady state was assumed.

d. Only binary systems were treated in this study.

e. The solute fluid of the mushy zone is considered to be a Newtonian fluid.

A general outline of the procedure of deriving the pressure equations is now presented.

The continuity equation[40] for the differential element is

$$\frac{\partial}{\partial t}(\rho_s g_s + \rho_L g_L) = -\nabla \cdot \rho_L g_L \vec{v} \qquad (11)$$

Since the relationship $g_s + g_L = 1$ must hold and since the density of the solid phase, ρ_s, is assumed constant within the interdendritic region Eq. (11) reduces to:

$$(\rho_L - \rho_s)\frac{\partial g_L}{\partial t} + \frac{\partial \rho_L}{\rho t} = -\nabla \cdot \rho_L g_L \vec{v} \qquad (12)$$

In order to solve this expression all time dependent terms $\vec{v}$, $\frac{\partial g_L}{\partial t}$ and $\frac{\partial \rho_L}{\partial t}$ must be transformed to time-independent relationships.

The first step is met if D'Arcy's Law for porous media is utilized so that:

$$\nabla = - \frac{K}{\mu g_L} (\nabla P + \rho_L \vec{g}) \tag{13}$$

From Chapter II Section B two separate relationships for specific permeability are expressed. "Equation (4)"

$$K = \gamma . g_L^{\,2}$$

used by Mehrabian et al.[3] to study macrosegregation based upon the experimental work of Piwonka and Flemings[9] is used in this study.

Step two is completed once time-independent expressions are found which equal the time-dependent terms $\frac{\partial g_L}{\partial t}$ and $\frac{\partial \rho_L}{\partial t}$. Since C_L is a function only of temperature the following is true:

$$\frac{\partial C_L}{\partial t} = \frac{dC_L}{dT} \frac{\partial T}{\partial t} = \frac{\varepsilon}{m} \tag{14}$$

where m is the liquidus slope from the equilibrium phase diagram, and ε is the cooling rate of the differential element. Based upon many of the same assumptions already outlined, the local solute redistribution equation has been derived. It gives volume fraction liquid as a function of the local composition of the interdendritic liquid (and hence, as a function of temperature during solidification); it is:

$$\frac{\partial g_L}{\partial C_L} = - \left(\frac{1-\beta}{1-K_p}\right) \left[1 + \frac{\vec{v} \cdot \nabla T}{\varepsilon}\right] \frac{g_L}{C_L} \tag{15}$$

where: $\beta = \frac{\rho_s - \rho_L}{\rho_s}$, and

K_p = partition ratio

From the chain rule multiply Eq. (14) times the LSRE, Eq. (15) to arrive at:

$$\frac{\partial g_L}{\partial t} = - \left(\frac{1-\beta}{1-k}\right) \left[1 + \frac{\vec{v}\cdot\nabla T}{\varepsilon}\right] \frac{g_L}{C_L} \cdot \frac{\varepsilon}{m} \tag{16}$$

The density of the interdendritic liquid, ρ_L, is a function of concentration and temperature. Since the liquid composition and the liquid density are both functions of the temperature an exact derivative, $d\rho_L/dC_L$, the slope of the plot of ρ_L versus C_L, is obtainable. Thus:

$$\frac{\partial \rho_L}{\partial t} = \frac{d\rho_L}{dC_L} \frac{\varepsilon}{m} \tag{17}$$

completing step two.

Upon inserting the three expressions from steps one and two into Eq. (12) a time independent expression of the continuity equation is arrived at:

$$\nabla \left(\frac{\gamma g_L^2 \rho_L}{\mu} \nabla P + \frac{\gamma g_L^2 \rho_L^2 \vec{g}}{\mu}\right) =$$

$$- (\rho_L - \rho_s) \left(\frac{1-\beta}{1-k_p}\right)\left[1 - \frac{\gamma g_L}{\mu\varepsilon} (\nabla P + \rho_L \vec{g})\cdot\nabla T\right] \frac{g_L}{C_L} \frac{\varepsilon}{m}$$

$$+ g_L \frac{d\rho_L}{dC_L} \frac{\varepsilon}{m} \tag{18}$$

For a given location within the mushy zone all of the physical terms of Eq. (18) are defined except pressure, P, which is the independent variable. The final step, then, is to unravel the difficult form of Eq. (18) making it more tenable. This form is:

$$\frac{\partial^2 P}{\partial r^2} + A\frac{\partial P}{\partial r} + \frac{\partial^2 P}{\partial z^2} + B\frac{\partial P}{\partial z} + C = 0 \qquad (19)$$

where: $A = \frac{1}{r} + \frac{2}{g_L}\frac{\partial g_L}{\partial r} + \frac{1}{\rho_L}\frac{\partial \rho_L}{\partial r} + \alpha\frac{\partial C_L}{\partial r}$

$$B = \frac{2}{g_L}\frac{\partial g_L}{\partial z} + \frac{1}{\rho_L}\frac{\partial \rho_L}{\partial z} + \alpha\frac{\partial C_L}{\partial z}$$

$$C = g\rho_L\{\frac{2}{g_L}\frac{\partial g_L}{\partial z} + \frac{2}{\rho_L}\frac{\partial \rho_L}{\partial z} + \alpha\frac{\partial C_L}{\partial z}\} - \frac{\varepsilon\mu}{m\gamma g_L}\{\alpha + \frac{1}{\rho_L}\frac{\partial \rho_L}{\partial C_L}\}$$

and $\alpha = \frac{\beta}{(1-k_p)C_L}$

The coefficients A, B, and C are referred to as the "primary" coefficients. Notice that A deals with the radial gradients of the physical terms. It is associated with $\partial P/\partial r$. Likewise, coefficient B dealing with the vertical gradient terms is linked with $\partial P/\partial z$ in the PDE. Term C deals again with the vertical gradients similar to that of B.

The coefficient $\mu\varepsilon/m\gamma g_L$ of the second term of coefficient C represents resistance to fluid flow within the interdendritic region. The viscosity, μ, represents the resistance due to fluid properties while the $\varepsilon/g_L\gamma$ term is resistance due to dendrite morphology. The cooling rate, ε, if high indicates that the interdendritic region will be composed of morphologies having large surface area to volume ratios. Alloys of higher nominal composition will have larger average values of fraction liquid if the partition ratio is less than unity. The effect is that the resistance to flow is lowered.

The (1/n)(dn/dL) form of the individual terms of the primary coefficients implies an exponential effect for incremental variations of property with respect to space. For instance, a tendency for liquid density to change upon freezing has very noticeable effects upon the fluid flow. The shrinkage potential is embodied within the α term and is found in all three primary coefficients. This concludes the brief analysis of the primary coefficients.

B. Finite Difference Approximations for the PDE and Boundary Conditions

One of the basic functions of the program is to determine the interdendritic velocity distribution within the mushy zone. The solute composition distribution follows. The velocity distribution, however, can only be found after the pressure distribution is computed. In this section boundary conditions and the partial differential equation for the interior of the mushy zone are defined in terms of finite difference pressure gradients.

1. Interior Nodes

Equation (19) is a second order partial differential equation (PDE), of elliptic type. The primary coefficients, A, B and C have been defined above and are also listed in Appendix B, Der. (2) in their finite difference forms in computer notation. The gradient $\partial C_L/\partial z$ in algebraic form is:

$$\frac{C_L(i,j+1) - C_L(i,j-1)}{2\Delta r}$$

In expanded form the first and second derivatives are:

$$\frac{\Delta P}{\Delta z} = \frac{P(i,j+1) - P(i,j-1)}{2\Delta z}$$

$$\frac{\Delta^2 P}{\Delta z^2} = \frac{P(i,j+1) + P(i,j-1) - 2P(i,j)}{\Delta z^2}$$

The same treatment applies to the radial gradient counterparts. The only assumptions are that the pressure distribution is continuous and that the vertical and radial increments, Δz and Δr, respectively are constant. The finite difference form of the PDE is given in Appendix B Der (3). The effects of unequal increment spacings for first and second order finite difference forms are listed in Appendix B, Der (4).

In the iteration sequence the step-by-step solution routine requires that one pressure value be computed at a time. At any given time all surrounding nodes contain values of pressure. Equation (19) is written as:

$$\begin{aligned} P(i,j) = {} & a \cdot P(i+1,j) + b \cdot P(i,j+1) \\ & + c \cdot P(i-1,j) + d \cdot P(i,j-1) \\ & + e \end{aligned} \qquad (20)$$

Discussions on the composite coefficients: a, b, c, d, and e are given in Chapter IV, Section (C.3).

2. Liquidus Boundary Condition

From experimental measurements the mushy zone geometry is determined and recourse to heat transfer for definition of the liquidus is not

necessary. This simplification alleviates the necessity of a "coupling" model and the pressure at the liquidus surface is calculated by the metallostatic height of the liquid pool. Therefore,

$$p = p_a + \rho_L \, gh \tag{21}$$

where p_a is the atmospheric pressure and h is the liquid pool depth. Since the liquid density term, ρ_L, is a function of the liquidus temperature, T_L, it is evident that the pressure gradient is only a function of the nominal alloy composition, C_o. There is a unique liquidus temperature for each value of C_o. The main assumptions for the liquidus boundary are:

1. the average temperature of the bulk liquid melt above the two phase zone is a constant, T_L;

2. the slag head affects only the absolute value of pressure and therefore is neglected; and

3. a flat top profile is assumed for the liquid metal pool.

3. Solidus-Interior Boundary Points

At the solidus boundary the last bit of liquid is freezing. This is of eutectic composition, C_E and volume fraction g_{LE}. This fraction of liquid eutectic is not constant except for the case of unidirectionally grown ingots. A mass balance yields:

$$\vec{V} = - \left(\frac{\rho_{SE}}{\rho_{LE}} - 1\right) \vec{U} \tag{22}$$

The components of Eq. (22) are

$$\vec{V}_{rE} = - \left(\frac{\rho_{SE}}{\rho_{LE}} - 1\right)\vec{U}_r \tag{23}$$

and

$$V_{ZE} = - \left(\frac{\rho_{SE}}{\rho_{LE}} - 1\right)U_Z \tag{24}$$

Since D'Arcy's law for laminar flow is applied to the two-phase region, the velocity components can also be written as

$$V_{rE} = - \frac{K}{\mu g_{LE}} \cdot \frac{\partial P}{\partial r} \tag{25}$$

and

$$V_{ZE} = - \frac{K}{\mu g_{LE}} \left[\frac{\partial P}{\partial Z} + \rho_{LE} g\right] \tag{26}$$

By equating like velocity terms the following results:

$$\left.\frac{P(i,j) - P(i-1,j)}{\Delta r}\right|_E \simeq \frac{\mu g_{LE}}{K} \left(\frac{\rho_{SE}}{\rho_{LE}} - 1\right)U_{rE} \tag{27}$$

and

$$\left.\frac{P(i,j+1) - P(i,j)}{\Delta Z}\right|_E \simeq \frac{\mu g_{LE}}{K} \left(\frac{\rho_{SE}}{\rho_{LE}} - 1\right)U_{ZE} - g\rho_{LE} \tag{28}$$

It is in finite difference form. Also known is that the isotherm velocities U_{ZE} and U_{rE} can be described in terms of the centerline velocity, U_Z, and the solidus isotherm slope, m_E, such that:

$$U_{ZE} = \frac{U_Z}{1+m_E^2} \tag{29}$$

and

$$U_{rE} = - \frac{m_E U_Z}{1+m_E^2} \tag{30}$$

A major problem is found at this boundary. The eutectic shrinkage for some alloys is considerable. However, expansion is occurring small distances away within the interior. Due to this singular behavior it was necessary to solve for pressures directly above the solidus isotherm and not on it. In this manner the gradients of pressure are "weighted" according to dominance. The radial pressure gradient at this "buffer" isotherm is approximated as:

$$\left.\frac{\Delta P}{\Delta r}\right|_{S-I} \quad \frac{1}{2}\left.\frac{\Delta P}{\Delta r}\right|_{E} + \frac{1}{2}\left.\frac{\Delta P}{\Delta r}\right|_{I} \tag{31}$$

In a similar manner the vertical pressure gradient is likewise written:

$$\left.\frac{\Delta P}{\Delta Z}\right|_{S-I} \quad \frac{1}{2}\left.\frac{\Delta P}{\Delta Z}\right|_{E} + \frac{1}{2}\left.\frac{\Delta P}{\Delta Z}\right|_{I} \tag{32}$$

Each gradient along the solidus-interior isotherm, S-I has two components. One is the eutectic portion subscripted E and the other is the contribution from the interior, subscripted I. Equations (27) and (28) are therefore substituted into Eq. (31) and (32) such that:

$$\left.\frac{\Delta P}{\Delta r}\right|_{S-I} = \frac{1}{2}\left[\frac{\mu g_{LE}}{K}\left(\frac{\rho_{SE}}{\rho_{LE}} - 1\right) U_{\bar{r}E}\right]_{E} + \frac{1}{2}\left[\frac{P(i,j)-P(i-1,j)}{\Delta r}\right]_{I} \tag{33}$$

and

$$\left.\frac{\Delta P}{\Delta Z}\right|_{S-I} = \frac{1}{2}\left[\frac{\mu g_{LE}}{K}\left(\frac{\rho_{SE}}{\rho_{LE}} - 1\right)U_{ZE} + g\,\rho_{LE}\right]_{E} + \frac{1}{2}\left[\frac{P(i,j+1)-P(i,j)}{\Delta Z}\right]_{I} \tag{34}$$

result.

4. Centerline and Ingot Radius Boundary Points

By symmetry, $v_r=0$ or $\partial P/\partial r = 0$ at the centerline. At the ingot circumference, $v_r=0$ so along this boundary $\partial P/\partial r=0$ is again implied. These boundary conditions are incorporated into the program by setting pressure at the centerline nodes equal to the pressure of the nodes directly adjacent to the centerline nodes. Similarly, the pressure at a node along the ingot radius is set equal to its connecting node. In finite difference form the boundary condition for the centerline is:

$$P(1,J) = P(2,J) \tag{35}$$

For the wall boundary:

$$P(IMAX,J) = P(IMAXN,J) \tag{36}$$

is the appropriate form where IMAX is the column representing the wall and IMAXN = IMAX-1. Notice that both forms are written in computer notation (CN).

C. Macrosegregation Calculations

1. Local Solute Redistribution Equation

The LSRE in exact form is seen in Eq. (15). In finite difference form it is:

$$g_L(i,j) = \sum_{j_{MAX}}^{j_{MIN}} \frac{1}{K_p-1} \frac{1}{2\rho_S} [C_L(i,j) - C_L(i,j+1)] \cdot [\ ] \tag{37}$$

where:

$$[\ ] = 1 + \frac{V_r(i,j)\ \frac{\partial T}{\partial r}\ (i,j) + V_Z(i,j)\ \frac{\partial T}{\partial Z}\ (i,j)}{\varepsilon(i,j)}$$

$$1 + \frac{V_r(i,j+1)\ \frac{\partial T}{\partial r}\ (i,j+1) + V_Z(i,j+1)\ \frac{\partial T}{\partial Z}\ (i,j+1)}{\varepsilon(i,j+1)}$$

The integration is directed from the liquidus to the solidus in a single pass. This is because the fraction liquid at the liquidus is always unity by definition whereas the value of fraction liquid eutectic, g_{LE}, is unknown. New values of fraction liquid are attained at each node in the column as the integration proceeds. The final value in the column is the revised value of the eutectic fraction liquid.

2. Radial Average Solute Composition

Macrosegregation in an ingot is given in terms of the local average composition of solid after solidification is complete. This is:

$$\bar{C}_s(r) = \frac{\rho_s K_p \int_o^{1-g_{LE}} C_L dg_s + \rho_{SE} g_{LE} C_E}{\rho_s(1-g_{LE}) + \rho_{sE} g_{LE}} \qquad (38)$$

In finite difference form it is

$$\bar{C}_s(r) = \frac{1}{2}\rho_s \sum_{j=j_{MAX}}^{j=j_{MIN}} \frac{[C_s(j) + C_s(j-1)] \times [g_s(j-1) - g_s(j)] + \rho_{SE} C_E g_{LE}}{\rho_s(1-g_{LE}) + \rho_{SE} g_{LE}} \qquad (40)$$

In the above equations g_{LE} is the volume fraction of eutectic, and C_E is the eutectic composition. The integration in the numerator can be carried out by picturing a fixed unit volume in which C_L continuously changes in a known manner as the alloy solidifies. For an ESR ingot, when the isotherms move at a steady velocity, the integration can be carried out by integrating from the liquidus (g_s=0) down to the solidus (g_s=1-g_{LE}) at a given radius

in a similar fashion to that of the LSRE. By doing this for different radial positions within the ingot, $\bar{C}_S(r)$ versus radius is determined which can be plotted to give the pattern of macrosegregation.

3. Average Ingot Composition

Occurring at the conclusion of the program is a method of determining the average solute content of the ingot. In exact form the integration appears as:

$$\bar{C}_s \text{ (ingot)} = \frac{2\pi \int_o^R \bar{C}_s(r)\, r\, dr}{\pi R^2} \tag{41}$$

In approximate form it is:

$$\bar{C}_s \text{ (ingot)} = \frac{2 \cdot \sum_{i=2}^{imax-1} \bar{C}_{si}\, r_i\, \Delta r}{R^2} \tag{42}$$

so long as the radial increments are equal.

IV. COMPUTER SIMULATION OF MACROSEGREGATION

This chapter has three sections. Section A examines both models for defining an appropriate grid for a mushy zone. Section B centers about Flow Chart I, Fig. (7) which is an overview of the entire program. Within this section major operations of the program are outlined. Section C contains each of the operations and details many of the sequences outlined in Section B. In Section C a very detailed flow chart, Appendix C, is given supplementing the presentation.

A. Grid Formation

Two versions of the program for predicting macrosegregation are constructed for use on the IBM 370. The nodal grid is an essential part of the program and is discussed here.

1. Model 1 (Three Zone Model)

Figure (4a), illustrates the superposition of nodes on a mushy zone. Observe that nodes actually delineate the boundaries. This is characteristic of the three zone model. Notice also that nodes tend to cluster in certain regions. Equations of the type:

$$z = a_1(r-n) \tag{43}$$

and

$$z = 2a_2r(r-n) \tag{44}$$

are used to define linear and parabolic isotherms, respectively. The value

$$n = \frac{d}{a_{1L}-a_{1S}} \tag{45}$$

is a constant term for the linear case where:

d = the depth of the mushy zone at the centerline,

a_{1L} = the slope of the liquidus isotherm, and

a_{1S} = the slope of the solidus isotherm

For the parabolic case:

$$n(r) = \frac{d(r)}{2r(a_{2L}-a_{2S})} \tag{46}$$

defines variable n(r) where:

a_{2L} = the coefficient of the second degree term for the liquidus;

a_{2S} = the coefficient of the second degree term for the solidus;

and $d(r)$ = the depth of the mushy zone at radius, r.

The simple equations are therefore:

$$z = a_o + a_1 r \tag{47}$$

for the linear case: and

$$z = a_o + a_2 r^2 \tag{48}$$

for the parabolic. It is apparent that Δz is a function of the radial increment, Δr. This is especially pronounced for the parabolic case where:

$$\Delta z \propto \Delta r^2$$

This means that regions of steep slopes will have large values of Δz which will diminish accuracy.

Model 1 is called a three zone type because each of the three zones is constructed separately. The first zone extends from the bottom of the grid at point 1 to point 2. Within this region, if Δr is a constant then Δz varies if the isotherms are not linear. Zone 2 extends from 2 to 3. A constant value of Δz is chosen for this region. Both Δr and Δz are constant

in this zone. Zone 3, from 3 to 4, is similar to zone 1.

2. Grid Features of Model 1

a. The liquidus and solidus isotherms form boundaries.

b. The z increments are functions of the isotherm shape and the value of Δr.

c. There is a major stipulation that point 3 must lie above point 2 due to grid construction techniques. If both points are at the same height the computer will automatically by-pass zone 2.

d. The number of nodal points lying in the mushy zone is (2*IMAX+NPTS)*IMAX where NPTS is the number of rows in zone 2.

e. Only certain basic polynominal types are allowed for describing isotherms. It is not possible to have

$$z = a_o + a_1 r + a_2 r^2 \tag{49}$$

3. Model 2 (Single Zone)

A simpler model for grid construction is Model 2. Two methods are permissible for defining the liquidus and solidus boundaries:

1. A polynomial with radius as the independent variable will define a boundary. The polynomial is determined by at least square approximations once the boundary is confirmed by experiment.

2. The "discrete linear segment" approach is a technique of defining linear approximations to the curve representing the solidus or liquidus. Linear segments of the actual curve are determined between neighboring vertical grid columns. The closer the columns, the more accurate the

approximations. This technique is described in Section (C).

As in Model 1 the centerline and wall boundaries are delineated once IMAX is determined. IMAX is the column representing the wall boundary. The centerline is always along column 1.

Constant radial and vertical increments, Δr and Δz, are utilized in this model for grid set-up. It is infrequent that a nodal point will define the liquidus or solidus boundary. An interpolation process is therefore carried-out at these isotherms. The node closest to the boundary, either above or below it, becomes the boundary. Observe Fig. (4b) for reference (where the dashed lines represents the true isothers and the solid curves denote the computer approximations). For this reason the depth of the mushy zone at a particular radius can be expanded or contracted slightly. The smaller the value of Δz the less significant is the distortion. These assignments of boundaries are implemented by "logical if" statements once the computer has stepped above a boundary in a given column. This is given in Oper. A, Loop 50 of Flow Chart II. The liquidus point for column I has a J value of NT(I) while the solidus point has a value of MT(I).

4. Grid Features of Model 2

a. The liquidus and solidus are seldom endpoints of the grid in the vertical direction. Interpolation is necessary.

b. The z increments are independent of the isotherm shape and the value of Δr.

c. There is no stipulation that one point of the grid must lie above or below another.

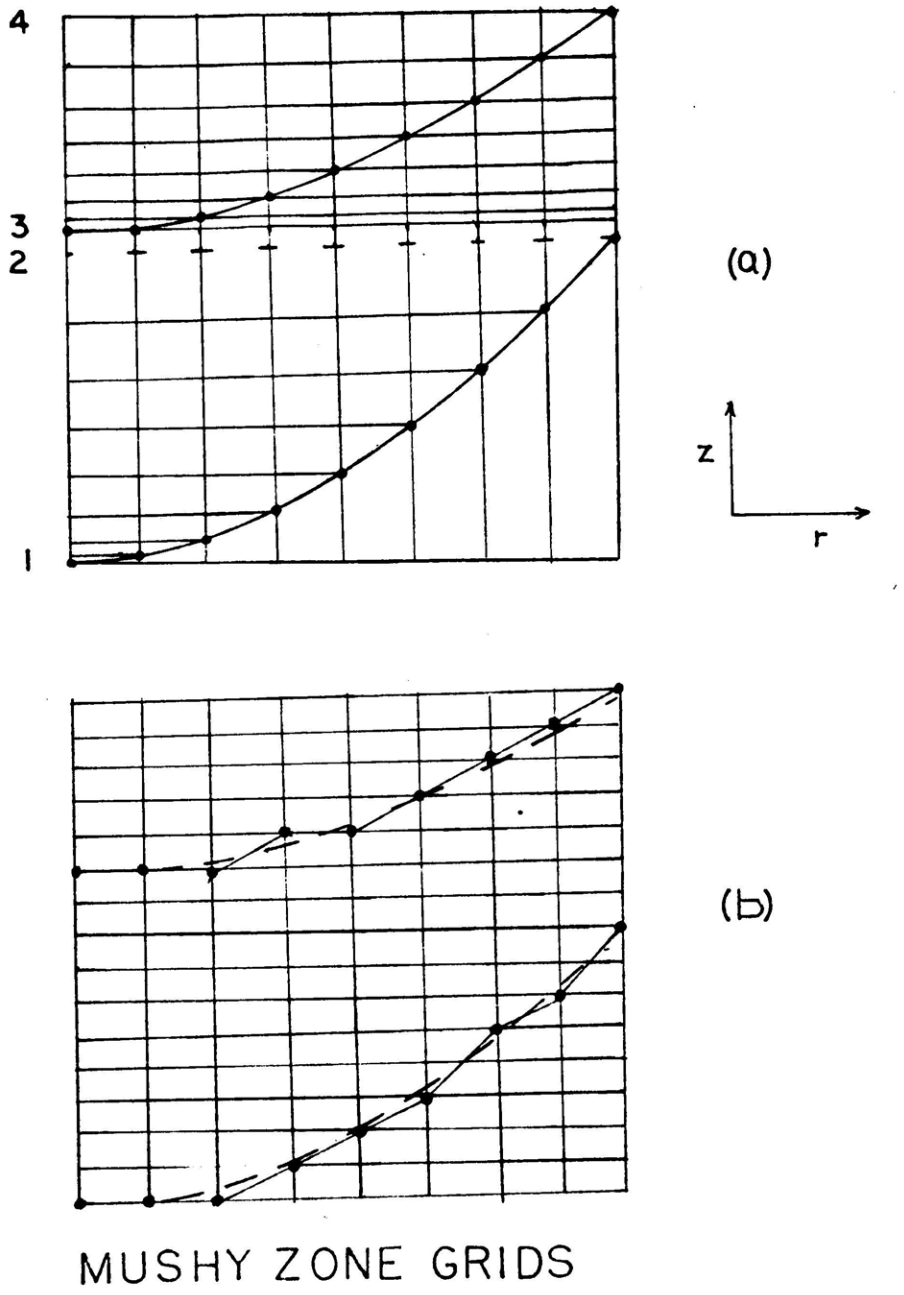

Fig. 4 - (a) Grid construction of Model 1 for the mushy zone. Note that the radial increment, h, is a constant whereas the z increment, k , varies. Boundary points are nodal points.
(b) Grid construction of Model 2. Neither h or k is affected by the mushy zone shape. Actual boundaries need not lie on assigned nodal positions. Dashed curves are actual boundaries.

d. It is no longer so simple to specify the total number of grid points within the grid. Unlike the three zone model the number of nodes within a column is no longer constant but instead is NT(I)-MT(I) for the Ith column.

e. Any type of isotherm function is permissible. Any curve that is monotonically increasing can be represented in terms of the discrete linear segments.

5. Contrast of Models 1 and 2

A major advantage of Model 2 over 1 is that it can handle complex mushy zone geometries whereas Model 1 relies upon simplicity of shape. Both steep and flat isotherm profiles are difficult to handle with Model 1. For example, if the isotherms are parallel then

$$\text{Limit } n = \infty \qquad \left.\frac{dz}{dr}\right|_{E} = \left.\frac{dz}{dr}\right|_{LIQ} \tag{50}$$

and since

$$z \propto n$$

$$\text{limit } z = \infty \tag{51}$$

The expression for z becomes meaningless in such cases. A less explicit difficulty is that there is uncertainty as to the relative amounts of error generated in different grid regions due to truncation. This is due to variations of Δz spacings in different regions as the isotherms slopes change. Thus, the final value of $\bar{C}_s$ are less consistent due to variations at different radii. This is not true in the case of Model 2 since values

of Δz and Δr are constant throughout the grid. The truncation error variations are not regional.

The one difficulty that can be encountered in Model 2 is that of expansion or contraction of mushy zone depth due to the two interpolations on each column at the liquidus and solidus boundaries. The maximum error can amount to

$$\underset{\max}{e(r)} = \frac{2\Delta z}{d(r)} \tag{52}$$

where d(r) is the depth of the mushy zone at radius, r. The effect is that this leads to inaccuracies in temperature gradients, dT/dz, which will detrimentally affect the finite difference form of the PDE. It will show up in the cooling rate term, ε, since:

$$\varepsilon = - U_z \cdot \frac{\partial T}{\partial z} \tag{53}$$

However, this error is controllable sinze Δz is chosen by the operator.

Difficult geometries of the mushy zones of continuous castings have been successfully simulated with satisfactory results with regards to composition distributions. Altogether, Model 2 is a more versatile model.

6. Direct Comparison of Models 1 and 2

A direct computer comparison was made of the two models for the Al-4.4% Cu of Ingot 1. Figure (5) shows the results of a 700 iteration run of both models. In these results $\gamma = 10^{-8}$ cm^2. Though Model 2 uses 46% more nodal points than Model 1 the comparison is justified. The greatest variation occurs beyond a radius of 2.6 cm. However, to choose

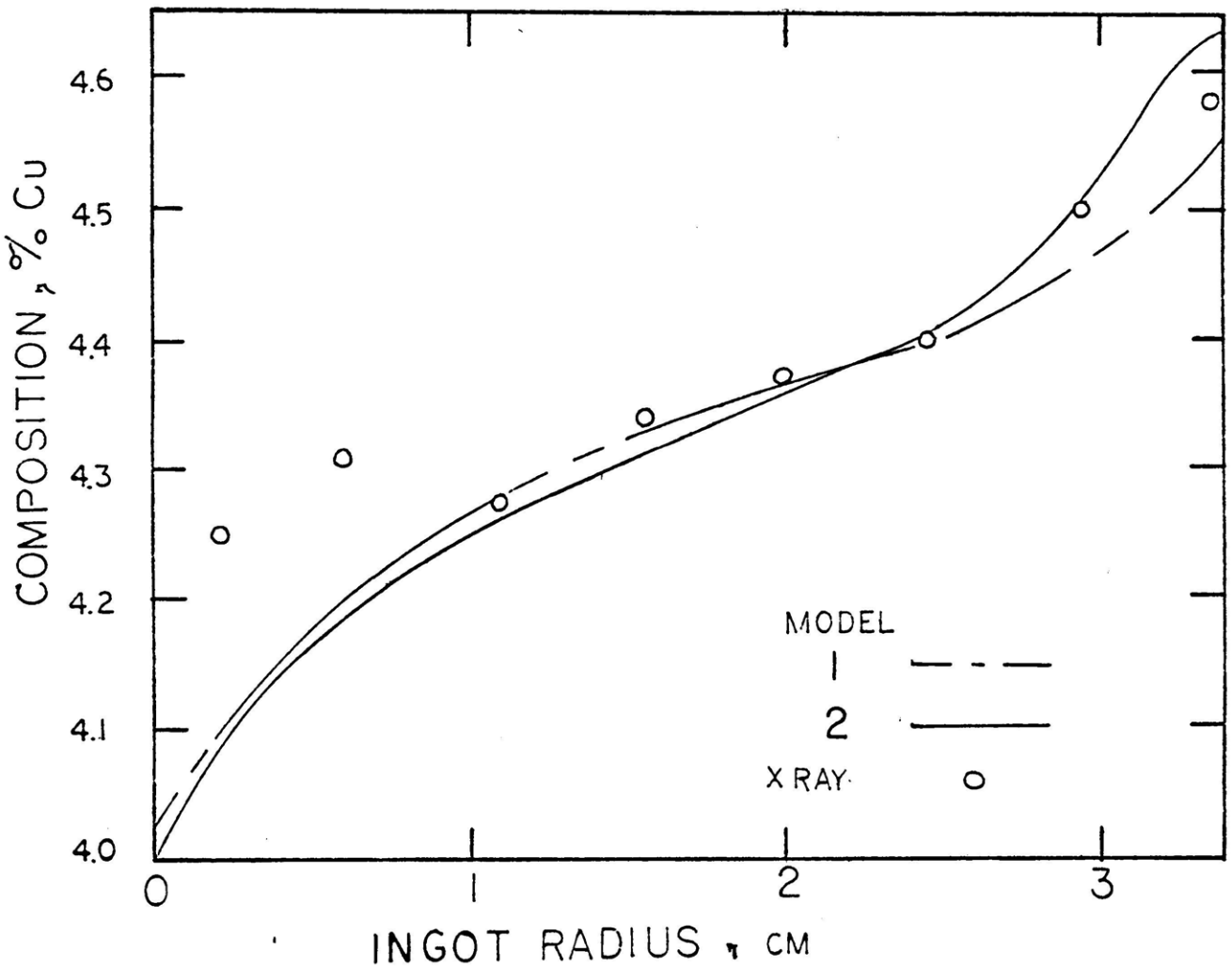

Fig. 5 - Comparison of Models 1 and 2 for an ingot of 4.4% Cu nominal composition. Experimental points are shown. Increment spacings are h = 0.2 cm and k = 0.1 cm. $\gamma = 10^{-8}$ cm^2.

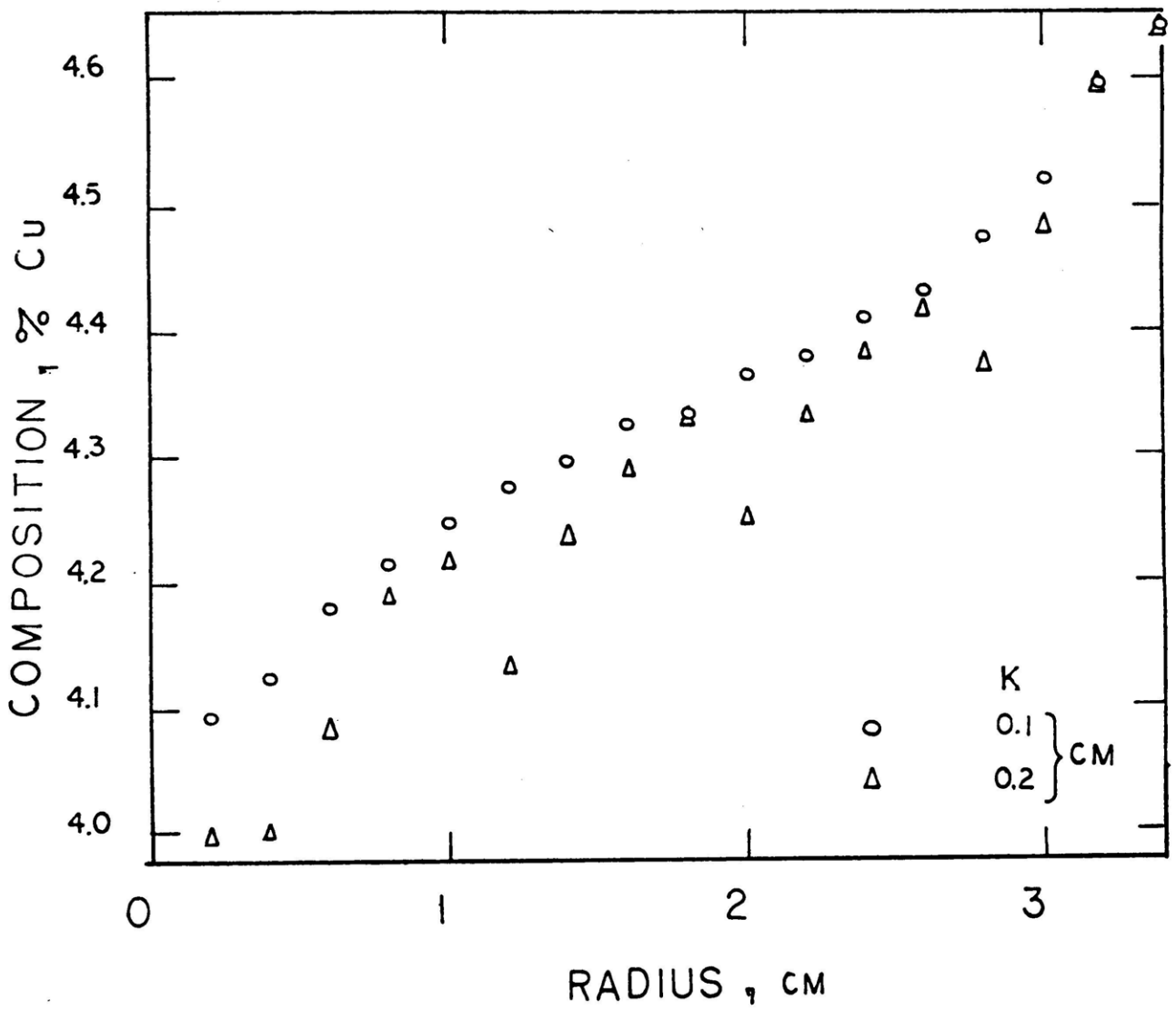

Fig. 6 - Model 2 yields both composition profiles if increment k is varied from 0.2 to 0.1 cm. Smoother profile results from smaller value.

which is more correct is not an easy task since an exact solution is not available and both simulation curves inscribe the experimental points in this region. Therefore, it appears that the results obtained from the models are comparable.

7. Coarseness of Computer Generated Profiles

An interesting feature of Model 2 is that it is possible to determine the correct z spacings in a step-wise manner. Figure (6) shows results of calculating the composition profile for two separate values of this increment. When a large spacing of 0.2 cm. is used an irregular pattern results from the interpolation method occurring at the liquidus and solidus. The value of e(r) is substantial.

A more regular profile is attained upon inputing a z spacing of 0.1 centimeters . This is half the former value. It is possible to determine the proper profile by adjusting the grid spacing. In Fig. (6) the 0.1 cm z increment necessitated 684 nodes whereas the coarser increment of 0.2 required half as many, 342 nodes.

B. Program Overview

This section is included to provide an overview of the operation of the computer program. A grasp of the overall system allows one to approach the detailed sections with an understanding of objectives. The flow chart of Fig. (7) embodies the most apparent sectors of the program . The following procedures are executed by the program. For each topic in Section B the program location (appropriate loop) is assigned in

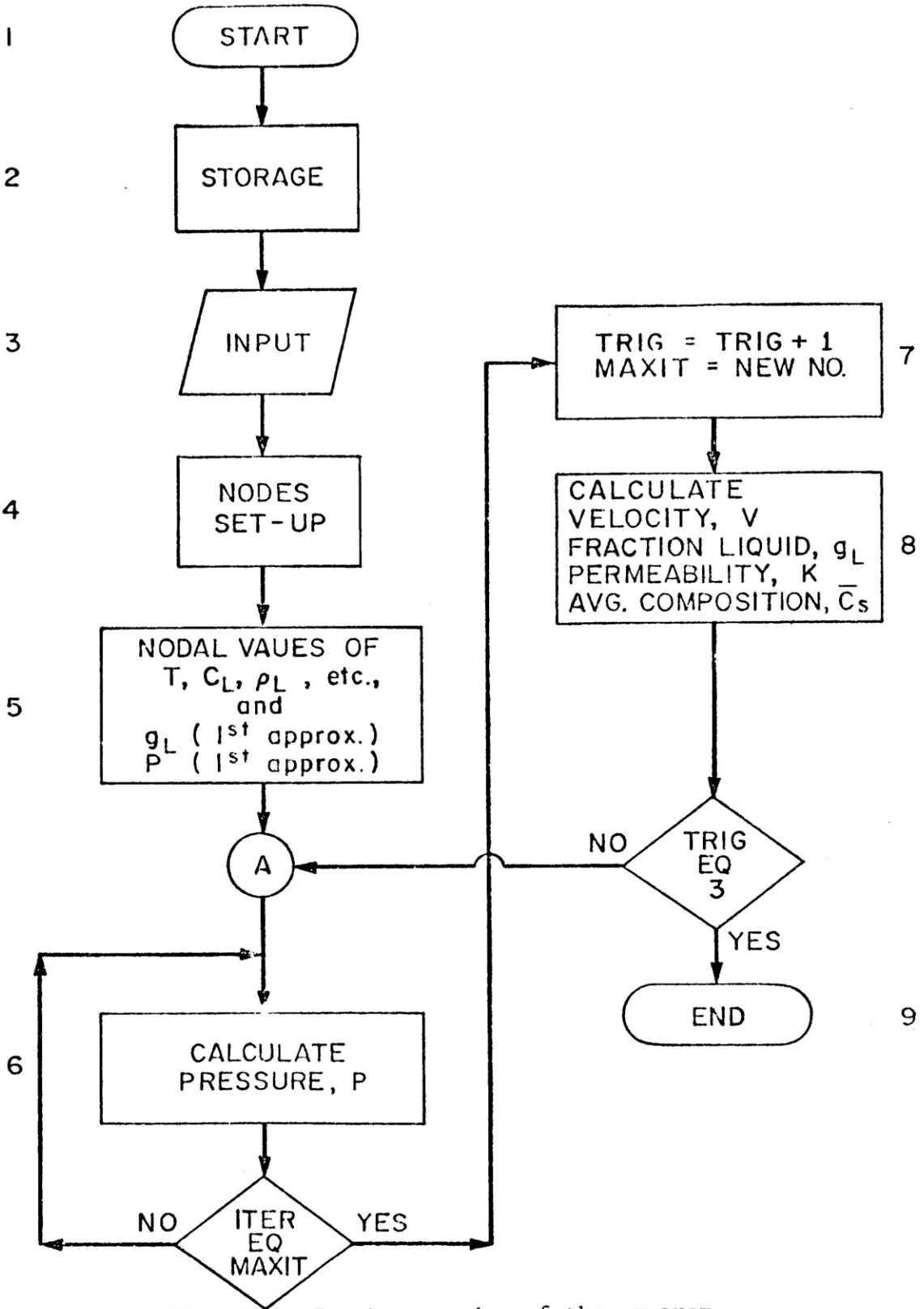

Fig. 7 - Flow Chart I. An overview of the program.

parenthesis. The number within parenthesis identifies the location of the process within Fig. (7). The loop specified is the actual placement within the program. Refer to Appendix E.

1. Storage (2, 3: Prior to Loop 10)

There are several items and properties which must be indexed and stored in memory. The mesh is composed of intersecting orthogonal lines. Each intersection is referred to as a node which is coded by two indices, I and J. For example if the operator wishes to invoke a certain fraction liquid he need only know its depth in the mushy zone and the corresponding radial position. Since I corresponds to radial position and J to vertical position, fraction liquid at a particular node is easily accessible to the operator by addressing its symbolic name GL(I,J).

2. Grid Formation (4: Loop 50)

Next encountered is the construction of the grid containing the two phase region. Once the liquidus and solidus contours and the vertical separation at the centerline, HTE, are specified, values of MT(I) and NT(I) are computed and stored by the computer. MT(I) is the J index for the lowest point for a given column with I corresponding to a given value of radius. NT(I) is the maximum point or liquidus point in the column. All intermediate points are located and specified for storage.

3. Temperature Field (5: Loop 70)

With the grid formed, the temperature, T(I,J) is determined at each nodal position within the grip. Values of T(I,J) are specified according

to experimental measurements of temperature.

Next identified are those physical properties which are temperature dependent such as density and liquid composition. These are filed individually within the appropriate memory arrays. The fraction liquid also is determined according to the Scheil equation as a first approximation. Section A of the flow chart of Fig. (7) has been reached.

4. Coefficient Determination (6: Loop 150)

At this stage the computer calculates the primary coefficients for the partial differential equation, Eq. (19). Once computed the primary coefficients A, B, and C are combined to form the "composite" coefficients a, b, c, d and e. The computer notation for these two sets of coefficients are:

A(I,J) = A

B(I,J) = B

C(I,J) = C

For the primary coefficients; and

ONE(I,J) = a

TWO(I,J) = b

TRE(I,J) = c

FOR(I,J) = d

KONST(I,J)= e

for the composite coefficients of the PDE, Eq. (20). Along with these values the cooling rate, ε, is designated EPPS(I,J), and the specific

permeability, K, is PERMI(I,J). These are used in calculations in later sections of the program.

5. Boundaries (6: Loops 200, 250, 300, 340)

There are four boundaries of the two phase zone. At each node along the boundaries, EPPS(I,J), PERMI(I,J) and other indexed properties are filed for later use in a manner similar to their counterparts within the interior sector.

6. Pressures at Boundary and Interior Nodes
(6: Loops 410, 430, 450, and 530)

Pressures are calculated by iterative calculations. The iteration sequence entails two processes:

1. the solving for new pressures at the boundaries; and
2. the solving for pressures at nodes within the grid interior .

Each node within the interior is surrounded by four adjacent nodes. Every node contains three primary coefficients and five composite coefficients. The inherent properties of the given binary investigated and the peculiar geometry of the mushy zone are contained within these few terms. Location 6 of Fig. (7) has been identified.

7. Interdendritic Velocities (8: Loop 790)

At the conclusion of the above loop (pressure iteration) the program determines the pressure gradients at all nodes in finite difference form. This accomplished, the algorithm based on D'Arcy's law is applied and

both components of the interdendritic velocity are calculated, numerically. Additionally, the dimensionless ratio, $\vec{v}\cdot\nabla T/\varepsilon$, called the "rate ratio" herein, is calculated for all nodes.

8. Local Solute Redistribution Equation (8: Loop 810)

The local solute redistribution equation (LSRE), Eq. (37), is integrated numerically along a given column using the components of velocity. This process yields updated values of fraction liquid, GL(I,J), at all nodes in the two phase zone except at the liquidus nodes where fraction liquid equals unity.

9. Radial Solute Composition Equation (8: Loop 850)

A simple series of equations follow the macrosegregation sequence. For each column, the computer determines the accumulation of solute through the radial solute composition equation (RSCE), Eq. (40). This value of radial composition coded as LOCCOM(I) in the program is found at each discrete radial column.

10. Average Ingot Composition (8: Loop 1020)

Another integration occurs after evaluation of the radial compositions. This is the determination of the overall average solute composition for the ingot. This is terms SUUM in the program. Values of SUUM should approach the nominal solute composition of the alloy as a limit.

11. Cycling the Program "UPDATE" (9: Loops 1030, 1040, 1050)

There is an outside loop which encompasses the entire program except the grid setup and introduction of memory arrays. A decision is made at the terminal of the program which returns the operation to point A of Fig. (7) immediately preceding the coefficient sector. Since the primary coefficients are functions of fraction liquid they too are updated. The iteration sequence to calculate pressures is again activated, Fig. (7). Thus, in a completed run several updates of the fraction liquid are made and the final evaluation of solute composition culminates in the prediction of yet another more recent set of fraction liquid values.

C. Investigation of Operations

1. Method of Inputing

An operator with little computer training will have no difficulty in "running" this computer program. This section deals with the general procedure a researcher undertakes in preparing the computer model to handle a given binary. More details related to this section are in Appendix C, Flow Chart II.

Input Data

There are four types of data to be inputed to the computer prior to loop 10. They are:

1. composition,
2. thermal,
3. physical, and

4. geometric data statements.

The composition parameters in wt % are:

liquid eutectic composition	CE	
solid eutectic composition, and	CSE	
alloy composition	CO	

The thermal parameters are:

melting temperature of pure solute (°C)	TM	and
eutectic temperature	TE	

Other related articles are:

liquids slope (phase diagram, °C/wt%)	EM	and
partition ratio	KAY	

Next, there are the physical properties related to temperature. They are:

density of solid (grams/cm^3)	RS	
density of solid eutectic	RSE	
density of liquid at TL	RO	and
density of liquid at TE	RLE	

Viscosity is not a function of temperature in the program. It is represented as MU and has the dimensions of poise. The density of the primary solid throughout the two phase zone is also assumed to be constant.

The geometric shape of the two phase zone along with related geometric functions are next represented as:

ingot radius (cm)	R	
radial spacing increment (cm)	HC	
depth of the mushy zone at the centerline (cm)	ZILIQ	and
isotherm velocity at the centerline (cm/sec)	UZCL	

To determine a value of NTOP which is the maximum number of nodes for a given column the operator must determine (external to the program) the difference of the highest z coordinate of the liquidus and the lowest value of the z coordinate of the solidus. The former is the value of z found at the junction of the liquidus and wall boundaries. The lowest point in the mushy zone is the centerline solidus. Then, the operator decides upon a reasonable value of vertical increment, KC, and divides it into this difference such that:

$$NTOP = \frac{ZL(IMAX) - ZS(1)}{KC} \qquad (54)$$

where:

NTOP = maximum number of rows, and

KC = the vertical increment spacing

In order to define the mushy zone the liquidus and solidus must be specified. On graph paper the operator traces the mushy zone as it is defined by experiment. The columns are superimposed on the trace. To determine the slopes of the liquidus and solidus isotherms at the intersections of the columns is the objective. In order to do this he merely divides HC, the incremental spacing, into the rise of adjacent intersections. This resultant slope is for the column to the left. In this single step operation the slopes of both the solidus and liquidus are determined. In computer notation slopes are defined as:

MLIQ = liquidus slope, and

MSOL = solidus slope

For the matrix containing the mushy zone which is NTOP*IMAX in size the operator needs to list IMAX slopes for the solidus and the same number for the liquidus where:

$$IMAX = RADIUS/HC + 1.00001$$

and RADIUS is the radius of the ingot. The number 0.00001 is added since the IBM 370 rounds numbers down. IMAX is an integer number representing the total number of columns from centerline to wall.

Cycling Inputs

A decision must be made as to the number of iterations made for calculating pressures in the relaxation process and the number of "updates" of fraction liquid. This is done by assigning values to the indices MAXIT1, MAXIT2, MAXIT3, etc. The indices TRIG1, TRIG2, TRIG3, etc. correspond to these values and are used for transferring the program into new "updates". For the nth update which is registered as TRIG(N), MAXIT(N) - MAXIT(N-1) iterations are performed (with a given distribution of volume fraction liquid) .N of course is some integer value. In this manner the pressures within the mushy zone are relaxed.

At present the program is set for a total of three updates. The first update always corresponds to pressure distributions related to Scheil values of fraction liquid. All updates thereafter correspond to fraction liquid values which are determined by the interaction of adjusted velocity distribution due to the local solute redistribution equation, Eq. (37). The number of cycles is arbitrary and must be amenable to the particular

alloy under study.

2. Temperature Fields

To determine temperature dependent parameters within the two phase zone it is essential that temperature be known. In this section the assumptions for temperature distributions and the mechanisms by which the computer executes this step are examined. This is Operation B, Loop 70 of Flow Chart II.

Vertical and Orthogonal Trajectories

Linear temperature distributions in the z direction have been detected during experimental runs. Therefore, the relationship:

$$\frac{T(r) - T_E}{T_L - T_E} = \frac{Z(r) - Z_E}{Z_L - Z_E} \tag{55}$$

is programmed where Z_E is the depth at the eutectic and Z_L is the liquidus endpoint for a given value of radius, r.

Also there is a section within the program in which orthogonal trajectories are evaluated. At present, however, this is by-passed but can be activated upon command. The formulation is:

$$\frac{T(r) - T_E}{T_L - T_E} = \frac{S_P}{S_T} \tag{56}$$

where S_P is the length of the arc extending from the solidus to the point of interest. This is a partial length. S_T is the total length of the arc having endpoints at both solidus and liquidus. The approximate method of determining values of S_P and S_T at a given node within the mushy zone is derived and illustrated in Appendix B, Der (5).

3. Coefficient Sequence and Pressure Determination

The pressure equation, Eq. (19), used at all interior nodes has the simple finite form:

$$\frac{\Delta(\frac{\Delta P}{\Delta z})}{\Delta z} + \frac{\Delta(\frac{\Delta P}{\Delta r})}{\Delta r} + A\frac{\Delta P}{\Delta r} + B\frac{\Delta P}{\Delta z} + C = 0 \qquad (57)$$

which approximates a second order partial differential equation of eliptic type. Individually, listed within Appendix B Der (2) are the primary coefficients in their finite difference form. Operation C of Flow Chart II, Appendix C shows their placement within the program.

The primary coefficients are composed of the finite difference forms of several gradients. These gradients are of properties such as the liquid density, RHO(I,J), the liquid composition, CL(I,J) and the fraction liquid, GL(I,J) to mention a few. These values are determined with Loop 70 of Operation B. Operation C contains the finite difference forms and the primary coefficients all of which are found in Loop 150.

As mentioned in Section B.1, Chapter III the composite coefficients a, b, c, d and e permit the unwieldy form of Eq. (19) to be simplified so that the independent variable, P(I,J), can be determined. The algebraic expression for this is Eq. (20). In computer notation it is written as:

```
P(I,J) = ONE(I,J) *P(I+1,J) + TWO(I,J) *P(I,J+1)
       + TRE(I,J) *P(I-1) + FOR(I,J) *P(I,J-1)
       + KONST(I,J)
```

These five composite coefficients are functions of:

1. the peculiar geometry of the grid; and
2. the primary coefficients already discussed.

All five values are calculated within Sequence (8) as the final part of Loop 150. A simple version of Appendix B Der (16) is:

```
ONE(I,J) = GEOM(HB) + GEOM(KA) *A(I,J)
TWO(I,J) = GEOM( ) + GEOM(HA) *B(I,J)
TRE(I,J) = GEOM(HA)-GEOM(KA) *A(I,J)
FOR(I,J) = GEOM( ) - GEOM(HM) *B(I,J)
KONST(I,J = GEOM *C(I,J)
```

Assumed is that the horizontal spacings are unequal. Each term is "weighted" linearly. If three colinear nodes have spacings HA and HB

```
          HB          HA
     X-----Y-------------------Z
```

property Y will require an HA/(HA+HB) contribution from property X and an HB/(HA+HB) contribution from property Z. The first term of coefficients TWO and FOR appear not to be so influenced but this is due to increment KA equaling KB. The sum of the above ratios is unity. Thus, each of the four surrounding nodes contain pressures which are weighted according to the composite coefficients. The following relationship must hold:

$$ONE + TWO + TRE + FOR = 1 \qquad (58)$$

To determine the appropriate pressure distribution for the two phase zone refer to Flow Chart II, Oper. D. Once the iteration portion is initiated an ordered sequence takes place. Firstly, the program addresses the separate discrete boundaries as follows:

1. solidus-interior boundary Loop 410
2. centerline boundary Loop 430
3. wall boundary Loop 450

For the same iteration a second sequence follows which is the determination of pressures at the interior nodes. A single pass is made for each column in a liquidus to solidus pattern, sweeping from the column adjacent to the centerline to that of the column next to the wall boundary. This two step procedure continues until the "stepping" mechanism addresses the appropriate value of MAXIT for the given cycle. That is ITER = MAXIT. At the conclusion of this iteration the loop is dormant until the command is given later in the program to reactivate this operation. Statement number 530 has been reached on Flow Chart II.

4. Boundary Conditions (Solidus-Interior)

Although Sections B.2, 3, and 4 of Chapter III dealt specifically with the boundary equations, further discussion is resumed in this section for the solidus-interior boundary. The slope of the solidus affects the final form of the finite difference equation at this boundary.

Examine the density versus liquid composition charts for both the aluminum-copper and tin-lead binaries of Fig. (8) and Fig. (9), respectively. Sharp jumps in solid density occur at the eutectic and the shrinkage,

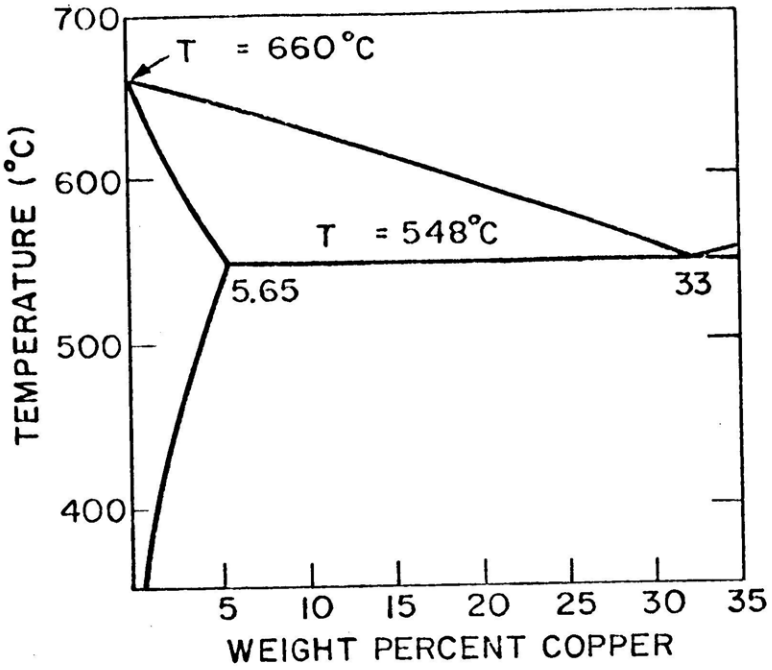

(a)

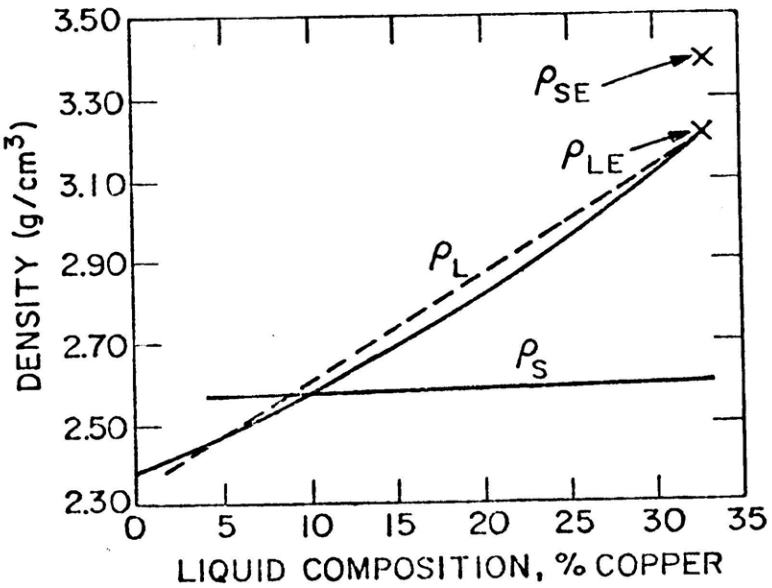

(b)

Fig. 8 - Phase diagram and density used for calculation of macrosegregation in Al-4% Cu ESR ingots.
(a) Phase diagram, Ref. 50; (b) density of solid and liquid during solidification, Ref. 3.

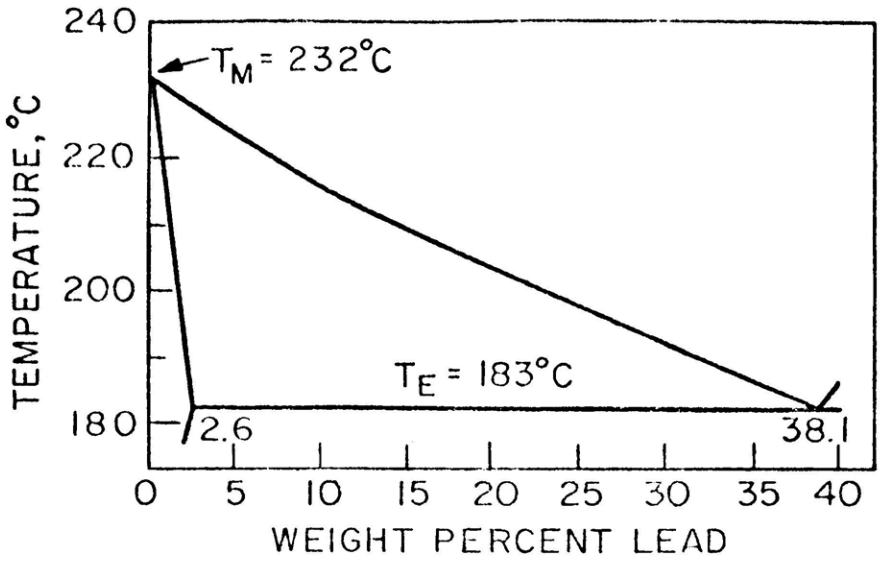

(a)

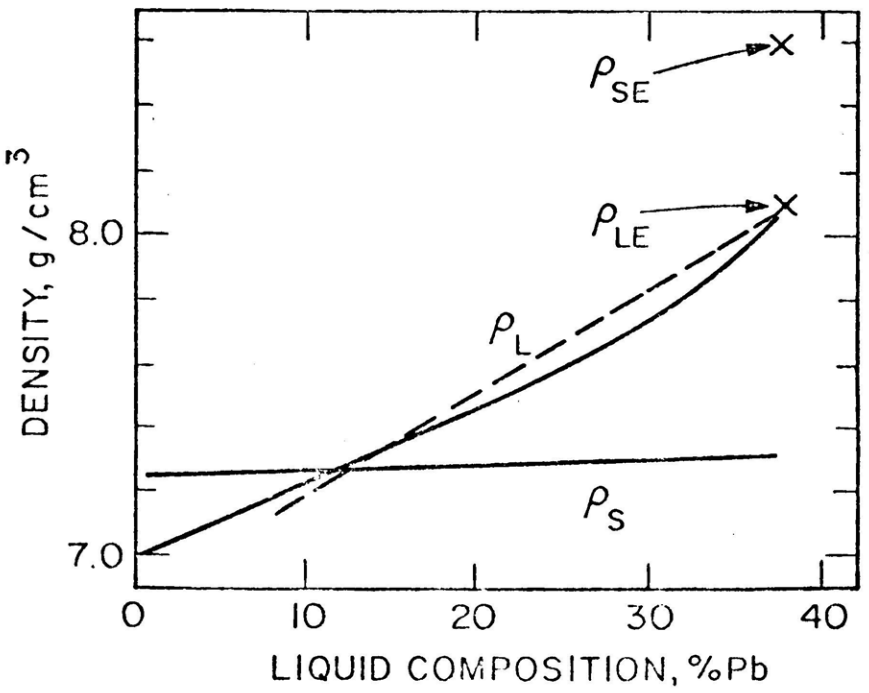

(b)

Fig. 9 - Phase diagram and density used for calculations of macrosegregation in Sn-20% Pb ESR ingots.
(a) Phase diagram, Ref. 51; (b) density of solid and liquid during solidification, Ref. 46-49.

$(\rho_s/\rho_L - 1)$, is strikingly affected. A change in sign as well as magnitude occurs.

The most tenable situation is not to solve for pressure along the solidus boundary but to solve for those pressures directly above them. This is the subtle change of tactics decided upon for assaulting this boundary dilemma. Direct reconciliation of the two differing gradients occurs only when both are assigned weights for a given nodal position. Discontinuity is thereby avoided.

The form which evolved is composed of both the vertical and radial pressure gradients along the solidus boundary. Refer to Appendix E. The radial component is represented as:

$$\left.\frac{\Delta P}{\Delta r}\right|_{S-I} = \frac{HB}{HA+HB}\left[\frac{P(I+1,J) - P(I,J)}{HA}\right] + \frac{HA}{HA+HB}\left[\frac{P(I,J) - P(I-1,J)}{HB}\right] \quad (59)$$

The abbreviation S-I is notation for solidus-interior. The interior nodes will always have pressures assigned to them. The solidus is made-up of pressure gradients and pressures need not be assigned. For the radial component Eq. (27) describes the gradient. If the solidus has a slope greater than zero it will have a radial pressure gradient described by Eq. (28) and this term is therefore substituted for the radial gradient of Eq. (59) such that

$$\left.\frac{\Delta P}{\Delta r}\right|_{S-I} = \frac{HB}{HA+HB}\left(\frac{RSE}{RLE} - 1\right)\frac{UR*MU*GLE}{PERMI(I,J)} + \frac{HA}{HA+HB}\left[\frac{P(I,J) \quad P(I-1,H)}{HB}\right] \quad (60)$$

This has already been defined by Eq. (33); however, Eq. (60) above allows

for unequal radial spacings. This is generally the case at the solidus boundary. The computer notation for the radial and vertical gradient substitutions, Eqs. (27) and (28) are SOLHZ and SOLVE, respectively. Equation (60) is in computer notation.

It is possible to solve for a single algebraic expression used for finding the pressures along the solidus-interior boundary. When completed, the final form is similar in type to that of the standard differential equation, Eq. (20) of the interior. The final form is:

$$\begin{aligned} P(I,J) = {} & TART(I,J)*P(I+1,J) + TATOP(I,J)*P(I,J+1) \\ & + TALEFT(I,J)*P(I-1) + TABOT(I,J)*P(I,J-1) \\ & + TAKONS(I,J) \end{aligned} \tag{61}$$

Coefficients TATOP and TALEFT will on all occasions be identified as the values associated with the interior whereas TABOT and TART can be associated with the solidus. That is, the value of SOLHZ or SOLVE can be substituted for the pressure gradients in these coefficients. Within derivation (7) are the three possible cases commonly occurring in ingot solidification. Equation (61) is altered for the three following cases of Sequence (7) of Flow Chart II:

1. flat and nearly flat isotherms (Loop 121);
2. steep isotherms, (Loop 123); and
3. moderate isotherms (Loop 125).

Flat and Nearly Flat Isotherms (Loop 121)

There are cases where the isotherms are flat as in the case of unidirectionally grown ingots. Notice the position of the solidus interior

nodes (S-I) to that of the solidus boundary nodes (S) in Fig. B.7(a). For this case the parameter SOLHZ does not appear within the final pressure expression. That is: TART(I,J)=0.

Steep Isotherms (Loop 123)

If much heat is extracted from the sides, the solidus will have a steep slant. In Fig. B.7(b) notice the extra positions along the solidus. These are "pseudo-nodes" (PS), extra nodes along the solidus boundary, present to accommodate adjacent interior nodes. This situation evolves when KC is less than HA and the solidus slope is significant. The SOLHZ term dominates in this situation making the term, TART(I,J) influential. Notice that SOLVE is not to be found in this situation. This is because the node under consideration is not immediately above a boundary node.

Moderate Isotherms (Loop 125)

Moderately sloped isotherms result if the heat extracted from the ingot is not biased to either the sides or the bottom to the extent of the two preceding cases. Both SOLVE and SOLHZ are displayed in this situation. This implies that coefficients TART(I,J) and TABOT(I,J) are of equal significant. Refer to Fig. B.7(c) for illustration.

5. Computer Simulation of Macrosegregation

This section is concerned with those sequences and operations which culminate in the determination of the radial composition profile of solute wihin the ingot.

Interdendritic Velocity Determination

The two phase region is a packed bed where the packing is dendrites. Equation (13) is D'Arcy's law which related the interstitial velocity, $\vec{v}$, to the linear pressure gradient, $\Delta P/L$. In computer notation the equations for fluid flow within the interior of the muzhy zone are written as:

$$VZ(I,J) = - \frac{PERMI(I,J)*}{MU*GL(I,J)} [PDZ+GRAV*RHO(I,J)] \tag{62}$$

for the vertical component, and as

$$VR(I,J) = - \frac{PERMI(I,J)}{MU*GL(I,J)} *PDR \tag{63}$$

for the radial component. PERMIT(I,J) is the value of specific permeability; MU is the viscosity; and GRAV represents the gravity force term. From these two components of velocity the quantity:

$$ANG = VZ(I,J)/VR(I,J) \tag{64}$$

is computed. The angle, TTHETA, in degrees is then calculated:

$$TTHETA = (180/PI) * DATAN(ANG) \tag{65}$$

where PI equals π and DATAN is the arc tangent in double precision. The rate ratio, $\vec{v}\cdot\nabla T/\varepsilon$ is:

$$RARA = \frac{VR(I,J)*GR(I,J) + VZ(I,J)*GZ(I,J)}{EPPS(I,J)} \tag{66}$$

where

GR(I,J) = the radial temperature gradient;

GZ(I,J) = the vertical temperature gradient; and

EPPS(I,J) = the cooling rate.

This completes the determination of the interdendritic velocities. On Flow Chart II this is represented as Operation E of major loop 790. Within it the radial and vertical pressure gradients (PDR and PDZ respectively) are computed prior to solving Eqs. (62) and (63). This is a single pass operation in which all interior nodes are assigned velocities.

Local Solute Redistribution Equation

Operation F within Loop 810 is the column by column solving for new values of fraction liquid. This is the local solute redistribution equation. Previously expanded in algebraic form in Chapter III, Section C it is shown here in computer notation:

$$GL(I,J) = \{\frac{CL(I,J) - CL(I,J+1)}{2.} * \frac{1}{KAY-1.} * \frac{1}{RS} * [\ ]\} \qquad (37)$$

where

$$[\ ] = 1 + \frac{VR(I,J)*GR(I,J) + VZ(I,J) * GZ(I,J)}{\varepsilon PPS(I,J)}$$

$$1 + \frac{VR(I,J+1)*GR(I,J+1)+VZ(I,J+1)*GZ(I,J+1)}{\varepsilon PPS(I,J)}$$

Integration is carried out from the liquidus, J=NT(I), to the solidus, J=MT(I), in a single sweep along a given column, I. In a more manageable compact form:

$$COEFT1 = - KON4 * RHO(I,J)/(CL(I,J)*RS) \qquad (67)$$

$$RATER1 = VR(I,J)*GR(I,J) + VZ(I,J)*(GZ(I,J) \quad (68)$$

and $$FN(J) = COEFT1*[1 + \frac{RATER1}{\varepsilon PPS(I,J)}] \quad (69)$$

where $KON4 = 1/1-K_p$

Similar terms: COEFT2, RATER2 and FN(J+1) require J+1 instead of J. The natural log of the fraction liquid is written:

$$NLGL(J) = 0.5*(CL(I,J)-CL(I,J+1))*(FN(J)+FN(J+1)) + SUM \quad (70)$$

where SUM is the total value of the integral from NT(I) to J. The fraction liquid is found upon taking the exponential form of this such that:

$$GL(I,J) = EXP(NLGL(J)) \quad (71)$$

Radial Average Solute Composition

Firstly, the integration term of Eq. (38) is computed. In computer notation this is:

$$SUMMS = 0.5*(CS(J) + CS(J-1))*(GS(J-1)-GS(J)) + SUMMS \quad (72)$$

This is Sequence (10), Loop 850 of Flow Chart II. Next, the new values of eutectic fraction liquid are taken care of:

$$GEE = 1.-GS(J) \quad (73)$$

The numerator of Eq. (38) is therefore equal to

$$TNT = RS*SUMMS + RSE*CE*GEE \quad (74)$$

and the denominator is

$$DDD = RS*(1.-GEE) + RSE*GEE \quad (75)$$

The radial composition for column I is symbolically termed LOCCOM(I), instead of $C_s(r)$. It is:

$$\text{LOCCOM(I)} = \frac{\text{TNT}}{\text{DDD}} \tag{76}$$

This terminates Operation G. The profile of the radial compositions versus radius for the ingot is available once the column at the wall, IMAX, has been solved.

Average Solute Content of the Ingot

Sequence (11) is now arrived at. This sequence carries out an approximation of the ingot composition as the values of LOCCOM(I) are registered column by column. From Eq. (41) the exact method was shown. In the computer, DELRAD is the average of radial spacings separating the columns for which values of LOCCOM(I) are known. It is computed. The value of radius is written as ROR(I) for the given column I. SUUM is the computer symbol equaling C_s(INGOT) of Eq. (41). This is the running tally of average ingot composition as the integration proceeds from the ingot centerline, I = 1 to the wall of the mold, I = IMAX. In computer notation:

$$\text{SUUM} = \frac{2.0*\text{ROR(I)}*\text{DELRAD}*\text{LOCCOM(I)}}{(\text{RADIUS}**2)} + \text{SUUM} \tag{77}$$

From this value of SUUM, values of SUUM from previous cycles, and a knowledge of nominal composition, CO, the operator is able to tell upon comparison whether the ingot composition is satisfactory. If the relative error (CO-SUUM)/CO is too large it may mean that:

1. not enough cycles were used (relaxation has not occurred); or
2. the phenomenon known as freckling is occurring to a major degree such that solute rich fluid is being rejected into the bulk liquid in large amounts

For case 2 the liquid pool continuously becomes enriched in solute throughout solidification. Axially, the ingot becomes solute rich at the top most section subject to transient solidification. This is not dealt with in this steady state model.

V. COMPUTER INTERACTION WITH EXPERIMENTS

Small ESR laboratory ingots of 6.8 centimeters diameter were cast within water chilled molds. Thermocouples inserted within the mold recorded the isotherm behavior as the ingot solidified. Figure 10 (a) is the mushy zone profile of Ingot 1 if a longitudinal section is taken. The uppermost curve is the liquidus while the lower curve is the solidus. Figures 10 (b) through (f) are similar profiles. The temperature distributions of Ingots 1, 2 and A are known to be linear within the mushy zone during steady state conditions.

Ingots 1 through 5 (Fig. 10 (a) through (e)) are of Al-4.4% Cu composition with the exception of Ingot 3 which is of 4.18% Cu composition. Ingot A is a Sn-15% Pb binary. Experimental details are given in Ref. D. R. Poirier, S. Kou, R. Furlong, and M.C. Flemings,"Electroslag Remelting," Interim Technical Report, Contract No. DAAG46-74-C-120, AMMRC, December 1976.

A. Analysis of Al-4% Cu Ingots

1. Determining γ

The first step is to vary γ over a broad range of values with the purpose of determining the value satisfying the experimental results. The term γ from Eq. (4) is a proportionality constant referred to here as flow factor. Upon analyzing Fig. (11) it is seen that in varying γ over two orders of magnitude from 10^{-6} to 10^{-8} cm^2 that a transformation occurs. The segregation of solute at the ingot center transforms from

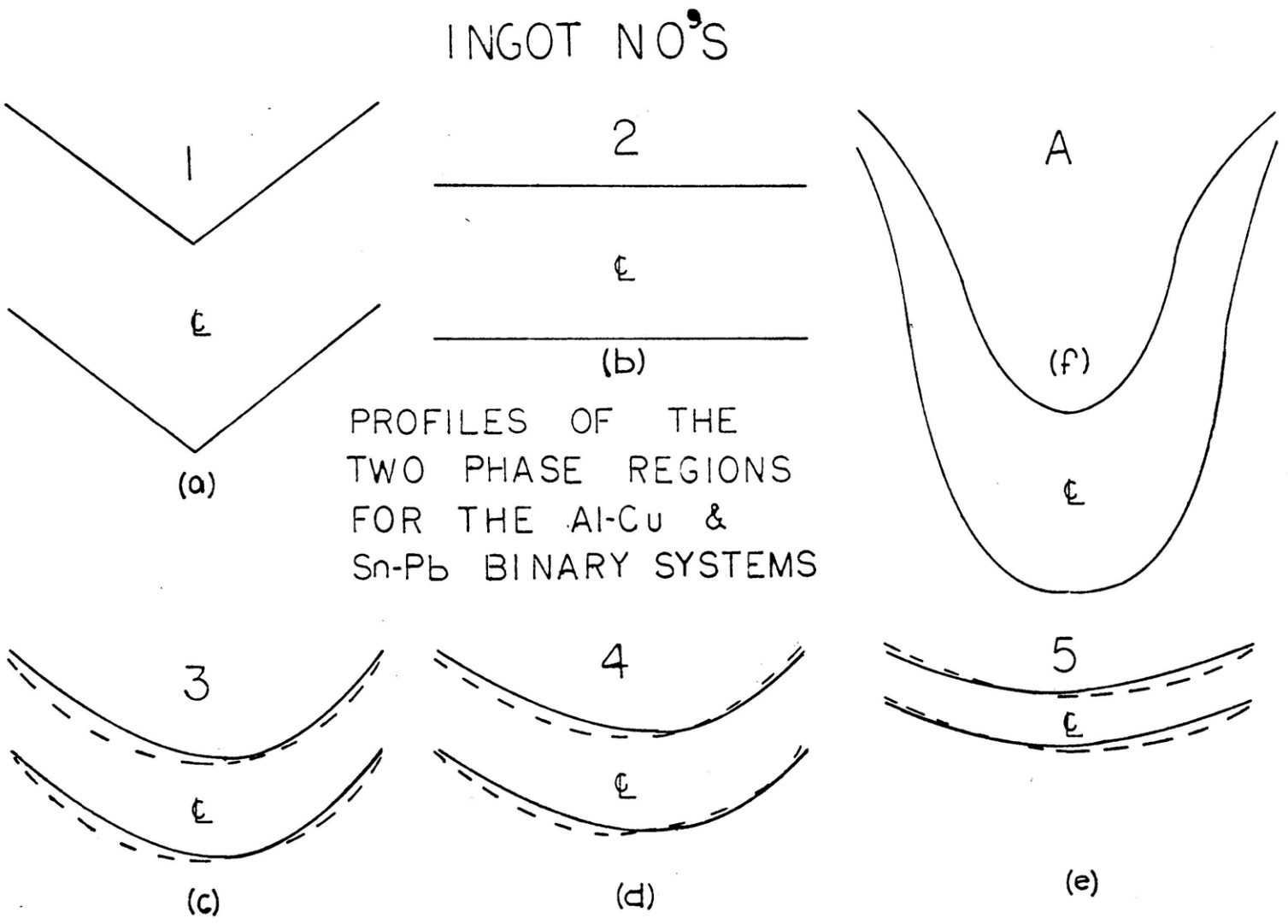

Fig. 10 - Five shapes of the two-phase region for the Al-Cu binary are listed from a to e. These correspond to Ingots 1 through 5, respectively. (f) Ingot A of the Sn-Pb system.

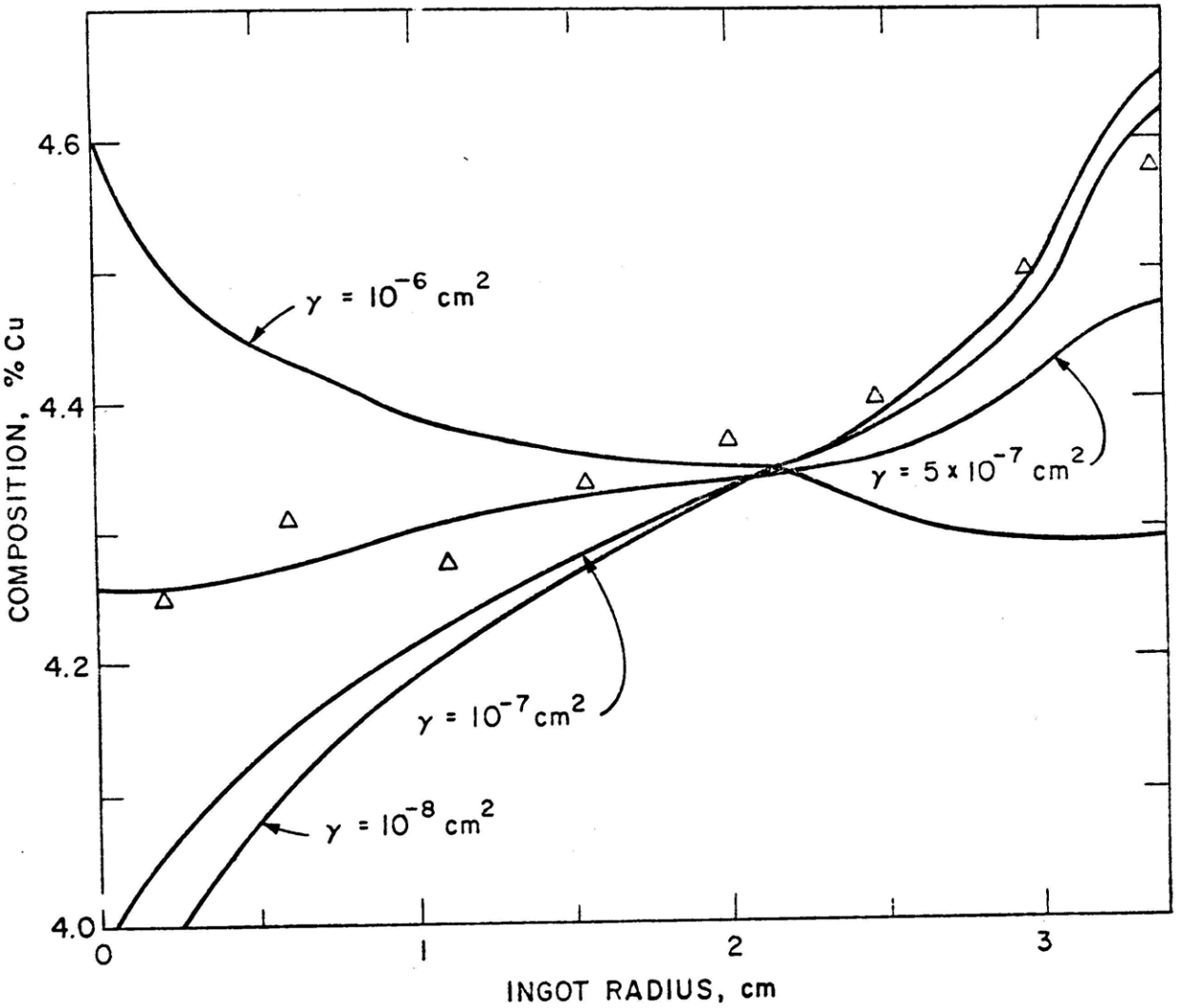

Fig. 11 - Composition profiles for Ingot 1 for various values of γ. Large values of γ, 10^{-6} cm^2, yield positive centerline segregation whereas small values, 10^{-8} cm^2, yield negative. Model 2.

the positive to negative type. Figure (11) results from using values of HC=0.2 and KC=0.1 cm in Model 2.

The experimental results (obtained through X-ray fluorescence) are also shown in Fig. (11). Negative segregation occurs at the centerline. A flow factor of appropriate magnitude lies between 10^{-7} cm^2 and 5.10^{-7} cm^2. Therefore, the proper range of flow factor allowing the simulation results conform to experimental measurements is identified. Figure (12), a plot of C_s versus radius, shows a small displacement of the composition profile if γ is varied by two orders of magnitude from 10^{-8} cm^2 to 10^{-10} cm^2. Figure (12) is the product of Model 1 if HC=0.2 and KC=0.1 cm.

2. Optimizing the Number of Iterations

Values of the average solute compositions corresponding to specific radii for given updates are compared with each other till the operator is satisfied that the solute composition distributions have relaxed. In the case of Ingot 1, for a constant value of γ equal to 6×10^{-8} cm^2 Fig. (13) shows the effect of this relaxation process. Again HC=0.2 and KC=0.1 cm for Model 1. The compositions tend to be high for the first 25 iterations. For the next few hundred iterations they drop as exemplified by the curve representing 400 iterations. From 400 to 700 iterations the compositions are climbing but at a diminishing rate.

The difference of values between 500 to 700 iterations is considerably less than between 400 to 500 iterations. Due to this behavior it was decided that the ceiling on iterations ought to be approximately 600 for the Al-4.4% Cu binary in the case of Ingot 1.

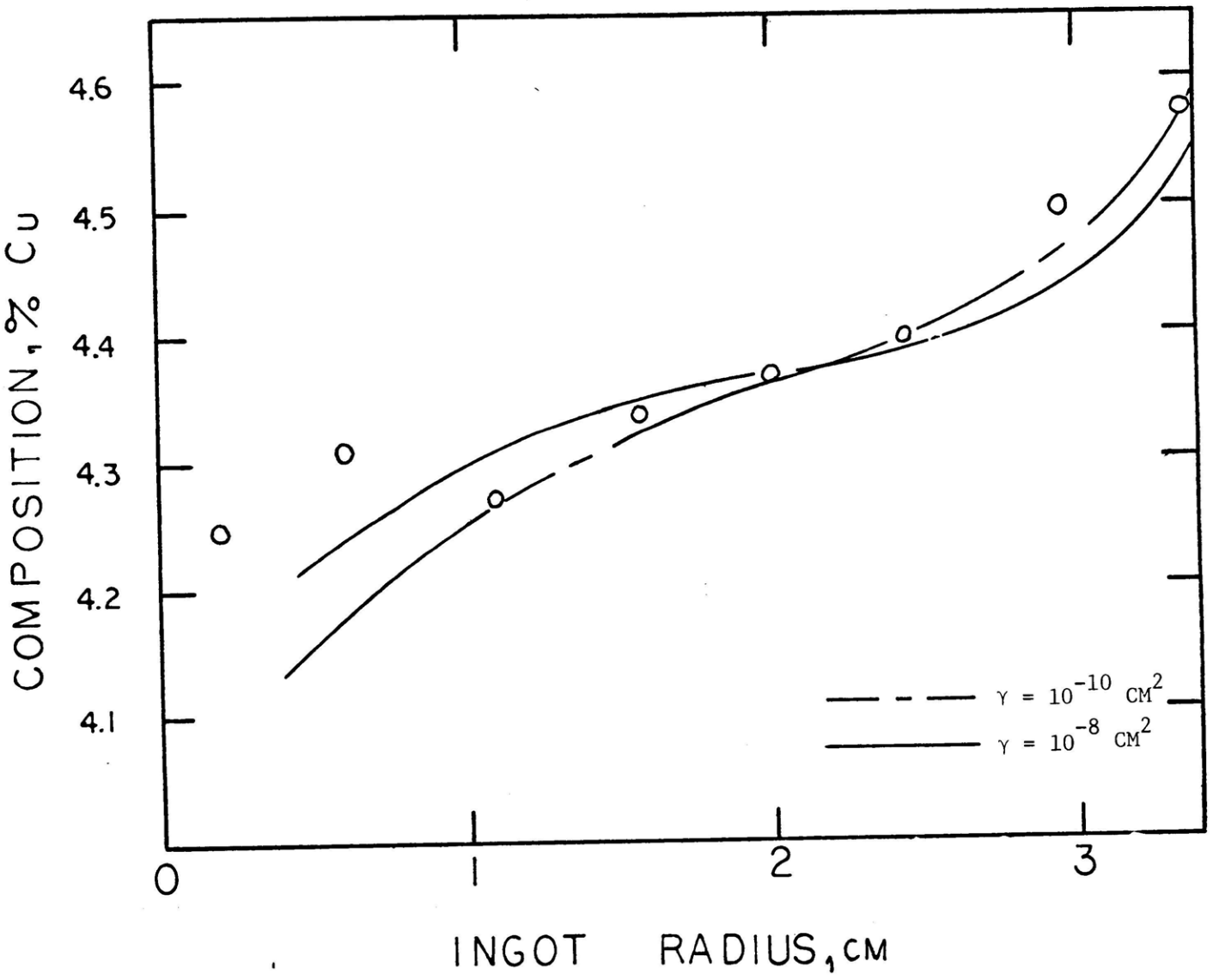

Fig. 12 - Radial solute profiles for Model 1. Values of γ are 10^{-8} cm^2 and 10^{-10} cm^2.

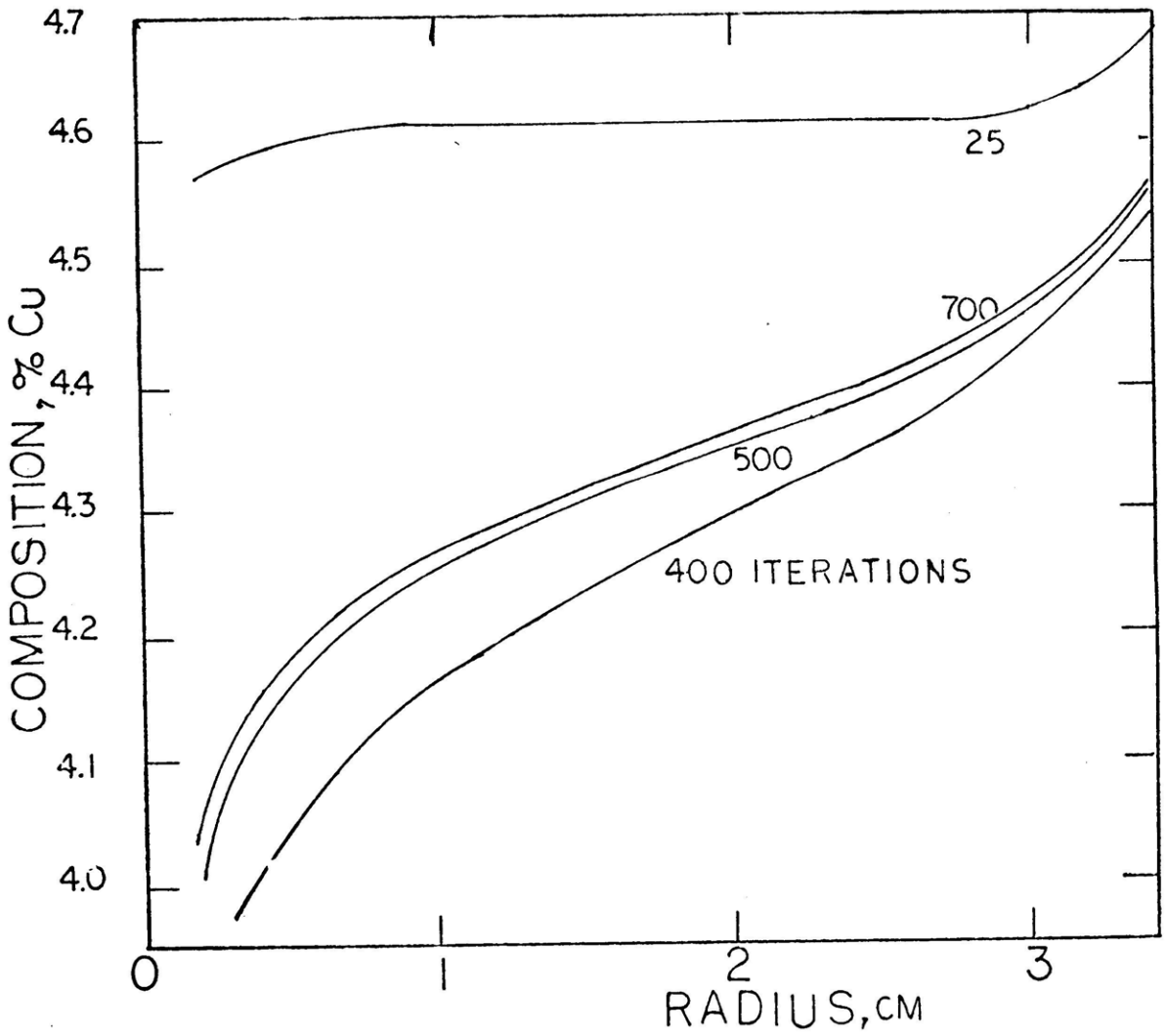

Fig. 13 - Radial solute profiles arranged according to total iterations completed. Little change between iterations 500 to 700. This is an illustration of the relaxation process. Model 1.

In this example updates are made at iterations 25,400, 500 and 700. It is evident that updating the values of fraction liquid throughout the mushy zone is required. At least 2 updates are necessary for relaxing the pressure field so that the fraction liquid distributions are approximated. Martin Keane in his Ph.D. thesis at MIT asserts that deviations between fraction liquid determined by the Scheil Equation and those approximated by the relaxation process are insignificant. Therefore, he proposed that for the Al-4.5% Cu alloy the Scheil Equation determined the proper fraction liquid distribution within the mushy zone. This conclusion is countered by the results of Figure (13) of this thesis.

3. Pressure Distributions within the Dendritic Region

Of basic importance is the distribution of pressures within the two phase zone. Refer to Fig. (14) Model 1 corresponding to a value of $\gamma = 2 \times 10^{-7}$ cm^2. Negative pressure gradients are associated with non-frictional regions. These are the regions of high fraction liquid. The free flow gradient is a characteristic of the given liquid alloy at temperatures equal to the liquidus temperature. It is the common Bernoulli relationship:

$$\frac{dP}{dZ} = -\rho_L(C_o)\cdot g \qquad (78)$$

Upon examining Fig. (14) it is not surprising to see pressure distributions of entirely negative slope for so high a flow factor, 2×10^{-7} cm^2. Frictional effects are minimal. The gradient at the liquidus and throughout most of the mushy zone is:

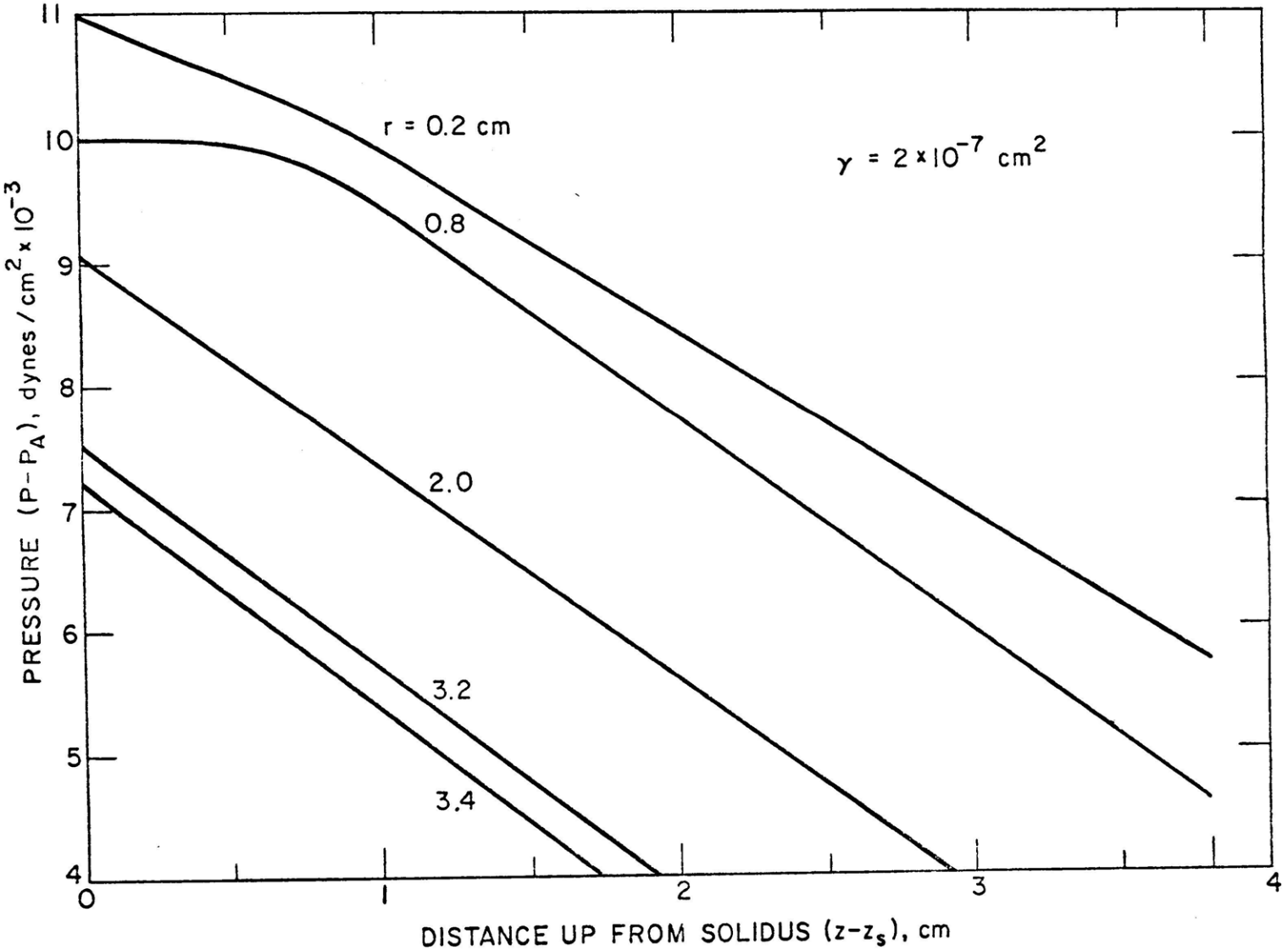

Fig. 14 - Pressure distribution from solidus to liquidus for Ingot 1. Gradient dP/dz is negative for $\gamma = 2 \times 10^{-7}$ cm^2. Model 1.

$$\frac{dP}{dZ} = - 1920 \frac{\text{dynes}}{\text{cm}^2}$$

For the liquid pool it is

$$\frac{dP}{dZ} = - 2401 \frac{\text{dynes}}{\text{cm}^2}$$

assuming the pool to be calm.

Figure (14) Model 1 corresponds to a value of γ equal to 6×10^{-8} cm^2. Notice that the pressure bars for specified radii have maxima. At the solidus region the gradient is positive but gradually becomes negative upon traversing the dendritic zone towards the liquidus. The dendritic array becomes more open as the liquidus is approached.

Comparing Figures (14) and (15) it is evident that a transformation of gradients from negative to positive values results as γ is diminished from 2×10^{-7} to 6×10^{-8} cm^2. This trend is indicative of the friction effect. The dominance of the friction effect (directly related to positive gradients) is increasing.

In Fig. (14) notice the orderly arrangement of the pressure bars according to radii. This indicates that the metallostatic head of the metal pool above the two phase zone influences the pressure distribution of the muzhy zone. The head above the mushy zone decreases linearly for Ingot 1 upon moving radially to the wall from the center for the free flow situation only. A better test for cases of parallel isotherms and large γ values would be to adjust the metal pool surface so that it lies parallel with the mushy zone isotherms. In this situation the

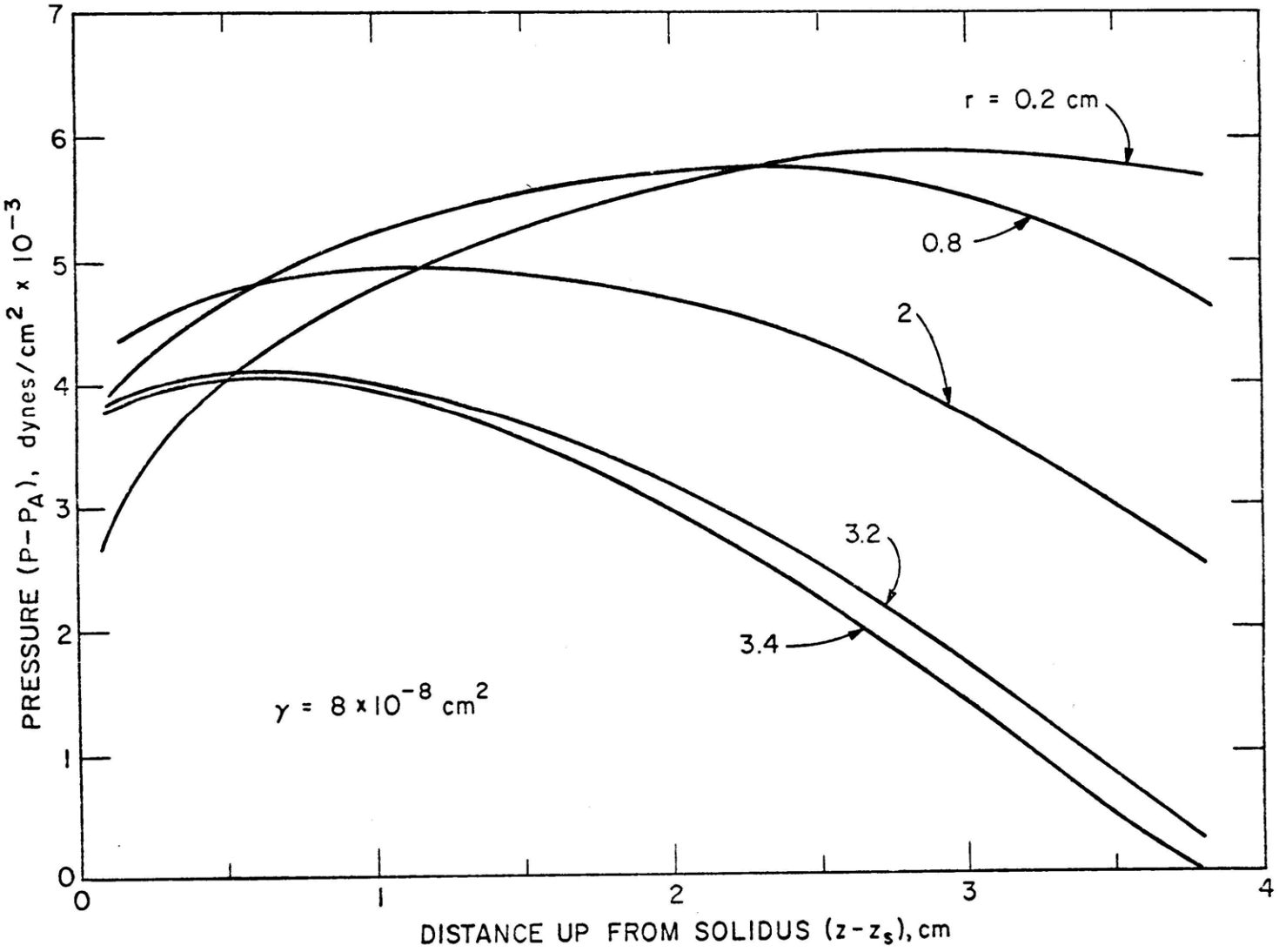

Fig. 15 - Pressure distribution of Ingot 1 for $\gamma = 8 \times 10^{-8}$ cm^2. dP/dz changes from negative to positive upon traversing the mushy zone from liquidus to solidus.

pressure bars for all radii would be equal. This is a good asymptotic solution check on the validity of the program.

4. Deflection of Streamlines

Observe Fig. (16). This is a plot of the steamlines for interdendritic fluid flow for Ingot 1 with $\gamma = 8 \times 10^{-8}$ cm^2 using Model 1. In this case flow throughout the mushy zone is downward and towards the eutectic isotherm. The shrinkage pressure is substantial. Proximity of streamlines indicates velocity along them. Those which are close together are traveling the fastest. The scale coefficient, $\hat{k}$ is 0.005 cm^2/sec for the equality:

$$v = \frac{\hat{k}}{s} \tag{79}$$

where s is the spacing between flow lines and v equals interdentritic velocity.

There is a very slight deflection of incoming streamlines towards the centerline. This is due to the attenuation of shrinkage forces almost immediately upon penetrating 15% of the depth of the mushy zone (approx. 0.57 cm). Half of the Al-4.4% Cu alloy solidifies within the first 15°C decrease below T_L. At the eutectic another deflection is observed due to the eutectic liquid (approximately 8-10%) solidifying with 5.625% shrinkage. The amount of eutectic solidifying is not necessarily the Scheil value. It can be considerably more or less. This would give even greater deflections at the solidus. One important realization is apparent from Fig. (16). Wherever substantial amounts of volume shrinkage occur the flowlines intersect the isotherms perpendicularly.

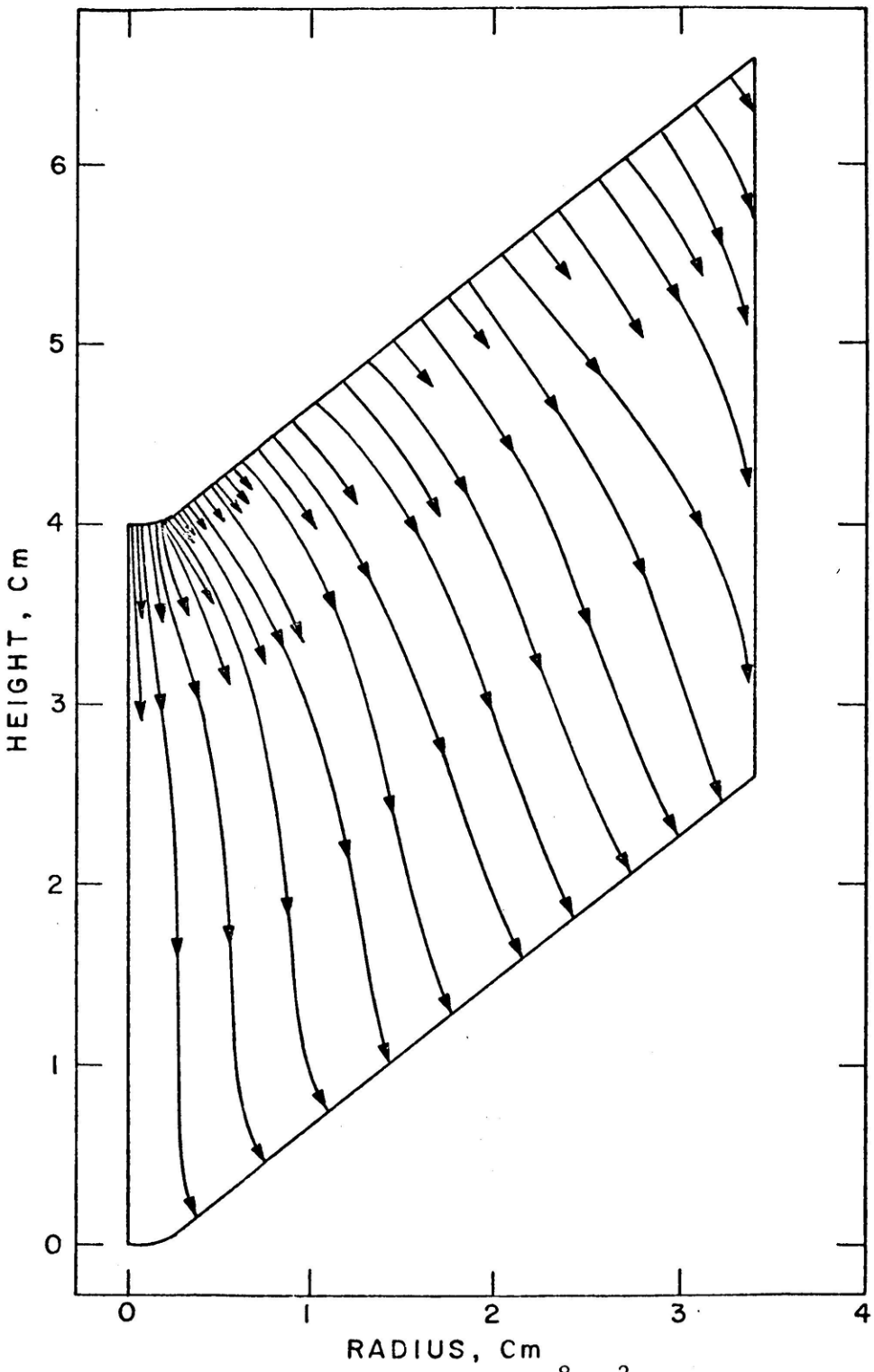

Fig. 16 - Streamlines of Ingot 1 for $\gamma = 8 \times 10^{-8}$ cm^2 show the deflection pattern. Streamlines give direction. Proximity is approximately proportional to the inverse of velocity. The scale coefficient, $\hat{K}$, is 0.005 cm/sec.

A graphical interpretation of the flow is next investigated. Figure (17) has both velocity components v_r and v_z plotted versus the depth within the mushy zone at a radius of 0.8 centimeters from the centerline. Calculations were done using Model 2. Since the shrinkage term outweighs the metallostatic effect in the radial direction for 10^{-8} cm^2 through 10^{-7} cm^2, v_r is positive. Notice that in all cases $\partial V_r/\partial Z$ is steepest at the liquidus and solidus regions and v_r is always greatest at the liquidus. The central zone from $Z-Z_s$ = 1 through 3.3 cm is concave upwards. The values of v_r diminish between $\gamma = 10^{-8}$ cm^2 to 10^{-7} cm^2 with a substantial drop between $\gamma = 10^{-7}$ cm^2 and 5×10^{-7} cm^2. An order of magnitude drop from 3.0×10^{-4} cm/sec to 2.1×10^{-5} cm/sec occurs at mid depth. The dashed line indicates negative radial velocities. For $\gamma = 10^{-6}$ cm^2 a reversal occurs and flow is towards the centerline. This indicates that free flow conditions are prevalent since friction is greatly reduced. The expansion forces exist in the central region of the mushy zone. There is no pull towards the wall. Note that shrinkage forces dominate at the eutectic and liquidus.

5. The Rate Ratio

The rate ratio, $\vec{v}\cdot\nabla T/\varepsilon$, with respect to depth within the mushy zone of Ingot 1 is now examined. Figure 18 (a), (b) and (c) consists of plots of this ratio as a function of the depth in the mushy zone for three different radii of Ingot 1 in which $\gamma = 10^{-8}$ and 10^{-6} cm^2. Referring to Figs. 11 and 18, simultaneously, a trend is noted. Going from Fig. 18 (a) to (c) the curves "flip-flop". At approximately the first moment radius (2.26 cm) both curves overlap each other as illustrated in

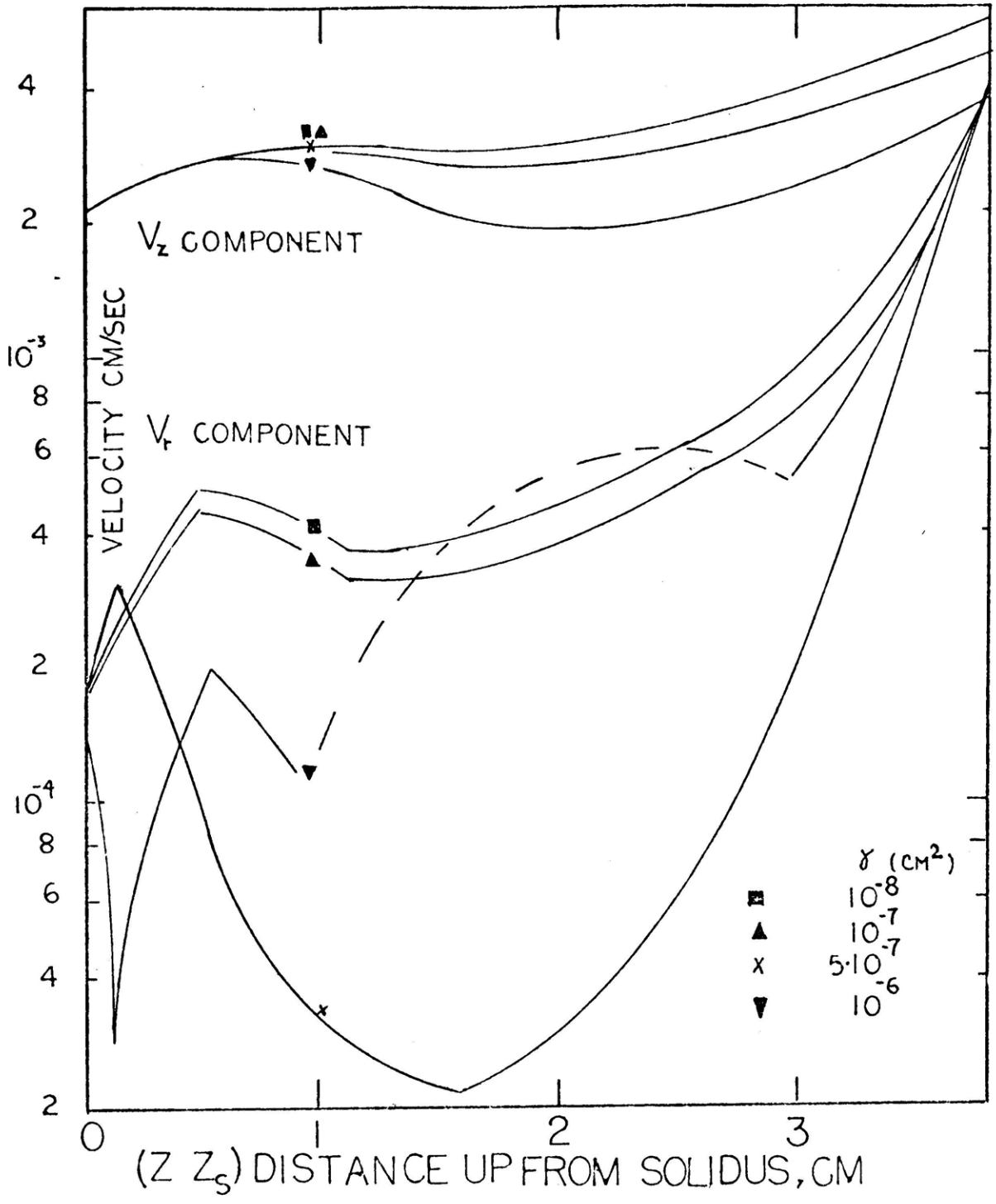

Fig. 17 - Velocity distributions for Ingot 1 at a radius of 0.8 cm. from the centerline. The value γ varies. Dashed curves for the V_r component represent flow towards the center.

Fig. 18 (b) at a radius of 2 cm. Upon looking at Fig. (11) it is noticed that all four curves converge at about this same location of 2.2 cm.

A simple relationship is derived in Appendix B. Der. (8) from the local solute redistribution equation (LSRE). It is found that any solute composition is inversely proportional to the rate ratio plus unity. Thus, in Fig. 18 (a) the lower value of γ yields a higher <u>average</u> value of rate ratio at one centimeter radius than the high flow factor. Using the simple form of the LSRE:

$$\bar{C}_s \propto \frac{1}{1 + (\frac{\overline{\vec{v}\cdot\nabla T}}{\varepsilon})} \tag{80}$$

it is realized that low values of γ yield low composition at one centimeter radius. The reverse is true for the high value of γ. Large γ produce positive segregation in the central region due to the corresponding low <u>average</u> values of $\vec{v}\cdot\nabla T/\varepsilon$. This behavior is graphically depicted in Fig. (11).

In Fig. 18 (b), both rate ratio curves corresponding to high and low flow factor have approximately the same value and therefore yield near equal solute compositions at this first moment radius, Fig. (11). With this method of analysis Fig. 18 (c), predicts positive segregation for γ of 10^{-8} cm^2 and negative segregation for the flow factor of 10^{-6} cm^2. This is in agreement with the two curves of Fig. (11).

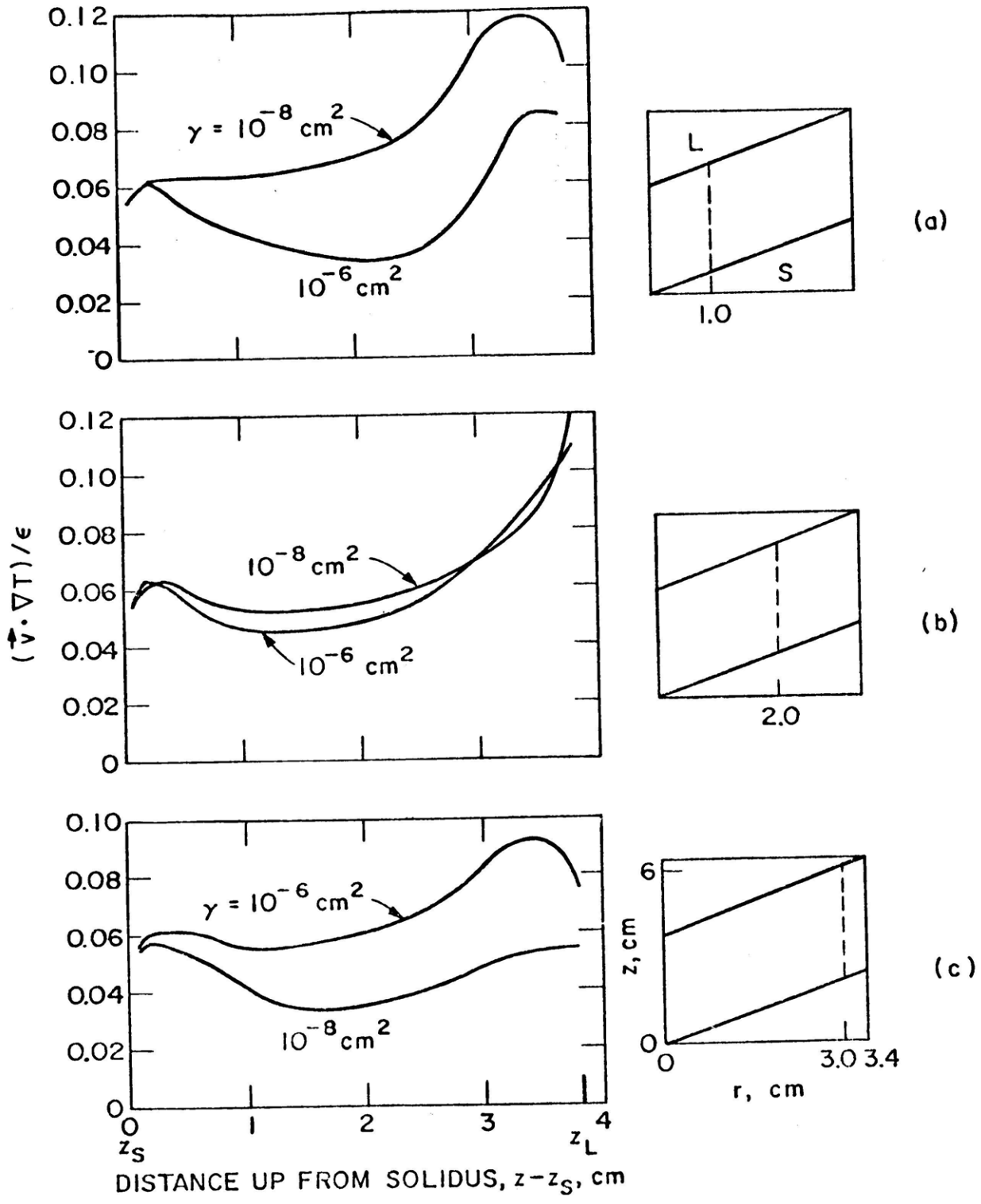

Fig. 18 - Calculated values of the rate ratio $\vec{v} \cdot \nabla T/\varepsilon$ in Ingot 1. (a) r = 1 cm; (b) r = 2 cm; (c) r = 3 cm.

6. Velocity Distributions

Figure (19) relates the interdendritic velocity to $Z-Z_s$ for radii equal to 0, 0.4, 1, 2, 3 and 3.4 centimeters for Ingot 1. Figure 19 (a) is for $\gamma = 10^{-8}$ cm^2 and (b) is for $\gamma = 10^{-6}$ cm^2. Since:

$$\varepsilon = - \frac{\partial T}{\partial Z} \tag{53}$$

where $\partial T/\partial Z$ and $U_{Z\ell}$ are constant for Ingot 1, the rate ratio is dictated solely by the interdendritic velocity. Therefore, the cooling rate, ε, is constant. Since

$$\frac{\partial T}{\partial r} = - m \frac{\partial T}{\partial Z} \tag{81}$$

where m = 0.75 for Ingot 1, $\partial T/\partial r$ is also constant. Notice that an average value of $\vec{V}$ for each radius is easily determined since the curves are smooth and without much variation. The average velocity is composed of two averaged components $\bar{V}_r$ and $\bar{V}_Z$,

$$\bar{V} = (\bar{V}_r^{\,2} + \bar{V}_z^{\,2})^{1/2} \tag{82}$$

and

$$\partial T/\partial r/\varepsilon = c_1 \qquad \text{(positive)}$$

and

$$\partial T/\partial Z/\varepsilon = c_2 \qquad \text{(negative)}$$

Equation (80) is now

$$C_s \propto \frac{1}{1 + c_1\bar{V}_r + c_2\bar{V}_z} \tag{83}$$

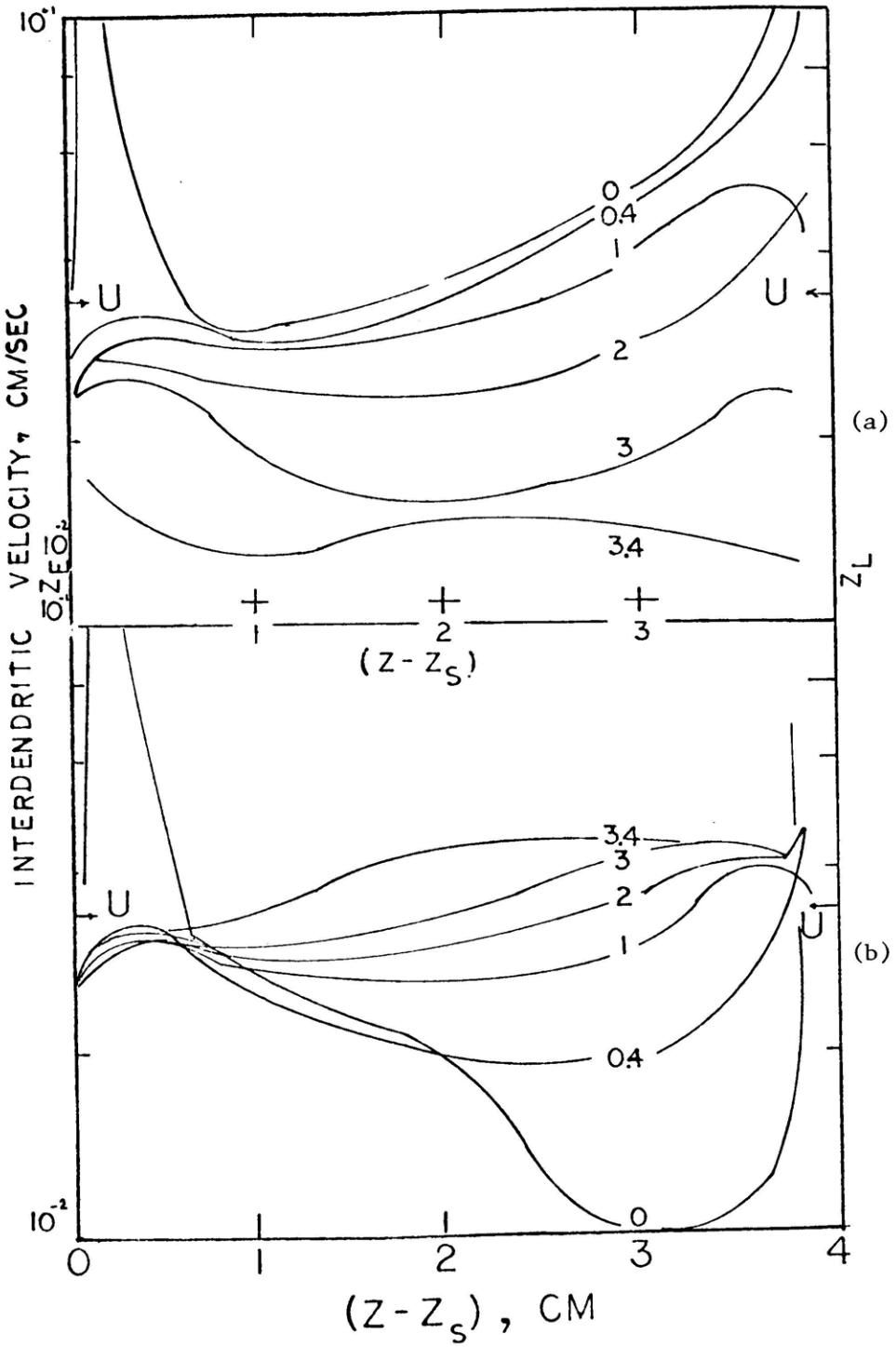

Fig. 19 - Interdendritic velocity distributions from center to wall for Ingot 1. Those for (a) are of $\gamma = 10^{-8}$ cm^2 whereas in (b) $\gamma = 10^{-6}$ cm^2. (a) Centerline velocities are highest, (b) centerline velocities are lowest.

Since products $c_1 \cdot \bar{V}_r$ and $c_2 \bar{V}_z$ are predominantly positive in Ingot 1 the composition is inversely proportional to the interdendritic velocity. For Figure 19 (a) $\bar{v}$ decreases with increasing radius so the composition, c_s, is increasing. The reverse is true for Fig. 19 (b). This behavior is illustrated in Figure (11). The analysis is not always so illuminating as it is in this special case.

7. Effect of Increasing Composition

Presumed is that an Al-15% Cu alloy has the same two phase geometry as Ingot 1 with the exception of the depth being 3.6 cm. instead of 3.8 centimeters. The average fraction liquid of the entire mushy zone is 0.5 whereas for Al-4.4% Cu the average is 0.25. $\gamma = 10^{-6}$ cm^2 for this simulation.

The cooling rate, ε, is permitted to vary in order to determine the effect of this parameter upon the final solute profile. It is seen from Fig. (20) that substantial accumulation of solute at the centerline results if the absolute value of the cooling rate is decreased. For a value of U_{ZCL} of 0.0053 cm/sec, C_s is 28% Cu at the centerline whereas a value of 16.1% Cu is attained if U_{ZCL} equals 0.053 cm/sec. The relationship of the cooling rate to the centerline velocity is:

$$\varepsilon = - U_{ZL} \cdot \frac{\partial T}{\partial Z} \qquad (53)$$

where $\partial T/\partial Z$ is a constant since the temperature is a linear function of the mushy zone depth. This derivation is found in Appendix B, Der (9). The information from Fig. (20) indicates the significance of cooling rates upon macrosegregation.

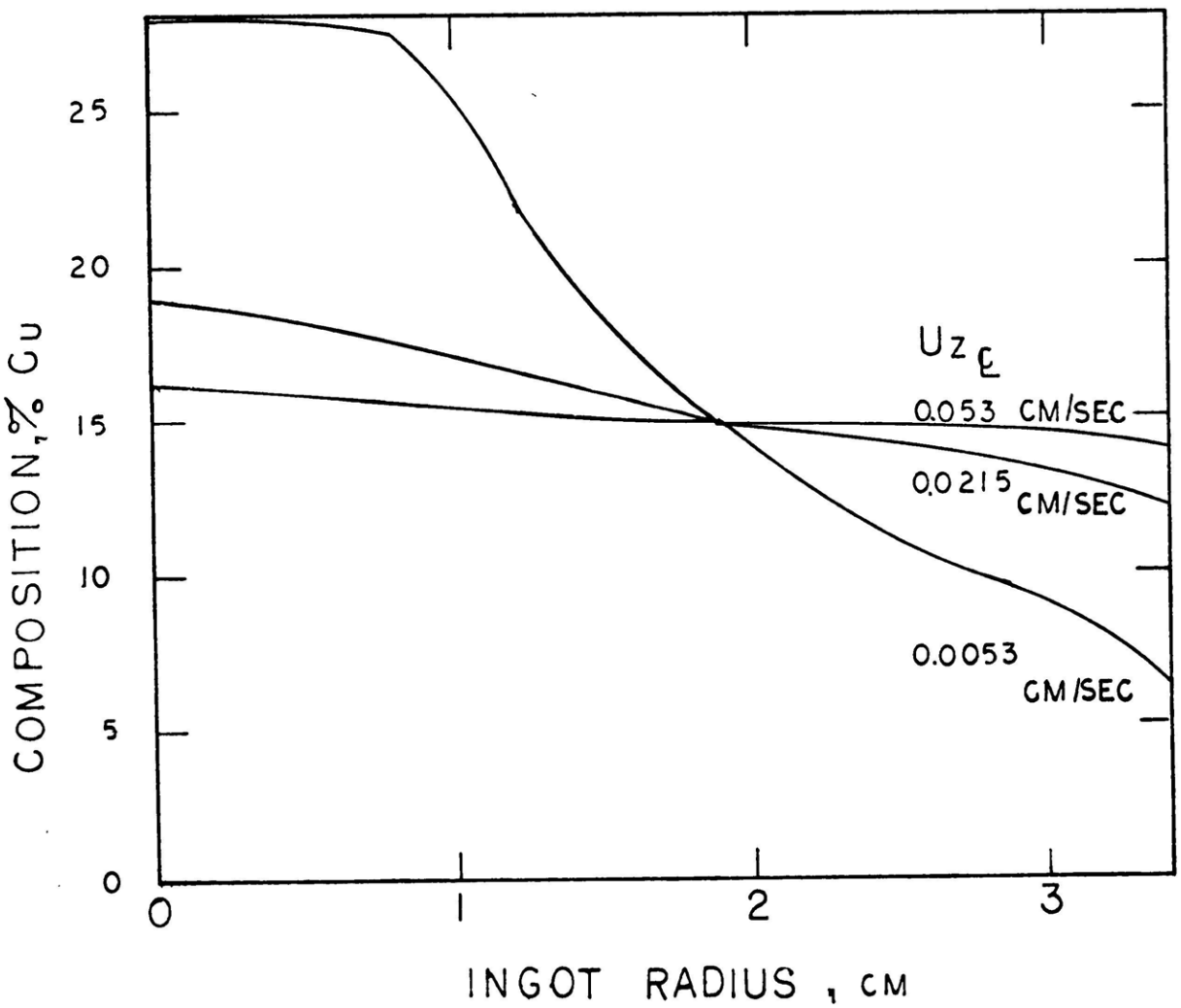

Fig. 20 - Composition profiles for Al-15% Cu if the centerline isotherm velocity UZCL varies from 5.3×10^{-2} cm/sec to 5.3×10^{-3} cm/sec.

B. Ingot 2

The special case of an Al-4.4% Cu ingot solidifying unidirectionally is simulated on the computer. Though it may appear to be a trivial case since no macrosegregation occurs in unidirectional ingots; it was analyzed because it does represent a limiting case against which the program could be tested.

The depth of the mushy zone is 2.18 centimeters with an isotherm velocity of 0.0239 cm/sec. A total of 230 iterations were specified with updates at iterations 30, 130 and 230. Both simulation and experiment agree. It was decided that to get the best results large z increments of 0.2 centimeters should be used for the bulk of the two phase region with the exception of the top 0.2 cm border extending to the liquidus. Spacings of 0.04 cm were chosen in this region. A more precise depth of the mushy zone is therefore achieved so that $\partial T/\partial Z$ is more accurate.

C. Al-Cu Alloy (Ingots 3, 4 and 5)

For these three ingots, thermal data was not obtained directly. However, all three ingots were "doped" with approximately fifty grams of molten Al-49% Cu during the steady state solidification. The three shapes of the mushy zone are in Fig. 10 (c, d and e).

1. Calculating the Depth of the Mushy Zone

Flemings et al. [5] have shown that the secondary dendrite arm spacing, λ_2, and the average cooling rate, ε, are related according to

$$\lambda_2 = \bar{c} \quad \varepsilon^{-0.39} \tag{84}$$

For steady state conditions the average cooling rate is:

$$\varepsilon = \left[\frac{d(r)}{U_{ZCL}}\right]^{-1} \tag{85}$$

where d(r) is the mushy zone depth at a given radius, r, and U_{ZCL} is the isotherm velocity at the centerline. Therefore, the relationship for steady state conditions is:

$$\lambda_2 = \bar{c}\ \left[\frac{d(r)}{U_{ZCL}}\right]^{0.39} \tag{86}$$

which when transposed is:

$$d(r) = U_{ZCL}\ \left[\frac{\lambda_2}{\bar{c}}\right]^{2.564} \tag{87}$$

The above is found in Appendix B, Der (10). Knowing the secondary DAS as a function of radius for all three cases it is possible to calculate the depth of the mushy zone. The fact that the DAS did not vary with radius indicates that the isotherms were parallel. Table A lists the DAS and the depths calculated using Eq. (86).

The value of $\bar{c}$ was calculated to be 848 versus the 1333 found in the literature. Having recorded the driving velocity of the electrode, V_D it was possible to "back calculate" the velocity of the liquid metal/slag interface, U_{ZCL}. According to Basaran[41]:

$$\left|U_{ZCL}\right| = \frac{A_E}{A_I - A_E}\ \left|V_D\right|$$

where A_E is the cross sectional area of the electrode and A_I is that of ingot. Values of V_D and U_{ZCL} are also found in Table A.

TABLE A

Measured and Calculated Parameters of the Al-Cu Ingots

Ingot Number		(Dimension)	1	2	3	4	5
Centerline Velocity	UZCL	cm/sec	0.053	0.028	0.025	0.024	0.024
Secondary DAS	λ_2	microns	61.0	61.0	62.0	62.0	51.0
Mushy Zone Depth	d(r)	cm	3.80	2.18	1.76*	1.74*	1.00*
1st Degree Coefficient	a_1**		0.75	0.00	0.00	0.00	0.00
2nd Degree Coefficient	a_2**		0.00	0.00	0.163	0.120	0.065

Comments:

*These are values of the mushy zone depth calculated by Eq. 8.7.

$$d(r) = Uz \quad [\lambda_2/\bar{c}]^{2.564}$$

**The equation for describing isotherms composing the muzhy zone is:

$$z = a_o + a_1 r + a_2 r^2$$

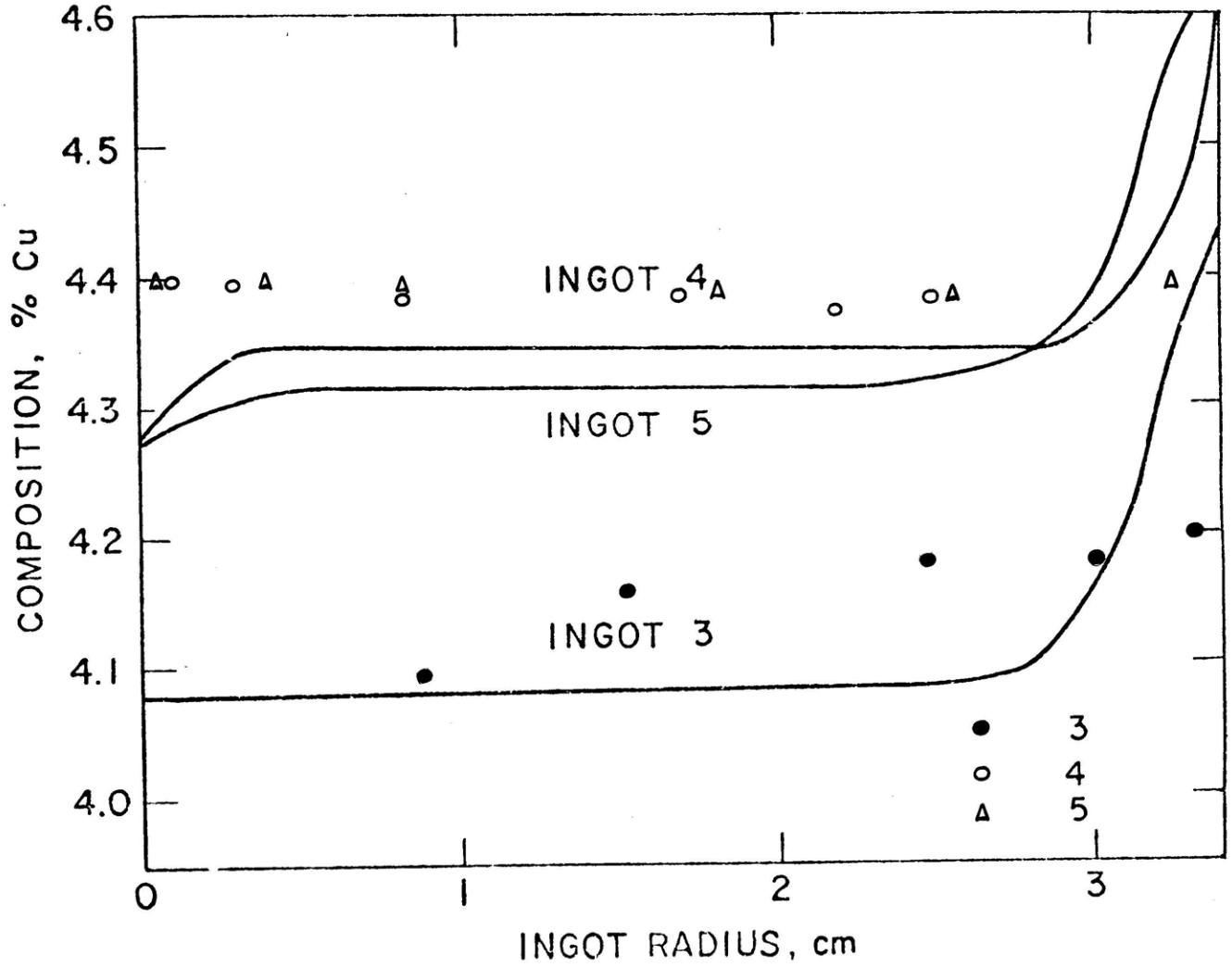

Fig. 21 - Computer simulated composition profiles for ingots 3, 4 and 5 with $\gamma = 10^{-7}$ cm^2.

All three composition profiles show substantial amounts of positive segregation at the wall. For ingots 4 and 5 this is not experimentally verified. The value of γ used for all three cases is 10^{-7} cm^2 since there is little variation of secondary DAS. It is constant in a radial sense due to a constant depth of the mushy zone (parallel isotherms).

It must be noted that the agreement between experiment and simulation results is not overwhelming for Ingots 3, 4 and 5. This is due to:

1. lack of thermal data during solidification; and
2. lack of mushy zone symmetry during solidification.

Values of HTE, UZCL, MSOL and MLIQ are therefore only approximate. However, it is very likely that the isotherms were in all cases parallel since the secondary dendrite arm spacings are independent of radial position. Profiles for the three ingots are found in Fig. (21).

D. Analysis of the Sn-15% Pb.

The methods employed in Section A are those utilized in Section D for analysis of a similar alloy: Sn-15% Pb. The main difference is that the Al-4.4% Cu alloy rates as a lean alloy whereas the Sn-15% Pb binary is a rich alloy. One of the most noticeable facts is that the average fraction liquid for the rich alloy is 0.59 and only 0.25 for the lean. The method of determining these averages is outlined in Appendix B, Der. (11). The Sn-Pb binary has a more "open" dendritic structure and so the specific permeability is also greater. The isotherm velocity at the centerline for the Sn-Pb binary is also 7.57 times slower than the case of the Al-Cu binary of Ingot 1.

1. Determination of γ

Scanning of a broad spectrum of flow factors was required as a routine step in determining the correct value of γ. For values of γ from 10^{-9} cm^2 to 10^{-7} cm^2 there was no noticeable effect upon the composition profile. It remained virtually flat from the centerline to the wall.

The dramatic change occurred upon increasing the flow factor from 5×10^{-7} to 10^{-6} cm^2. Three cycles of 150 iterations per cycle were used for these calculations. Figure (22) depicts two curves approximating the true composition profile. Experimental data points are also evident. Comparing the two curves to the experimental points it was decided that the actual flow factor lies closer to the high value of 10^{-6} cm^2. A high value of $\gamma = 10^{-5}$ cm^2 indicated that the central ingot core would be of nearly eutectic composition upon freezing.

The result of this routine "scanning" procedure is that an appropriate value of flow factor was determined as approximately 10^{-6} cm^2. Again, this indicates that the dendritic packed bed is more open than the leaner alloy of Al-4.4% Cu binary.

2. Variable γ

From the Karman Kozeny Equation, Eq. (8) it was seen that specific permeability was proportional to $1/S_o^2$ where:

$$\lambda_2 = \hat{c}/S_o \qquad (9)$$

This is true if the fraction liquid is low and the predominant fraction volume of solid packing within the mushy zone is composed of secondary

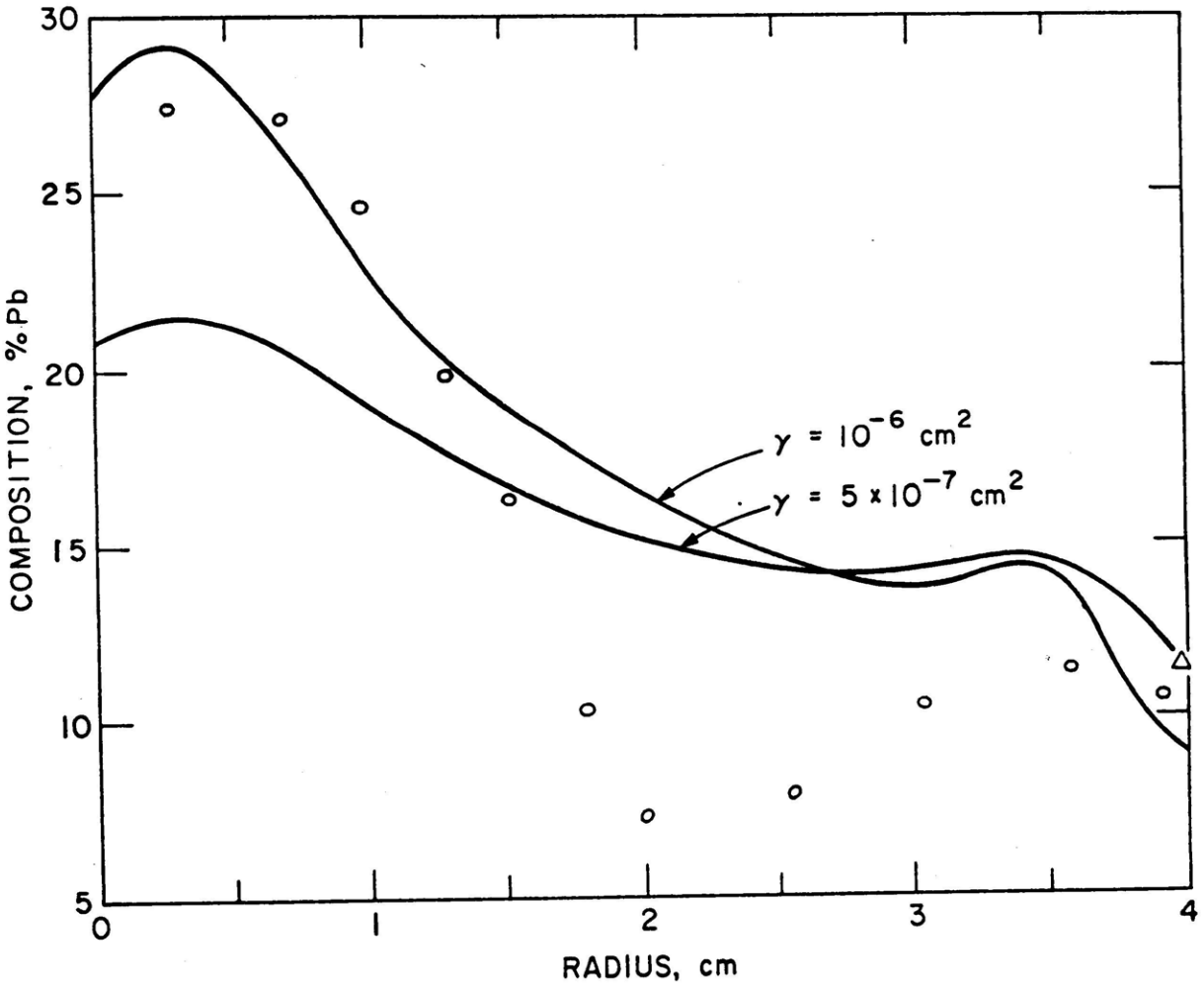

Fig. 22 - Determination of the proper range of γ for Ingot A. Comparisons of simulation profiles to experimental data are made. Values of 5×10^{-7} cm^2 and 10^{-6} cm^2 are investigated for a Sn-15% Pb ingot.

dendrites. Otherwise the relationship is:

$$\lambda_1 = \tilde{\tilde{c}}/S_o \tag{88}$$

and resistance to flow is controlled by primary dendrites. Using the relationship

$$K = \gamma g_L^2 \tag{4}$$

in which

$$\gamma \propto \lambda_2^2$$

the specific permeability was permitted to vary according to secondary DAS of the ingot through γ. From the inset in Figure (23) the secondary DAS is illustrated to vary from a maximum of 60 μm at the centerline to 30 μm at the wall. Therefore, the proportionality

$$\frac{\gamma_{\text{Ł}}}{\gamma_w} = \frac{\lambda_{2(\text{Ł})}^2}{\lambda_{2(w)}^2} = \frac{4}{1}$$

exists for this system. The dendrite distribution was programmed as a linear relationship. Since $\gamma = 10^{-6}$ cm^2 (Fig. 23) gave a good approximate profile of composition, the centerline value of γ, $\gamma_{\text{Ł}}$, was set to 10^{-6} cm^2. $\gamma = 2.5 \times 10^{-7}$ cm^2 is appropriately the wall value, γ_w.

In computer notation this linear relationship is:

```
ZAT(I) = GADSCL - ((GADSCL-GADSWL)/RADIUS)*ROR(I)
```

where ZAT(I) = $\gamma(r)$,

GADSCL = $\gamma_{\text{Ł}}$,

GADSWL = γ_w, and

ROR(I) = r, the radial location.

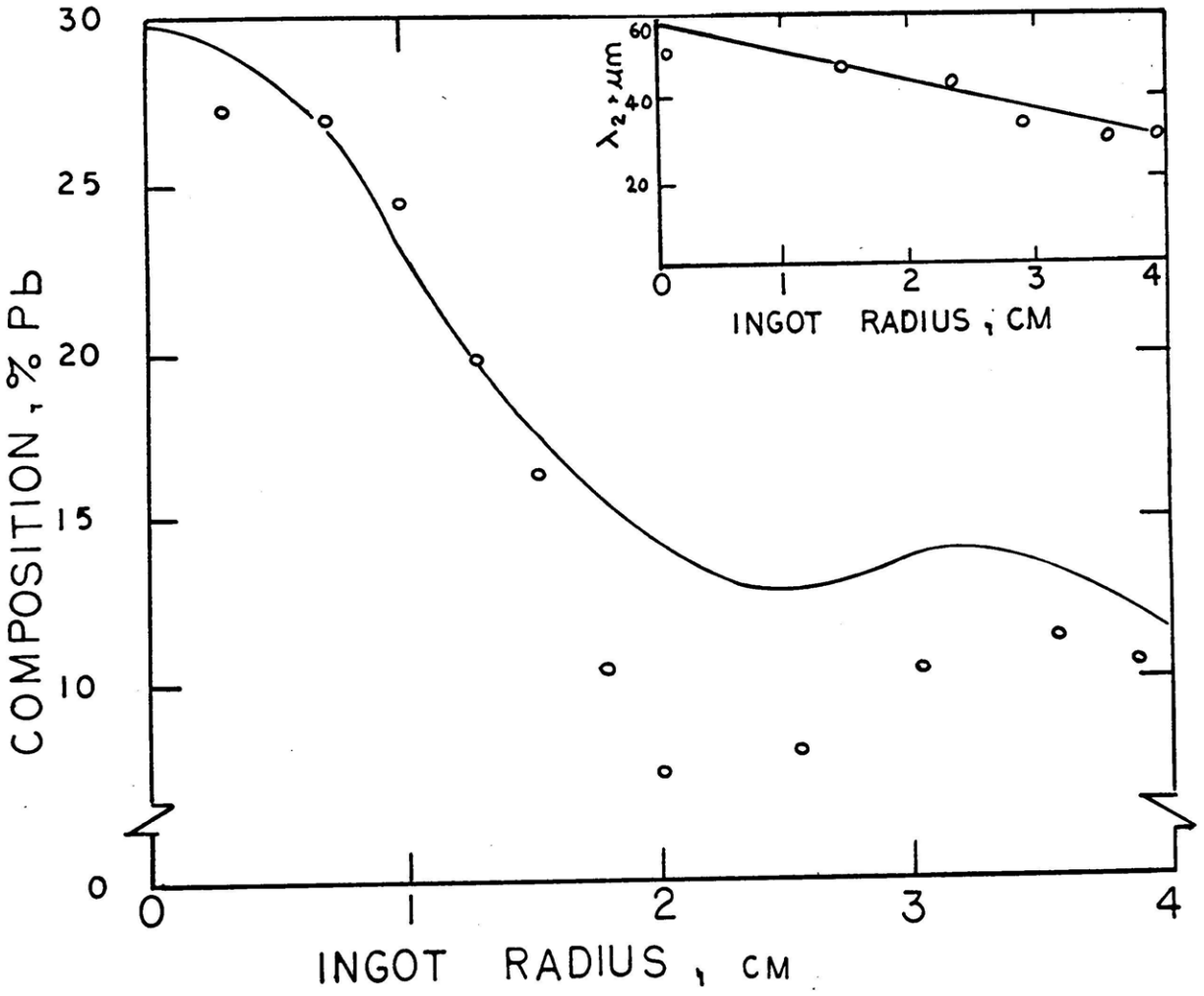

Fig. 23 - Variable value of γ for Sn-15% Pb system. γ is proportional to λ_2^2 with a maximum value of 10^{-6} cm^2. Inset figure illustrates the radial distribution of secondary DAS.

Figure (23) represents the composition profile generated after 450 iterations for Model 2. Updates are at iterations 150, 300 and 450. The trend is accurate and experimental measurements of composition are closely approximated by the simulation. This, I believe supports the premise that in castings in which interdendritic flow is controlled by secondary dendrite arms that resistance is inversely proportional to the square of these dendrite arm spacings. If this is true, then simulations can be made more amenable to direct experimental measurements. This is not the case for the model in which tortuosity factor, τ, and channel number, n, are utilized.

3. Iteration Ceiling and Frequency of Recycling

Since the eutectic fraction liquids in the Sn-15% Pb alloy as well as most fraction liquid distributions within the two phase region were markedly different from the Scheil approximation by the end of the first cycle, it was possible to have a eutectic fraction liquid of 0.77 at the centerline and less than the Scheil value of 0.3^9 at the ingot wall. Values of 0.25 were common. Therefore, it was decided that more cycles (updates) should be incorporated with a reduction in total iterations per cycle as a strategy. The main emphasis is that several updates are required for rich alloys having low values of isotherm velocity since the fraction liquid is expected to vary considerably in cases of low freezing rate whereas the fraction liquid has a narrower range of values for the lean alloys. A lean alloy is one which yields an average fraction liquid of less than 0.3 with a Scheil approximation. Figure (24)

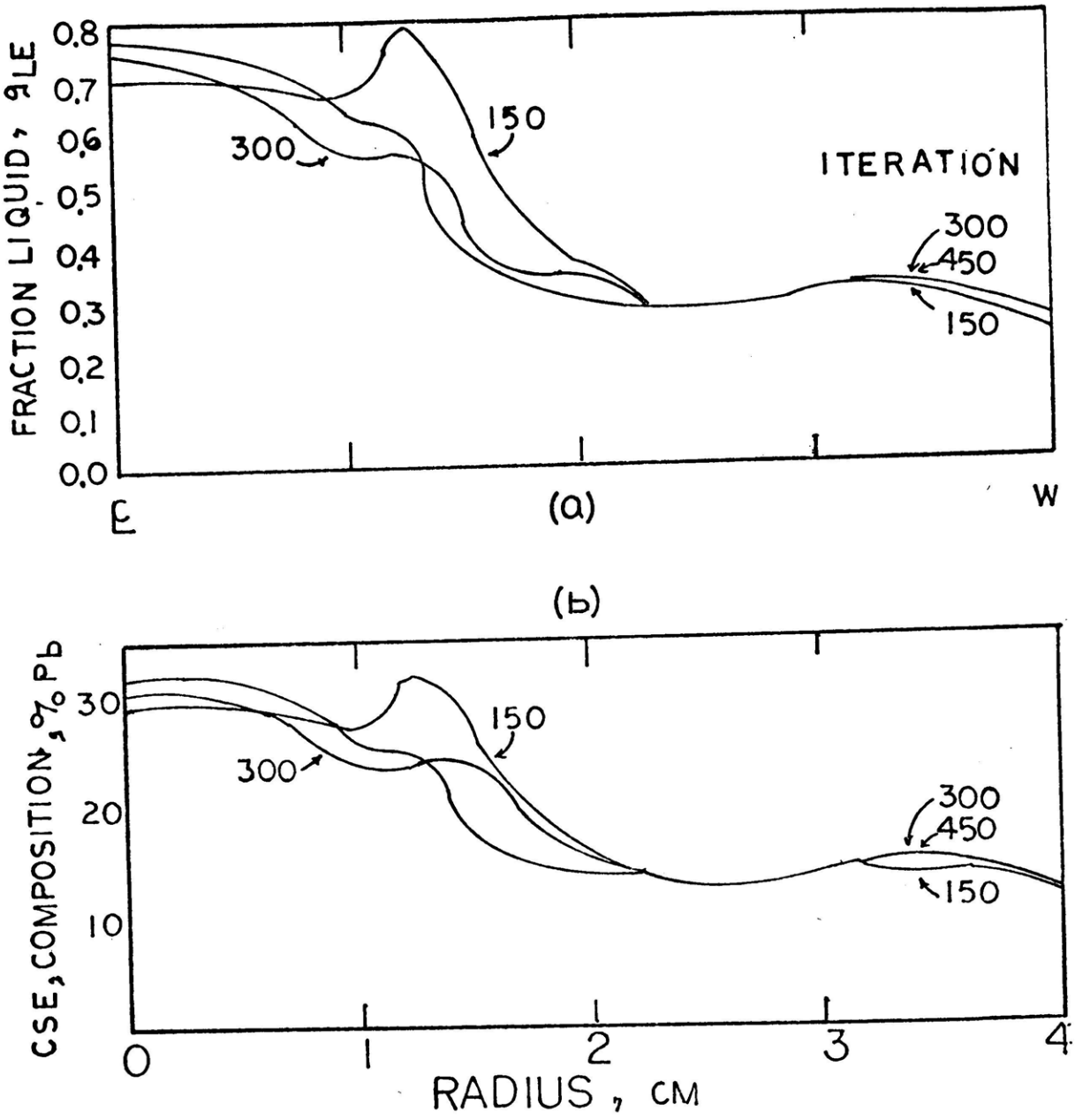

Fig. 24 - Change in fraction liquid (a) and the composition (b) profiles at the eutectic isotherm for a 3 cycle program at iterations of 150, 300 and 450 iterations. Pb - 15% Sn ingot using Model 2.

demonstrates the need for high cycle, frequency-low iteration per cycle design.

4. Deflection of Streamlines

Within Figure (25) are the streamlines of the interdendritic fluid for the mushy zone of Ingot A. Since this is an alloy rich metal having an average fraction liquid of 0.59 the flow resistance is reduced substantially over the Al-4.4% Cu system. Nearly an order of magnitude difference in γ exists between the systems. Whereas Ingot 1 had flow lines essentially downward and toward the solidus those shown in Fig. (25) are downward and towards the ingot center. In the central core, flow is towards the liquidus.

Incoming streamlines are not perpendicular to the isotherms. This is due to lesser amounts of metal solidification in this region than in the Al-4.4% Cu system. Good streamline deflection occurs at the solidus due to substantial metal solidification. Approximately 39% of the metal solidifies in this zone.

Since velocity is inversely proportional to streamline proximity it appears that relative flow at the central core is significant. If it is faster than the isotherm velocity at the liquidus isotherm as indicated by Fig. 26 (a), solute is escaping the interdendritic region and flowing into the bulk liquid. The ingot composition was predicted to be 13.7% Pb for this example. This is noticeably less than the nominal ingot composition of 15% Pb.

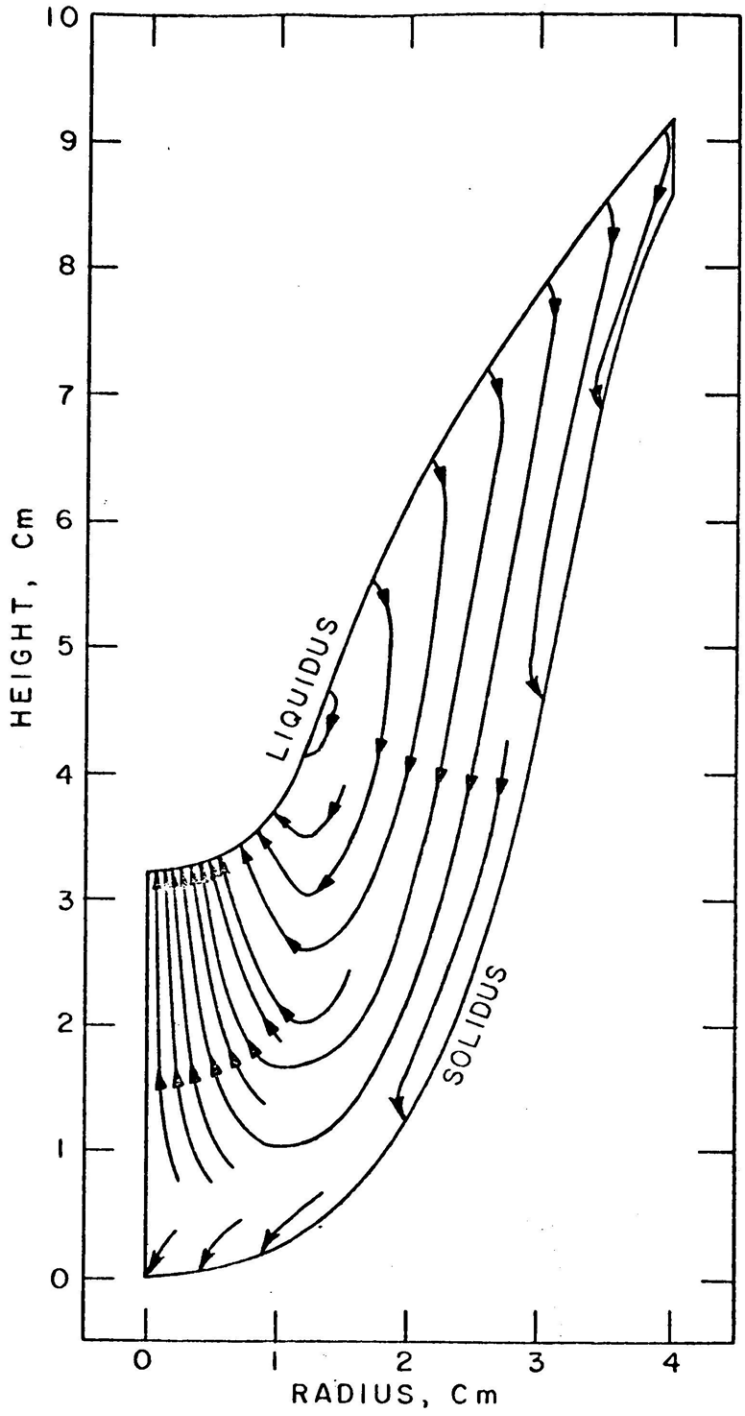

Fig. 25 - Streamlines for the Sn-15% ingot calculated using $\gamma = 10^{-6}$ cm^2. Spacings are approximately equal to the inverse of the relative magnitude of velocity.

5. Rate Ratio and Average Radial Composition

Plots $\vec{v}\cdot\nabla T/\varepsilon$ versus depth in the mushy zone for the Sn-15% Pb alloy of Ingot A are plotted in Fig. (26). In Fig. 26 (a), notice that each of the three curves has a definite relationship to the others. It is either entirely above or below its neighbor. It is important to realize that even though the curve for radius of zero goes as low as -2 its average falls well above -1. This will always be true. These curves of Fig. 26 (a) and (b) indicate that the compositions steadily decrease upon moving away from the centerline. This agrees with Fig. (22). The trend of diminishing solute compositions continues out to a radius of approximately two and a half centimeters.

By now it is understood that the analysis concerns itself with the average value of the rate ratio for a specific radius. Thus, the operator is concerned only with the integral:

$$\left.\frac{\vec{v}\cdot\nabla T}{\varepsilon}\right|_r = \frac{\int_{Z_s}^{Z_L} \vec{v}\cdot\frac{\nabla T}{\varepsilon}\,(Z)\,d_Z}{\int_{Z_s}^{Z_L} d_Z} \qquad (89)$$

holding radius constant. Summing the areas between curve and axis $(z-z_s)$ for both positive and negative regions it is possible to determine the total net area for each radius. This value divided through by the total depth of the mushy zone at this radius gives the average value of rate ratio for the particular column.

Insert the average value of rate ratio into the simple approximation:

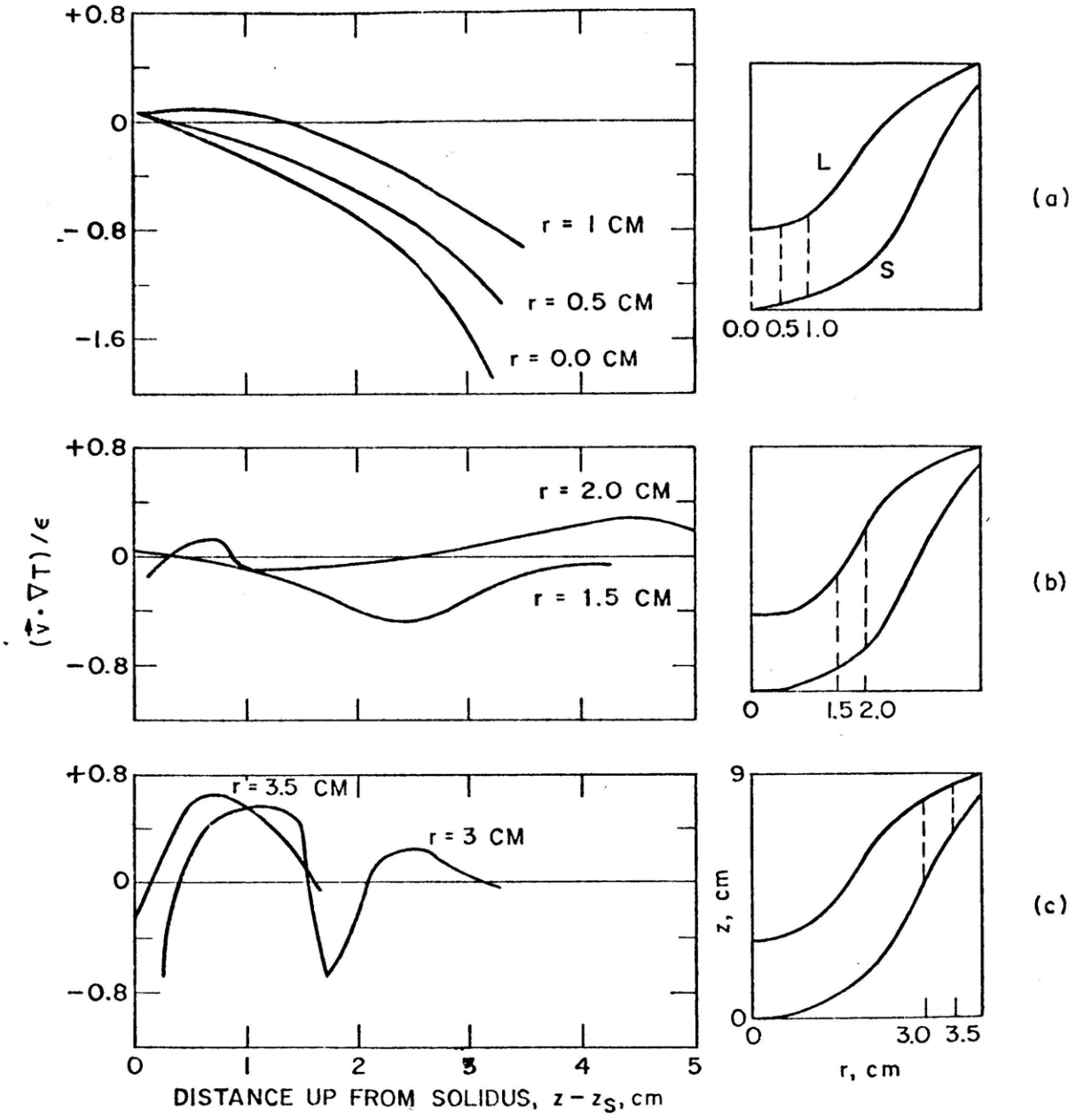

Fig. 26 - Calculated values of the rate ratio $\vec{v}\cdot\nabla T/\varepsilon$ in the Sn-15% ingot with $\gamma = 10^{-6}$ cm^2.

$$\bar{C}_s \propto \frac{1}{1 + \frac{\vec{v}\cdot\bar{\bar{\nabla T}}}{\varepsilon}} \tag{80}$$

to get a relative value of local solute content for the given radius. After this is done the operator compares these relative values for each curve (w/r to a constant radius) and notes the total relationship. This informs him in advance what the final composition trend will be.

The difficulty of giving an immediate approximation of trend when comparing Fig. 26 (b) and (c) for curves corresponding to radii of 2, 3 and 3.5 cm indicates that their compositions are not too different. This is shown best in Fig. (23) where the radial composition curve appears as a gentler sloping curve than that of the slope for radii less than two centimeters. The analysis can of course be made without rigorous manipulation.

For Fig. 26 (a) and (b) notice that the rate ratio is negative out to a radius of 1.5 centimeters from the center. This indicates channeling within the mushy zone at the central ingot core. From Fig. (25) notice that flow is upwards in this region. Severity of channeling appears marked such that "freckling" might occur. Stability criteria, Appendix F, indicates that freckling occurs if $\vec{v}\cdot\nabla T/\varepsilon<-1$. This is the case of radii from r=0.0 to 1.0 cm as shown in Figure 26 (a). Further investigation reveals that freckling continues beyond 1 cm but doesn't occur at r=1.5 cm where $\vec{v}\cdot\nabla T/\varepsilon= -0.5$ is the lowest value. Experiments conducted by Sindo Kou on Sn-15% Pb ingots reveal severe "freckling" within a radius of 1.5 centimeters of the center line. The central ingot core

contains a high liquid content as reported from output. Fig. 24 (a) shows values of fraction liquid eutectic within a radius 1.3 cm as being high. Values as high as 0.78 at iteration 450 are predicted. The Scheil value is 0.39; half the actual value.

Figure (22) and (26) are from the same simulation output. The composition profile is accurately simulated within the first 1.3 cm of the centerline. Freckling is predicted correctly for this region. Beyond this radius the results of Fig. (26) have less credibility. Since the trend is good, however, analysis is continued. From radius 1.5 cm to 2.0 cm, Fig. 26 (b) shows increasing values of $\vec{v}\cdot\nabla T/\varepsilon$ at mid depth. Positive values of $\vec{v}\cdot\nabla T/\varepsilon$ are seen at the solidus and liquidus zones. This trend continues out to 3 cm as illustrated in Fig. 26 (c) as the pronounced negative dip at mid depth within the mushy zone. $\vec{v}\cdot\nabla T/\varepsilon$ is positive above and below this "channeled" region. The value of $\vec{v}\cdot\nabla T/\varepsilon$ for this region is -0.8. Freckling criteria is approached. From Fig (25) marked solute flow is directed through this hollowed corridor originating at about 1 cm from the ingot wall and extending to the central ingot core. At r = 3.5 cm the value of $\vec{v}\cdot\nabla T/\varepsilon$ is positive. The hollowed region is thus sealed.

Computer simulation results for Ingot A concur with experimental measurements in the following ways:

1. composition profiles from centerline to approximately 1.3 cm from center for the case of a constant γ of 10^{-6} cm (Fig. 22). Thereafter, the trend is decent but the relative error of simulation to experiment is sifnificant except at the wall where order is again restored.

2. prediction of freckling phenomena within a radius of 1 cm and possibly as far as 1.3 cm from the centerline.

3. a significantly better composition profile from centerline to wall is achieved if γ is varied according to the square of the secondary DAS. This is shown in Fig. 24.

The agreement of simulation computations to experimental measurements indicates the predictive ability of the model. The accuracy of the joint prediction suggests the correctness of the models treatment of underlying fluid flow phenomena. Also the accuracy indicates that the discrete linear segment method of Model 2 is satisfactory in approximating mushy zone isotherms.

6. Comments on Both Systems

Comments on both the Al-4.4% Cu system and the Sn-15% Pb system are addressed in this section. The instrument used for discussion is the rate ratio with attention given to Appendix E.

For the Al-4.4% Cu system, Ingot 1, notice in Figure (18) that $0.12>\vec{v}\cdot\nabla T/\varepsilon>0.03$ is the range for the rate ratio. This is a case (1) class (a) type (Refer to Appendix E). In Figure 26 (a) of the Sn-15% Pb system, Ingot A, the range is $-1.8<\vec{v}\cdot\nabla T/\varepsilon\leq 0.1$. At radii r=0.0, 0.05 and 1.0 cm, $\vec{v}\cdot\nabla T/\varepsilon<-1$ in the liquidus zone. This is an example of case (3). Freckling is predicted.

In contrasting the systems the following are observed:

1. The magnitudes of the absolute value of $\vec{v}\cdot\nabla T/\varepsilon$ for the Al-4.4% Cu system are substantially smaller than those of the Sn-15% Pb system.

The low values of $\vec{v}\ \nabla T/\varepsilon$ for Al-4.4% Cu convinced Martin Keane that the relaxation and Scheil methods of predicting fraction liquid were synonymous.

2. The Al-4.4% Cu system is a case (1) class (a) type throughout the mushy zone; whereas, for the Sn-15% Pb system, regions exist within the mushy zone representing all three cases. The Al-4% Cu system is entirely stable whereas the Sn-15% Pb system has a central crater containing nearly twice the Scheil predicted value of fraction liquid at the eutectic. This region is unstable and freckling is predicted out to 1 cm and perhaps to 1.3 cm from the center.

VI. CONTINUOUS CASTING

The continuous casting (CC) method is similar to the ESR method in that it is a steady state process. Commercially, it is more suited to production than is ESR. On the average it is about five to ten times faster than the ESR method which derives its importance from its "refining" capabilities. The ESR method is employed where specialty products of high quality are needed.

Lewis in 1958 documented some work on the CC process.[42] He determined the isotherms for a CC aluminumalloy for two different casting speeds: 3 and 9 inches/minute for an ingot diameter of 8 inches during steady state solidification.

Due to the heat extraction methods and melting velocities employed in the CC process, solidification profiles differ markedly from ESR profiles. This is due to the two modes of heat extraction. There is a primary extraction unit followed by a secondary extraction unit. The basic shape occurring in ingots produced by CC are comprised of:

1. a steep solidification front at the mold wall (it is nearly parallel to the wall); and
2. a region of lesser sloped isotherms in the central core. A distinct nexsus where both types meet is observed.

Work has been done on the isotherm velocity as related to the crystal structure (secondary DAS) within the ingot cast as described by Altenpohl et al.[43]

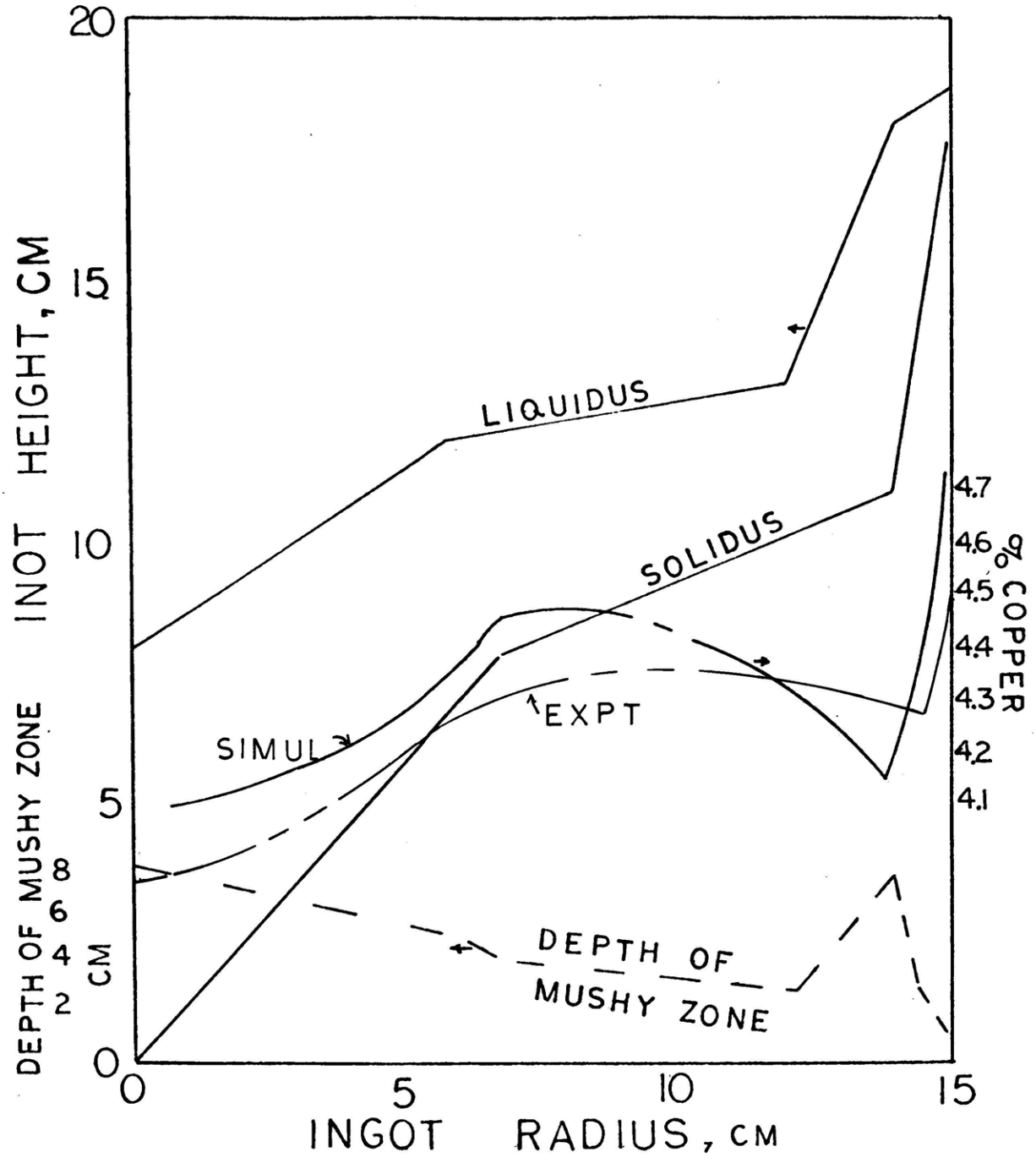

Fig. 27 - Mushy zone shape of an Al-4.5% Cu alloy continuously cast is illustrated. The dashed curve depicts the corresponding depth. The computer simulated composition profile is determined.

Since

$$\varepsilon = - \vec{u} \cdot \nabla T$$

and

$$\lambda_2 \propto - 1/\varepsilon$$

then approximately $\lambda_2(r) \propto 1/d(r)$

Therefore, the secondary DAS is inversely proportional to the isotherm velocity at a given radius. On page 582 of Ref. 43 a graph of DAS versus ingot radius and one of isotherm velocity versus radius are shown (Bild 12). Secondary DAS is the "mirror image" of the isotherm velocity. Important to note is that both graphs have sharp curves. Significant differences of d and λ_2 exist along the radius. This is a distinct feature of the CC process.

Non-uniform coarsening occurs in the CC process due to differences of the heat extraction modes. Again consider equation (85) for Al-Cu alloys. Since

$$\gamma(r) \propto \lambda_2^2 (r)$$

then Eq. (86) squared is:

$$\lambda_2^2 = \bar{c}^2 \left[\frac{d(r)}{U_{z\bar{b}}}\right]^{0.78} \qquad (90)$$

This variable γ situation causes the computer program to invoke the specific permeability relationship:

$$K(r) = \lambda_2^2 (r) \cdot g_L^2 \qquad (91)$$

When Eq. (90) is substituted into Eq. (91) the form in computer notation is:

```
PERMI(I,J) = ZAT(I)*(GL(I,J)**2)
```

where:

```
ZAT(I) = (DEPMZ(I)/UZCL)**0.78
```

Also ZAT(I) = $\gamma(r)$

DEPMZ(I) = $d(r)$

Figure (27) shows the mushy zone shape used for the simulation study. The radius is fifteen centimeters. Notice that depth of the mushy zone varies with radius as shown by the dashed curve in Fig. (27). The maximum depths occur at the center and within two centimeters of the mold wall. It is not surprising that large values of λ_2 occur in both regions. This is verified by both Altenpoh[43] and Peel and Pengelly[44] in studies done on Al-Cu ingots of this size at equal isotherm velocities (2 inch/minute).

Results of computer simulations for an alloy of Al-4.5% Cu composition are illustrated in Fig. (27). Updates are at iterations 130 and 260; spacings are KC = 0.1 cm and HC = 1.0 cm through to radius 13 cm. Thereafter, HC = HCC = 0.25 cm. Thus, the radial increment is allowed to vary in this case. Similarity between this simulation profile and that of the profile for an Al-4.5% Cu C.C. ingot measured by Peterson as presented by Flemings[1] is indisputable. There is a very sharp peak at the mold wall followed by a trough. This trough corresponds to the region of deep mushy zone near the wall. Upon closer examination of Fig. (27) it is noted that the depth of mushy zone is roughly a "mirror image" of the composition profile.

An approximate prediction expression for composition can be derived from Eq (80) if the following hold:

$$V_Z \propto -\lambda_2^2 \propto - d^2(r)$$

$$V_r \propto +\lambda_2^2 \propto + d^2(r)$$

$$dT/dr = - m\Delta T/d(r)$$

The expression is:

$$\bar{c}_s \propto \frac{1}{1 + c \cdot d^2(r)(1+m)}$$

where $m = dz/dr$ and c is some constant. Thus, diminishing the slope of isotherms has the effect of increasing the composition. If d(r) and m are simultaneously large than $\bar{c}_s$ will increase significantly. This is apparent from Fig. (27). The assumption that v_r is positive, however, is not always legitimate. If flow is towards the center than $m<0$.

Results of the computer simulation in this chapter indicate the following:

1. The fluid flow model is applicable to other steady state processes (it correctly predicts the composition profiles of CC processes).

2. It satisfies criteria for larger-than-lab sized ingots (at least in the cases of lean alloy types).

3. Specific permeability for lean alloys of variable cooling rates is proportional to λ_2^2 and ultimately to depth of mushy zone squared.

4. The discrete linear segment feature of Model 2 is well suited for treatment of complicated mushy zone shapes. Model 1 could not be used.

VII. CONCLUSIONS

1. A macrosegregation model for steady state ESR casting has been developed. Simulated profiles of composition versus radius in laboratory-scale ESR ingots are attained. The model applies to CC under steady state conditions as well. A continuously cast ingot was simulated. The ingot had a radius of 15 cm meaning that larger than laboratory-sized ingots can be simulated also.

2. Computer calculations are successful in determining macrosegregation profiles for laboratory sized ingots. Accurate composition profiles for Al-4% Cu ingots of 6.8 cm diameter have been simulated. Temperature distribution, mushy zone shape and depth, symmetry as well as solidification rate are pertinent input. Simulation accuracy depends on these measurements. The method of determining the mushy zone shape by "doping" methods yields questionable simulation results since definition of liquids and solidus regions is not correlated to thermal measurement.

For the Sn-15% Pb ingot of 8.0 cm diameter "freckling" was predicted within the central 1.3 cm radius. A constant value of $\gamma = 10^{-6}$ cm^2 was utilized in the program. Experimental, measurements indicated "freckling" to extend from the ingots central axis to $r = 1.5$ cm. Composition profiles of simulation and experimental measurements correlate well from r=0 to r=1.3 cm. From r=1.3 to r=4 cm comparison is satisfactory. This joint concurrence of simulation calculations to experimental measurements suggests the correctness of the model's treatment of underlying fluid flow phenomena.

3. Varying the conductivity term, γ, according to the relationship

$$\gamma = \hat{c}\, \lambda_2^2$$

yielded a slightly better composition profile for the Sn-15% Pb system. Since secondary DAS is proportional to the depth of mushy zone, d,

$$\gamma = \bar{c}\, d^2$$

was the explicit relationship programmed for the Cu ingot. The CC mushy zone utilized illustrates an example of significant variations of mushy zone depth. Thus "non-uniform" coarsening prevails.

4. A 30 cm diameter Al-4.5% Cu ingot continuously cast has been simulated for macrosegregation assuming a mushy zone profile similar to those found in literature for equivalent casting rates . The composition profile generated is indisputably similar to profiles found in literature. The profile is not a simple type.

5. For small ingots the operational parameter, ε, (cooling rate) is significant in its role in macrosegregation determination. It affects γ through DAS such that

$$\lambda \propto 1/\varepsilon$$

for instance. The creation of a large surface area to volume ratio by augmenting ε impedes gravitational seepage of solute enriched fluid within the mushy zone. Small ingots which are alloy lean can have negative centerline segregation. In large ingots this characteristic is far less likely. For large ingots ε is relatively small and the surface area to volume ratio of the mushy zone packing material (primary or secondary)

dendrites is diminished correspondingly. Resistance to flow decreases. In large ingots λ_1 rather than λ_2 is the resistance controlling parameter. Since cooling rate is low there is more time for the seeping fluid to travel. For large ingots "gravity induced" convection predominates due to low ε. In small ingots ε is high and convection is "solidification induced".

6. Expansion of metal above the solidus isotherm and shrinkage at the eutectic defines a discontinuity situation. A buffer boundary was necessitated which "weighted" pressure gradients from the solidus and interior regions. A solidus-interior boundary evolved.

7. The condition $\vec{v}\nabla T/\varepsilon<-1$ occurring at nodes adjacent and along the liquidus implies that interdendritic fluid is escaping the mushy zone and feeding the bulk liquid. For the Sn-15% Pb system in which UZb = 0.007 cm/sec this occurrence was evident. The average ingot composition was given as 13.7% Pb instead of the nominal value of 15% Pb. This may imply non-steady state conditions since nominal composition is continuously changing. Increment spacings were HC = 0.25 cm and KC = 0.14 cm.

8. Due to the overall satisfactory correlation of simulated profiles to experimental measurements it is acknowledged that the discrete linear segment approach of approximating isotherms is itself satisfactory. This characteristic of Model 2 is especially appreciated when difficult isotherm shapes are encountered.

9. The absolute value of $\vec{v}\nabla T/\varepsilon$ in the Al-4% Cu system is considerably lower than that of the Sn-15% Pb system. More updates per computer run are necessary for the latter. The effect of $\vec{v}\cdot\nabla T/\varepsilon$ on the Al-4% Cu system does, however, cause significant alteration of the fraction liquid distributions within the mushy zone. Martin Keane's conclusion that the Scheil Equation could be substituted for the relaxation process in the case of Al-4% Cu is therefore contended.

VIII. FUTURE WORK

1. The assumption that the metal pool is calm is not realistic. Coupling of the flow within the metal pool[45] to that of the flow within the mushy zone ought to be incorporated into the program. The pool flow may influence the interdendritic flow pattern significantly and thereby affect the macrosegregation profile. This therefore should be investigated.

2. Since magnetic forces can be used to alter the flow within the metal pool and mushy zone this subject deserves special attention also. Control of fluid flow within sizeable ingots by this method would result in ingots of more uniform composition.

3. The physical basis of parameter γ must be revealed. The earlier interpretation involving tortuosity factor, τ, and channel number, n is difficult to correlate to experimental measurements. The latest approach involves a single parameter, S_o. Qualitatively, S_o can be related universely to λ_1 or λ_2 depending upon which is the predominant resistance controlling factor.

4. The Karman-Kozeny Equation should be used to derive a relationship for the specific permeability. This is:

$$K = \frac{\bar{c}}{S_o^2} \cdot \frac{g_L^3}{1-g_L}$$

From experimental work done, the $g_L^3/1-g_L$ relationship holds in the region $g_L > 0.4$ whereas the relationship

$$K = \gamma g_L^2$$

holds for the region $g_L < 0.3$ for the case of alloy lean Al-4% Cu. In order

to make the proper investigation the partial differential equation (PDE) must be re-derived in terms of the former relationship.

5. Work on orthogonal trajectories is sometimes justified in cases of steep solidification fronts. Temperature distributions are then related to these trajectories. In lab sized ingots this situation is not so common.

6. The basic structure of the program is complete. In order to expedite future computer investigations of the steady state ESR or CC processes I suggest that more emphasis be placed upon graphical displays of computational results. Topography charts of $\vec{v}\cdot\nabla T/\varepsilon$ and fraction liquid superimposed on the mushy zone map at the completion of each cycle would greatly aid the researcher. With a different symbol, also superimposed on the same map would be the Scheil values of fraction liquid for instantaneous comparison. Maps of flow lines (streamlines) such as those in this thesis could be easily be generated. One dimensional data printout plots of these parameters should also be generated. The emphasis of upcoming research on the computer investigation level must be on outputing techniques. Much time was lost previously due to tedious plottings of output data and mistakes made therein.

REFERENCES

1. Flemings, M., Solidification Processing, McGraw-Hill, N.Y., p. 244 (1974).

2. Flemings, M., Nereo, G., Macrosegregation: Part 1, Trans. Met. Soc. AIME, vol. 239: 1449 (1967).

3. Mehrabian, R., Keane, M., Flemings, M., Interdendritic Fluid Flow and the Macrosegregation, Influence of Gravity, Met. Trans., vol, 1: 1209 (1970).

4. Young, K., Kirkwood, D., The Dendrite Arm Spacings of Aluminum-Copper Alloys Solidified Under Steady State Conditions, Met. Trans. A, vol.6A: 197 (1975).

5. Bower, T., Brody, H. and Flemings, M., Trans. AIME, vol. 236: 624 (1966).

6. Chien, K., Kattamis, T., The Role of Dendritic Coarsening and Coalescence in the Establishment of Cast Microstructure, Zeit Metallkde, vol. 61: 475 (1970).

7. Jacobi, H., Schwerdtfeger, K., Dendrite Morphology of Steady State Unidirectionally Solidified Steel, Met. Trans. A., vol. 7A: 811-820 (1976).

8. Takayashi, T. Hagiwara, Significance of Solidifying Zone on the Ingot Solidification, Trans. ISIJ, vol. 12: 412 (1972).

9. Piwonka, T., Flemings, M., Pore Formation in Solidification, Trans. of Met. Soc. AIME, vol. 236: 1157-1165 (1966).

10. Apelian, D., Flemings, M., Mehrabian, R., Specific Permeability of Partially Solidified Dendritic Networks of Al-Si Alloys, Met. Trans., Vol. 5: 2533-2537 (1974).

11. Streat, N., Weingerg, F., Interdendritic Fluid Flow In a Lead-Tin Alloy, Met. Trans. B, Vol. 7B: 417-422 (1976).

12. Burton, J., Prim, R. and Slichter, W., J. Chem. Phys., vol. 21: 1987 (1953).

13. Jackson, K., Hunt, J., Uhlmann, R., Steward, On the Origin of the Equiaxed Zone in Castings, Trans. Met. Soc. AIME, vol. 236: 149 (1966).

14. Kirkaldy, J., Youdelis, W., Trans. AIME, vol. 239: 1449 (1967).

15. Flemings, M., Mehrabian, R., Nereo, G., Macrosegregation, Part II, Trans. Met. Soc. of AIME, vol. 242: 41 (1968).

16. McDonald, R., Hunt, J., Trans. AIME, vol. 245: 1993 (1969).

17. Hebditch, D., Hunt, J., Fluid Motion within the Partially Solid Region of a Casting, Met. Trans., vol. 4: 2008 (1973).

18. Fisher, B., Aspects of Macrosegregation, Ph.D. Thesis, Dept. of Metallurgy and Science of Materials, Univ. of Oxford (1974).

19. Szekely, J., Chen, J., Thermal Natural Convection in the Two-Phase Region of a Solidified Alloy, Ch. Metal. Conf., Sheffield: 218 (1971).

20. Chen, J., The Effect of Thermal Natural Convection on the Solidification of Alloys, Ph.D. Thesis, State Univ. of N.Y. (1971).

21. Narita, K., Mori, T., Freezing Rate and Internal Structure of Heavy Carbon Steel Ingots, Trans. ISIJ, vol. 12: 92 (1972).

22. Copley, S., Giamei, A., The Origin of Freckles in Unidirectional Solidified Castings, Met. Trans., vol. 1: 2193 (1970).

23. Gould, G., Freckle Segregation in Vacuum Consumable Electrode Ingots, Trans. Met. Soc. AIME, vol. 233: 1345 (1965).

24. Burns, D., Beech, J., Growth of Blowholes during the Solidification of Iron-Base Alloys, Ch. Metal. Conf., Sheffield: 229 (1971).

25. Oeters, F., Ruttiger, K., Solidification Mechanisms of Steel, ISI, no. 123: 162 (1969).

26. Pfann, W., Zone Melting, 2nd ed., John Wiley & Sons, Inc., N.Y. (1966).

27. Fischer, W., et al., Arch. Eisenh, vol. 31: 361-371 (1960).

28. Graham, S., Math Model for the Macrosegregation of Alloy Elements in VAR Ingots, p. 225 (1973).

29. Joy, G., Nutting, J., Effects of Intermetallic Phases and Non-Metallic Inclusions Upon Ductility and Fracture Behavior of Alloy Steeels, ISI, No. 145: 95 (1971).

30. Little, J., Henderson, W., Effect of Sulphides Inclusions on the Anisotropy of Ductile Charpy Shelf Energy, ISI, No. 145: 182 (1971).

31. Thornton, P., Colangelo, V., Variations of Mechanical Properties in Large Steel Formings, Met. Trans. B vol. 7B: 425 (1976).

32. Kay, et al., Thermodynamic Aspects of ESR, First International Symposium, Pittsburgh, Pa.

33. Kluyev et al., Abscheidung und bildung nichtmetallischer Einschlusse im Metall bein ESU Stal in Deutsch 590-594 (1969).

34. Frederiksson, H., Jarleborg, O., Solidification of ESR Ingots, Jour. of Metals: 32 Sept. (1971).

35. Sun, R., Pridgeon, J., Predicting Pool Shapes in a Laboratory ESR Process, Union Carbide Corp., Matl's. Systems Div., Kokomo, Indiana (1969).

36. Gulya, J., Swift, R., Improved 2 1/4 Cr-1Mo Pressure Vessel Steel through Electroslag Remelting, Trans. ASME, J. of Pressure Vessel Tech. vol. 98, Series J. (1976).

37. Maslenkov, S., Burova, Influence of Melting Methods on Segregation and Property Anisotropy in EI835 Steel, Steel in USSR, No. 2 (1972).

38. Edwards, K., Spittle, J., Inverse Segregation in Unidirectionally Solidified Al-Cu Alloys, Met. Trans.; 1004 (1972).

39. Melberg, P., Sandberg, H., Solidification Studied by ESR Remelting of High Speed Steel Scan. J. Metal: 2 (1973).

40. Sindo Kou, private communication.

41. Basaran, M., A Study of the Heat and Fluid Flow in Electroslag Remelting, Ph.D. Thesis, MIT (Appendix A), p. 112, 1974.

42. Lewis, D., J. Inst. Met. 82: 395 (1954).

43. Altenpohl, D., Fornerod, R., und Steinegger, A., Uber den Erstarrungsverlauf beim Kontinuierlichen Gieben, Z. Metallkunde, Bd.60: 576-583 (1969).

44. Peel, D., Pengelly, A., Heat Transfer, Solidification and Metallurgical Structure in the Continuous Casting of Aluminum, ISI, P123: 186 (1970).

45. Dilawari, A., Szekely, J., A Mathematical Model of Slag and Metal Flow in the ESR Process, Munich Conference, Autumn (1976).

46. Thresh, H., Crawley, A., and White, D., Trans. TMS-AIME, vol.242:819 (1968).

47. Fisher, H., and Phillips, A., Trans. TMS-AIME, vol.200: 1060 (1954).

48. Lee, J. and Raynor, G., Proc. of the Physical Soc., London, 67B: 737 (1954).

49. Tyzack, C., Raynor, G., Acta Cryst., vol.7: 505 (1954).

50. Metals Handbook, Vol. 8, A.S.M.: 259 (1973).

51. Metals Handbook, Vol. 9, A.S.M.: 330 (1973).

APPENDIX A

LIST OF SYMBOLS

(Single Terms)

Computer Notation	Algebraic Notation	Explanation of Symbols
A1L(I)	a1L	Coefficient of first degree polynomial (liquidus)
A1S(I)	a1s	Coefficient of first degree polynomial (solidus)
AOL	aOL	First coefficient of polynomial expansion (liquidus)
AOS	aOs	First coefficient of polynomial expansion (solidus)
CE	C_E	Composition of liquid eutectic
CL(I,J)	C_L	Composition of liquid
CO	C_o	Composition of liquid (liquidus)
CSE	C_{SE}	Composition of solid eutectic
CS(J)	C_S	Composition of solid
DELKA(J)	Δz	Vertical spacing increment
DEPMZ	d(r)	Depth of mushy zone
DTT		Depth of metal pool
GADS	γ	Constant value of flow factor
GE,GLEUT(I)	g_{LE}	Fraction liquid at eutectic Scheil; 2nd--non-Scheil
GL(I,J)	g_L	Fraction liquid
GRAV	g	Gravitational acceleration
GS(J)	g_s	Fraction solid

Computer Notation	Algebraic Notation	Explanation of Symbols
HC,HCC	Δr	Radial spacing increment
HEIT(I)		Maximum depth of metal pool
HTE	d	Depth of mushy zone at the center
I		Column designation
IMAX		Column at wall
ITER		Iteration step
J		Row designation
k	Δz	Vertical spacing increment
KA(I,J)	k_a	Vertical spacing increment
KAY	k_p	Partition ratio
KC	k_c	Vertical spacing increment (critical)
LOCCOM(I)	$\bar{C}_s(r)$	Average composition of column I
MAXIT1		Number of iterations in the 1st cycle
MLIQ	m_{LIQ}	Slope of liquidus
MO(I,J)	m_o	Slope of isotherm at node (I,J)
MSOL	m_{SOL}	Slope of solidus
MT(I)		Lowest row for column I
MU	μ	Viscosity
NLGL(J)	$\ln(g_L)$	Natural log of fraction liquid
NTOP		Maximum number of rows
NT(I)		Top row of column I
P(I,J)	P	Pressure at node (I,J)
PA	P_a	Atmospheric pressure

Computer Notation	Algebraic Notation	Explanation of Symbols
PDR	dP/dr	Radial pressure gradient
PDZ	dP/dz	Vertical pressure gradient
R(I,J)	r	Radius at node (I,J)
RADIUS	R	Radius of ingot
RHO(I,J)	ρ_L	Liquid density at node (I,J)
RLE	ρ_{LE}	Density of liquid eutectic
ROR(I)	r	Radius at column I
RS	ρ_s	Solid density
RSE	ρ_{SE}	Density of eutectic solid
T(I,J)	T	Temperature at node (I,J)
TE	T_E	Eutectic temperature of alloy
TL	T_L	Liquidus temperature of alloy
TM	T_M	Melting temperature of alloy
TRIG1, 2...N		Cycling command (trigger)
UR	U_r	Radial isotherm velocity
UZ(I,J)	U_z	Vertical isotherm velocity at node (I,J)
Z(I,J)	z	Z coordinate
ZILIQ		Z coordinate of liquidus center line
ZISOL		Z coordinate of solidus (cntr 1)
ZL(I)	z_{LIQ}	Z coordinate (liquidus) at column I
ZS(I)	z_{SOL}	Z coordinate (solidus) at column I

(Composite Terms)

Computer Notation	Algebraic Notation	Composite Expression	Explanation of Symbols
A1,A2,Ae			Components of AX
ANG		VZ(I,J)/ VR(I,J)	Flow line direction (radians)
AX	A	A1+A2+A3	Primary coefficient
B	B	B1+B2	Primary coefficient
B1,B2			Components of B
C	C	C3-C4*C5	Primary coefficient
CONTR	$\rho_{SE}/\rho_{LE}-1$	RSE/RLE-1	Eutectic shrinkage
CRAT	C_o-C_E	CO-CE	Composition difference
DECLR	dC_L/dr	finite diff.	Radial gradient of CL
DECLZ	dC_L/dz		Vertical gradient of CL
DEGIR	dg_L/dr		Radial gradient of GL
DEGLZ	dg_L/dz		Vertical gradient of GL
DERHOR	$d\rho_l/dr$		Radial gradient of RHO
DERHOZ	$d\rho_L/dz$		Vertical gradient of RHO
EM	m	(TE-TM)/CE	Phase Diagram slope of the Liquidus
EPPS(I,J)	ε	-UZCL*GZ(I,J)	Cooling rate
FOR(I,J)			Coefficient of the PDE
GAMMA(I,J)	γ		Flow factor
GR(I,J)	dT/dr	finite diff.	Radial gradient of T
GZ(I,J)	dT/dz		Vertical gradient of T

Computer Notation	Algebraic Notation	Composite Expression	Explanation of Symbols
HM		(HA+HB/2)	Average value of r increment
HORAT	$\rho_o - \rho_{LE}$	RO-RLE	Density difference
HTT(I)		ZL(I)-ZS(I)	Depth of mushy zone at the centerline
ONE(I,J)			Coefficient of the PDE
PERMI(I,J)	$\vec{v}\cdot\nabla T/\ \varepsilon$	GADS*(GL(I,J)**2) ZAT*(GL(I,J)**2)	Specific permeability
RARA			Rate ratio
SOLHZ	$(dP/dr)_{EUT}$	finite diff.	Pressure gradient (eut.)
SOLVE	$(dP/dz)_{EUT}$		Pressure gradient (eut.)
tart			Coefficient for the solidus-interior boundary
TATOP			Coefficient for the solidus-interior boundary
TRAT		TL-TE	Temperature difference
TRE(I,J)			Coefficient of the PDE
TTHETA	θ	$*180/\pi)*TAN^{-1}$(ANG)	Streamline angle: degrees
TWO(I,J)			Coefficient of the PDE
U		$(U_r^2 + U_z^2)$**1/2	Isotherm velocity
VTOT	v_T	(v_r+v_z)**1/2	Interdendritic velocity
W	ω		Angular velocity of mold
ZAT(I)	$\gamma(r)$	GADS(HTT(I)/ UZCL)**0.78)	Specific permeability (variable)

APPENDIX B

DERIVATIONS AND DETAILED FORMULATIONS

1. Alternative Form of the Specific Permeability

For flow through packed beds the Ergun equation of the form :

$$\frac{\Delta P}{L} = 150\frac{(1-e)^2 \mu v_0}{e^3 \ (\phi_s \ d_p)^2} + \text{Turbulent Term} \qquad (1.1)$$

relates the pressure gradient to the superficial velocity, v_0 . In the case of the mushy zone the void space, e, is in fact the fraction liquid(volume) , g_L. The turbulent term is ignored . ϕ_s is the shape factor .

$$g_L = e \qquad (1.2)$$

The particle diameter, d_p, is related to the secondary DAS :

$$d_p = \frac{4}{\pi} \lambda_2^2 (1-g_L) \qquad (1.3)$$

Inserting 1.2 and 1.3 into Eq.(1.3)

$$v_0 = \frac{\phi_s^2}{\pi \ 150\mu} \frac{\Delta P}{L} \frac{g_L^3}{(1-g_L)} \cdot \lambda_2^2 \qquad (1.4)$$

The interdendritic velocity, v :

$$v = v_0 / g_L \tag{1.5}$$

Equation (1.5) inserted into Eq.(1.4) yields

$$v = \frac{4}{\pi} \frac{\phi_s^2}{150} \frac{g_L^3}{1-g_L} \cdot \lambda_2^2 \frac{\Delta P}{L} \tag{1.6}$$

D'Arcy's law holds for the mushy zone region and is of the form :

$$v = \frac{-K}{g_L} \frac{\Delta P}{L} \tag{1.7}$$

The specific permeability can thus be specified as :

$$K = \frac{4}{\pi} \frac{\phi_s^2}{150} \frac{g_L^3}{1-g_L} \lambda_2^2 \tag{1.8}$$

The flow factor is therefore :

$$\gamma = \frac{4}{\pi} \frac{\phi_s^2}{150} \cdot \lambda_2^2 \tag{1.9}$$

2. Primary Coefficients A,B and C

The three primary coefficients are written in their expanded form in computer notation .

$$A(I,J) = \frac{1}{R(I,J)} + \frac{1}{RHO(I,J)} \frac{RHO(I+1,J) - RHO(I-1,J)}{(HA + HB)}$$

$$+ \frac{2}{GL(I,J)} \frac{GL(I+1,J) - GL(I-1,J)}{(HA + HB)}$$

$$+ \frac{1}{KAY - 1} \left\{ \frac{RHO(I,J)}{RS} - 1 \right\} \frac{1}{CL(I,J)} \frac{CL(I+1,J) - CL(I-1,J)}{(HA + HB)}$$

$$B(I,J) = \frac{1}{RHO(I,J)} * \frac{RHO(I,J+1) - RHO(I,J-1)}{2*KA}$$

$$+ \frac{2}{GL(I,J)} * \frac{GL(I,J+1) - GL(I,J-1)}{2*KA}$$

$$+ \frac{1}{KAY - 1} \left\{ \frac{RHO(I,J)}{RS} - 1 \right\} \frac{1}{CL(I,J)} * \frac{CL(I,J+1) - CL(I,J-1)}{2*KA}$$

$$C(I,J) = GRAV*RHO(I,J)*\left\{\frac{2}{RHO(I,J)}\,\frac{RHO(I,J+1)-RHO(I,J-1)}{2*KA}\right.$$

$$+\quad \frac{2}{GL(I,J)} * \frac{GL(I,J+1)-GL(I,J-1)}{2KA}$$

$$+\quad \left\{\frac{1}{KAY-1}\right\}\left\{\frac{RHO(I,J)-1}{RS}\right\}\frac{1}{CL(I,J)}\,\frac{CL(I,J+1)-CL(I,J-1)}{2*KA}\left.\right\}$$

$$-\quad \frac{EPPS(I,J)*MU}{EM*GAMMA*GL(I,J)}\left\{\frac{1}{RHO(I,J)}\,\frac{RHO(I,J+1)-RHO(I,J-1)}{CL(I,J+1)-CL(I,J-1)}\right.$$

$$+\quad \frac{1}{KAY-1}\left\{\frac{RHO(I,J)}{RS} - 1\right\} * \frac{1}{CL(I,J)}\left.\right\}$$

3. FINITE DIFFERENCE FORM OF THE PARTIAL DIFFERENTIAL EQUATION (PRESSURE TERMS)

The pressure gradients for the mushy zone are examined . Exact gradients are approximated by finite difference forms .Refer to Fig.(B7) for nodal arrangement .The first order term in algebraic form for node (i,j) are :

$$\frac{\partial P}{\partial z} \quad \cong \left\{\frac{\Delta P}{\Delta z}\right\}_j = \frac{P(i,j+1)-P(i,j-1)}{k_a+k_b}$$

and

$$\frac{\partial P}{\partial r} \quad \cong \left\{\frac{\Delta P}{\Delta r}\right\}_i = \frac{P(i+1,j)-P(i-1,j)}{h_a+h_b}$$

The second order terms are now investigated .Let

$$h_a = h_b \qquad \text{and}$$

$$k_a = k_b .$$

$$\frac{\partial^2 P}{\partial z^2} \cong \frac{\left\{\frac{\Delta P}{\Delta z}\right\}_{j+\frac{1}{2}} - \left\{\frac{\Delta P}{\Delta z}\right\}_{j-\frac{1}{2}}}{\Delta z} = \frac{P(i,j+1)+P(i,j-1)-2P(i,j)}{k_a^2}$$

and

$$\frac{\partial^2 P}{\partial r^2} \cong \frac{\left\{\frac{\Delta P}{\Delta r}\right\}_{i+\frac{1}{2}} - \left\{\frac{\Delta P}{\Delta r}\right\}_{i-\frac{1}{2}}}{\Delta r} = \frac{P(i+1,j)+P(i-1,j)-2P(i,j)}{h_a^2}$$

The simple form of the PDE of elliptic type is :

$$\frac{\Delta^2 P}{\Delta r^2} + \frac{\Delta^2 P}{\Delta z^2} + A\frac{\Delta P}{\Delta r} + B\frac{\Delta P}{\Delta z} + C = 0$$

In expanded form(algebraic notation) it is :

$$\frac{P(i+1,j)+P(i-1,j)-2P(i,j)}{h_a^2} + \frac{P(i,j+1)+P(i,j-1)-2P(i,j)}{k_a^2}$$

$$+ A*\left\{\frac{P(i+1,j)-P(i-1,j)}{2*h_a}\right\} + B*\left\{\frac{P(i,j+1)-P(i,j-1)}{2*k_a}\right\}$$

$$+ C = 0$$

4. Finite Difference Form of Pressure Derivatives Having Unequal Grid Spacings

Since the program is written so that unequal grid spacings are possible the form of the finite difference approximations for the 1_{st} and 2_{nd} order derivatives will be more involved than those found in Derivation 3 .Ultimately, the form of the pressure equation is altered .This is seen in Derivation 6 .

The 1_{st} order derivative in finite difference form (FD) is now written :

$$\frac{\Delta P}{\Delta r} = \frac{h_b}{h_a+h_b}\left\{\frac{P(i+1,j) - P(i,j)}{h_a}\right\} + \frac{h_a}{h_a+h_b}\left\{\frac{P(i,j)-P(i-1,j)}{h_b}\right\} \tag{4.1}$$

In expanded form it is :

$$\frac{\Delta P}{\Delta r} = \frac{h_b^2 \cdot P(i+1,j) - h_a^2 \cdot P(i-1,j) + (h_a^2 - h_b^2) \cdot P(i,j)}{\left(h_a + h_b\right) h_a \cdot h_b} \tag{4.2}$$

In (FD) form the 2_{nd} derivative is written as :

$$\frac{\Delta^2 P}{\Delta r^2} = \frac{\frac{h_b}{h_m}\left\{\frac{P(i+1,j)-P(i,j)}{h_a}\right\} - \frac{h_a}{h_m}\left\{\frac{P(i,j)-P(i-1,j)}{h_a}\right\}}{h_m} \tag{4.3}$$

In expanded form it is :

$$P = \frac{h_b^2 P(i+1,j) + h_a^2 P(i-1,j) - (h_a^2 + h_b^2) P(i,j)}{h_m^2 \, h_a \, h_b} \qquad (4.4)$$

where :

$$h_m = \frac{h_a + h_b}{2.0}$$

5. Segmented Orthogonal Trajectories

Within the program there is a sequence which allows for temperature distributions to be determined along orthogonal trajectories .The orthogonal trajectories are approximate .For a given node two linear segments are coupled Each is linear One is orthogonal to the solidus isotherm and the other is orthogonal to the liquidus isotherm .

Examine Fig.(B5) a point ,P_o .Segment s_L joins P_0 to the liquidus and segment s_S joins the solidus to P_0 .If the slope of the liquidus ,m_L, is :

$$m_L = c/a \qquad (5.1)$$

where c and a are the lengths shown in Fig (B5) a then angle θ_L :

$$\theta_L = \tan^{-1}(m_L) \qquad (5.2)$$

This angle is shown in Fig.(B5) b .The segment length s_L :

$$s_L = c \cdot \cos(\theta_L) \qquad (5.3)$$

Likewise, since :

$$m_S = d/b \qquad (5.4)$$

and

$$\theta_S = \tan^{-1}(m_S) \qquad (5.5)$$

then

$$s_S = d \cos(\theta_s) \qquad (5.6)$$

The total length of the approximated arc ,s_T :

$$s_T = s_L + s_S \qquad (5.7)$$

If the temperature distribution along the arc length s_T is linear then :

$$T_o = T_E + \left\{ \frac{s_S}{s_S + s_L} \right\} (T_L - T_E) \qquad (5.8)$$

is the temperature at point P_o .If the slope of the isotherm passing through point P_o need be calculated ,m_o,then the following expressions are used .Refer to Fig.(B5) c .

$$x = s_H / \left\{ \frac{\tan\theta_S}{\tan\theta_L} - 1 \right\} \quad \text{and} \quad m_o = \tan\psi = x \cdot \tan\theta_{S/(b+x)} \qquad (5.9,10)$$

Figure B 5

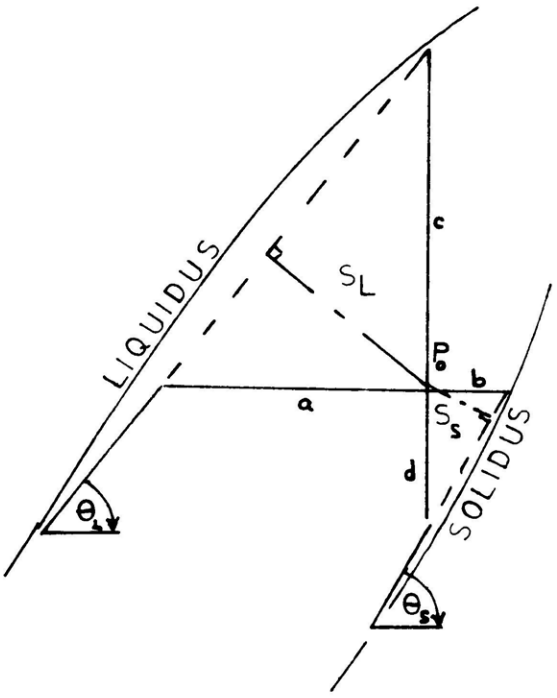

(a)

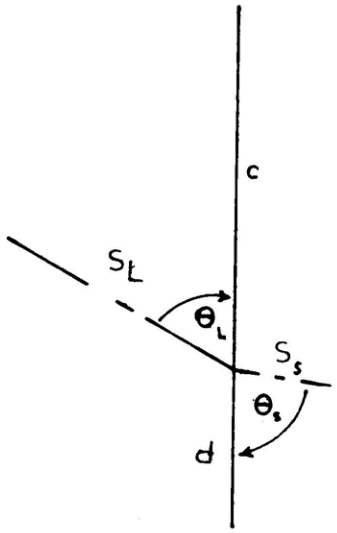

(b)

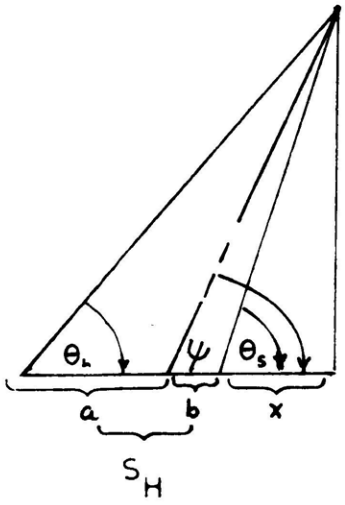

(c)

6.Composite Coefficients in Expanded Algebraic Form

The composite coefficients in algebraic form are referred to as :a,b,c,d and e .The first four are composed of two separate terms . The first term is an arrangement of the spatial increments of the grid The second is a geometrical term multiplied times a primary coefficient A,B or C .Notice that all the terms except e include $\theta_{i,j}$ which is given as :

$$\theta_{i,j} = 2*(h_a \cdot h_b \cdot h_m \cdot k_a + k_a^3 \cdot h_m) \qquad (6.1)$$

The five composites are listed :

$$a(i,j) = \frac{k_a^3 \cdot h_b}{\theta_{i,j}} + \frac{k_a^3 \cdot h_a \cdot h_b}{2\theta_{i,j}} * A(i,j)$$

$$b(i,j) = \frac{h_a \cdot h_b \cdot h_m \cdot k_a}{\theta_{i,j}} + \frac{k_a^2 \cdot h_a \cdot h_b \cdot h_m}{2\theta_{i,j}} * B(i,j)$$

$$c(i,j) = \frac{k_a^3 \cdot h_a}{\theta_{i,j}} - \frac{k_a^3 \cdot h_a \cdot h_b}{2\theta_{i,j}} * A(i,j)$$

$$d(i,j) = \frac{h_a \cdot h_b \cdot h_m \cdot k_a}{\theta_{i,j}} - \frac{k_a^2 \cdot h_a \cdot h_b \cdot h_m}{2\theta_{i,j}} * B(i,j)$$

$$e(i,j) = k_a^3 \, h_a \, h_b \, h_m * C(i,j)$$

The terms simplify considerably if

$$h_a = h_b \quad .$$

Equivalent terms in computer notation for the composite coefficients are :

$$ONE(I,J) = a(i,j) \quad , \quad TRE(I,J) = c(i,j)$$

$$TWO(I,J) = b(i,j) \quad , \quad FOR(I,J) = d(i,j)$$

and $KONST(I,J) = e(i,j)$

where : $THETA(I,J) = \theta(i,j)$.

The final form of the pressure equation (PDE) in computer notation is written as :

$$\begin{aligned} P(I,J) = {} & ONE(I,J)*P(I+1,J) + TWO(I,J)*P(I,J+1) \\ & + TRE(I,J)*P(I-1,J) + FOR(I,J)*P(I,J-1) \\ & + KONST(I,J) \end{aligned}$$

7. Solidus - Interior Boundary

The solidus-interior boundary needs special boundary conditions .In finite difference form the pressure equation is composed of two parts :

1) terms including pressures from the interior of the mushy zone , and

2) the pressure gradient equivalents at the eutectic .

Both parts are essential for defining the pressure distribution in this region of the mushy zone .

Also it is realized that the shape of the isotherms plays an important role .Three cases are presented for the 3 possible geometries .Refer to Figures (B7) a,b and c .

a.(Flat & Nearly Flat Isotherms)

The pressure gradient at the eutectic as symbolized by k_v for the vertical component is :

$$k_v = \frac{P(i,j) - P(i,j-1)}{k} = \frac{\mu g_{LE}}{K}\left\{\frac{\rho_{SE}}{\rho_{LE}} - 1\right\} U_{ZE} + g\rho_{LE} \qquad (7.1)$$

If $$\theta_o = \frac{1}{k^2} + \frac{2}{h_a(h_a+h_b)} + \frac{2}{h_b(h_a+h_b)} + \frac{B}{2k} + \frac{(h_b-h_a)\cdot A}{(h_a+h_b)} \qquad (7.2)$$

then the final form of the pressure equation at the solidus-interior incorporating both Eq.'s(7.1) and (7.2) is written as :

$$P(i,j) = \frac{1}{\theta_o}\left\{\left\{\frac{2}{h_a(h_a+h_b)} + \frac{h_b\cdot A}{h_a(h_a+h_b)}\right\} * P(i+1,j) + \left\{\frac{1}{k^2} + \frac{B}{2k}\right\}P(i,j+1) + \left\{\frac{2}{h_b(h_a+h_b)} - \frac{h_a\cdot A}{h_b(h_a+h_b)}\right\}P(i-1,j) + k_v\left\{\frac{B}{2} - \frac{1}{k}\right\} + C\right\} \qquad (7.3)$$

b.(Steep Isotherms)

If on the other hand the isotherms are steep then the solidus-interior equation for pressure involves the radial pressure gradient of the eutectic , k_H , which is :

$$k_H = \frac{P(i+1,j) - P(i,j)}{h_a} = \frac{\mu g_{LE}}{K}\left\{\frac{\rho_{SE}}{\rho_{LE}} - 1\right\} U_{rE} \qquad (7.4)$$

Also the term $$\theta_1 = 2 + \frac{2k^2}{h_b(h_a+h_b)} - \frac{h_a \cdot k^2 \cdot A}{h_b(h_a+h_b)} \qquad (7.5)$$

Both Eq. (7.4) and (7.5) are incorporated in the final pressure expression :

$$P(i,j) = \frac{1}{\theta_1}\left\{(1 + \frac{B\cdot k}{2})P(i,j+1)\right.$$
$$+ \left\{\frac{2\cdot k^2}{h_b(h_a+h_b)} - \frac{h_a \cdot k^2 \cdot A}{h_b(h_a+h_b)}\right\}P(i-1,j)$$
$$+ \left\{1 - \frac{B\cdot k}{2}\right\}P(i,j-1)$$
$$\left. + \frac{k_H \cdot 2 \cdot k^2}{(h_a+h_b)} + \frac{k_H \cdot h_b \cdot k^2 \cdot A}{(h_a + h_b)} + k^2 * C\right\} \qquad (7.6)$$

c.(Moderate Isotherms)

For moderate isotherm geometries at the solidus it is necessary to incorporate both gradients,Eq.'s (7.1) and (7.4) along with the following expression :

$$\theta_2 = \frac{1}{k^2} + \frac{2}{h_b\cdot(h_a+h_b)} + \frac{B}{2\cdot k} - \frac{h_a\cdot A}{h_b\cdot(h_a+h_b)} \qquad (7.7)$$

to attain the following expression :

$$P(i,j) = \frac{1}{\theta_2}\left\{\left\{\frac{1}{k^2} + \frac{B}{2\cdot k}\right\}P(i,j+1) + \left\{\frac{2}{h_b(h_a+h_b)} - \frac{h_a A}{h_b(h_a+h_b)}\right\}P(i-1,j) + \frac{k_H(2+h_b A)}{(h_a+h_b)} + \left\{\frac{B}{2} - \frac{1}{k}\right\}k_v + C\right\} \qquad (7.8)$$

Notice that the term containing k_H should be visualized as a $P(i+1,j)$ term as the k_v term ought to be recognized as the $P(i,j-1)$ term .

In computer notation the following equivalents exist :

$$\text{SOLVE} = k_v \; ; \quad \text{COFO} = \theta_o \; ;$$

$$\text{SOLHZ} = k_H \; ; \quad \text{COF1} = \theta_1 \; ;$$

$$\text{and} \quad \text{COF2} = \theta_2$$

Likewise the pressure expression in computer notation is :

```
P(I,J) = TART(I,IXX)*P(I+1,J) +TATOP(I,IXX)*P(I,J+1)
       +
         TALEFT(I,IXX)*P(I-1,J) +TABOT(I,IXX)*P(I,J-1)
       +
         TAKONS(I,IXX)          .
```

The five terms :SOLVE,COFO , etc. are found in the TA____ coefficients .Notice the similarity of this expression with that of the partial differential equation (in expanded algebraic form) for the interior .

Figure B 7

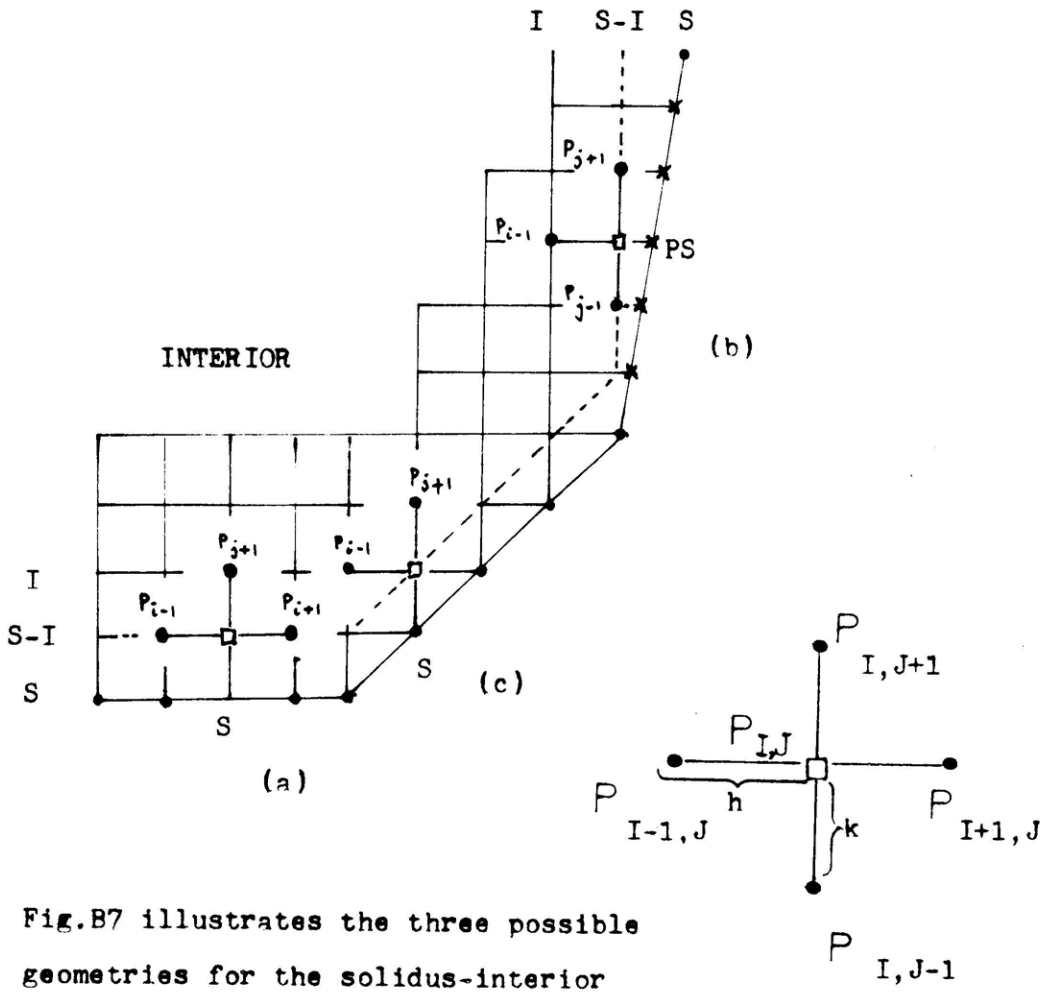

Fig.B7 illustrates the three possible geometries for the solidus-interior boundary . The flat geometry is (a) while (b) is steep and (c) is moderate .

8. Simple Device for Approximating Solute Composition Trends

The local solute redistribution equation is :

$$\frac{\partial g_L}{\partial C_L} = -\frac{1-\beta}{1-k_p}\left\{1 + \frac{\vec{V}\cdot\nabla T}{\varepsilon}\right\}\frac{g_L}{C_L} \qquad (8.1)$$

Since β and k_p are constants let :

$$c = \frac{1-\beta}{1-k_p} > 0 \qquad (8.2)$$

Let $R = \frac{\vec{V}\cdot\nabla T}{\varepsilon}$ for convenience also .Rearranging Eq.(8.1) and inserting (8.2)

$$\frac{\partial C_L}{C_L} = -\frac{1}{c}\left\{\frac{1}{1+R}\right\}\frac{\partial g_L}{g_L} \qquad (8.3)$$

The integral

$$\int_1^{1-g_{LE}} \frac{1}{g_L}\, dg_L < 0 \qquad (8.4)$$

is always negative .For simplification assume that R is independent of fraction liquid. Though not strictly true since velocity is a function of g_L this allows Eq.(8.3) to be integrated .The result is :

$$\ln C_L \propto \frac{1}{1+R} \qquad (8.5)$$

In other words

$$C_L \propto \exp\left\{\frac{1}{1+R}\right\} \tag{8.6}$$

Since

$$e^x = 1+x+x^2/2! +....$$

then

$$C_L \propto 1 + \frac{1}{1+R} + \frac{1}{2}\left(\frac{1}{1+R}\right)^2 \tag{8.7}$$

For small values of $1/(1+R)$:

$$C_L \propto \frac{1}{1+R} \tag{8.8}$$

and therefore :

$$C_s \propto \frac{1}{1+R} \tag{8.9}$$

Assuming an average value of R ,$\bar{R}$, the ingot composition at discrete radii ,$\bar{C}_s$, can be determined .For a given column the final form is :

$$C_s(r) \qquad \frac{1}{1+\frac{\vec{\nabla}\cdot\nabla T(r)}{\epsilon}}$$

where $\frac{\vec{\nabla}\cdot\nabla T(r)}{\epsilon}$ is the average value of the rate ratio for a given radius ,r .

9. Cooling Rate in Terms of UZCL and dT/dz

The major assumptions are : 1)steady state ,and
2)linear temperature distributions

hold for the mushy zone during solidification .If m is the slope of an isotherm then the following hold :

$$U_z = U_{ZCL}/(1+m^2) \qquad \text{and} \qquad U_r = -m \cdot U_Z \qquad (9.1,2)$$

$$dT/dz = \Delta T/d(r) \qquad \text{and} \qquad dT/dr = -m \cdot dT/dz \qquad (9.3,4)$$

The cooling rate in this 2D situation is :

$$\varepsilon = -\left\{U_Z \cdot dT/dz + U_r \cdot dT/dr\right\} \qquad (9.5)$$

Upon inserting Equations (9.1 - 9.4) into (9.5) the following results :

$$\varepsilon(r) = -\, U_{ZCL} \frac{\Delta T}{d(r)} \qquad (9.6)$$

where d(r) is the depth of the mushy zone at radius r and

$$\Delta T = T_L - T_E \qquad (9.7)$$

In computer notation (CN) Eq.(9.6) is:

```
EPPS(I,J) =-UZCL*GZ(I,J)                    (9.6)
```

10. Relationship of the Secondary DAS to UZCL and the Depth of the Mushy Zone (DEPMZ)

From Bower et al[5] the relationship :

$$1/\lambda_2 = \tilde{c}\ \theta_f^{-n}(r) \qquad (10.1)$$

was determined for secondary DAS, λ_2, where $\theta_f(r)$ is the local solidification time at radius,r .The exponent ,n, is experimentally determined .The relationship :

$$\theta_f(r) = -\ \Delta T/\dot{\varepsilon}\ (r) \qquad (10.2)$$

is the local solidification time expressed in terms of the cooling rate at the given radius .Recalling Derivation (9.6) for $\dot{\varepsilon}(r)$ insert it into (10.2) to get :

$$\theta_f(r) = d(r)/U_{ZCL} \qquad (10.3)$$

Upon inserting (10.3) into (10.1) the form :

$$\lambda_2 = \frac{1}{\tilde{c}}\left\{\frac{d(r)}{U_{ZCL}}\right\}^n \qquad (10.4)$$

emerges .This says that the secondary DAS, λ_2, is proportional to the depth of the mushy zone .The depth is allowed to vary as a function of radius .Assuming the specific permeability to be pro-

portional to λ_2^2, then :

$$K = \text{constant}\ \lambda_2^2 g_L^{\ 2} \ . \qquad (10.5)$$

This is written in the program as :

```
PERMI(I,J) = nO.*(( DEPMZ/UZCL)**2*n))
           * (GL(I,J)**2)                    (10.6)
```

11. The Average Fraction Liquid, $\bar{g}_L$, for a Given Nominal Composition

The fraction liquid average is a function of the temperature, T such that :

$$\bar{g}_L = \int_{T_E}^{T_L} g_{L(T)}\ dT \Big/ \int_{T_E}^{T_L} dT \qquad (11.1)$$

Assume that a good approximation of this temperature relationship is the Scheil equation :

$$g_L(T) = \frac{-m\,C_o}{T_M - T}^{\frac{1}{1-k_p}} \qquad (11.2)$$

Inserting Eq.(11.2) into (11.1) and carrying out the integration yields :

$$\bar{g}_L(T) = \frac{-mC_o}{T_o}^{\frac{1}{1-k_p}} * \frac{\left(T_M - T\right)\left(1 - \frac{1}{1-k_p}\right)}{\left\{1 - \frac{1}{1-k_p}\right\}\left(\frac{-1}{1}\right)}\Bigg|_{TE}^{T_L} \qquad (11.4)$$

where : $T_L = m(C_O - C_E) + T_E$ (11.4)

and m is the slope of the liquidus on the phase diagram .It is important to realize that the functional relationship of fraction liquid to temperature is ultimately tied to the nominal composition, C_O which is evinced in Eq.(11.4) .If $k_p < 1$ then $g_L(T)$ or $g_L(C_O)$ increases as C_O increases .The limiting value of unity occurs at the eutectic composition .

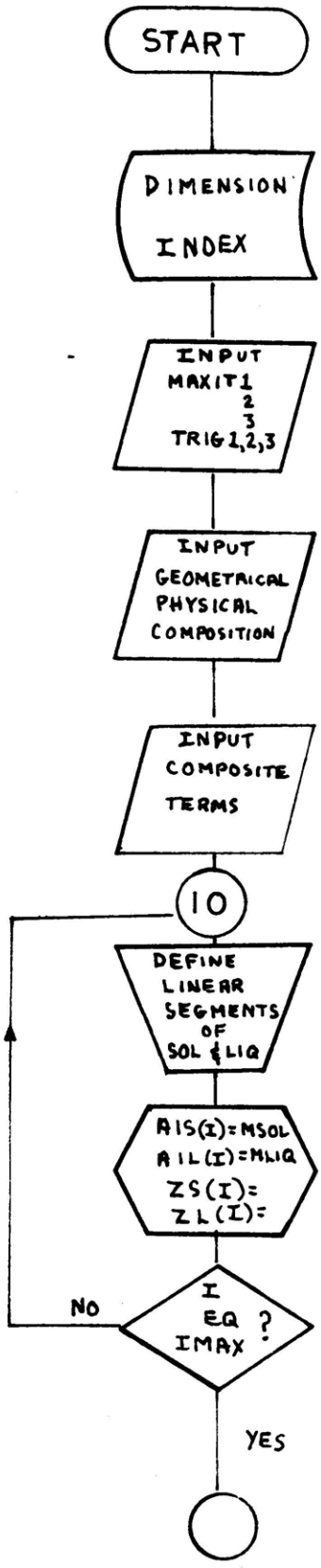

COMPUTER FLOW CHART II

This is a two dimensional system and therefore parameters within the grid will have 1 or 2 indices for ID . Storage is based upon size .

Input Region

Within this zone specified are :

Iteration requirements ,
Geometric stipulations and
Physical-thermal data

Sequence 1

The solidus and liquidus are constructed of joined linear segments.

Slopes { solidus A1S(I); liquidus A1L(I) }

Tentative coordinates are assigned :

Liquidus point--(ROR(I), ZL(I))

Operation A

Determination of column endpoints :
liquidus--NT(I)
solidus --MT(I)

for nodes ZL(I) andZS(I) respectively .The depth of the mushy zone is labeled HTT(I) .

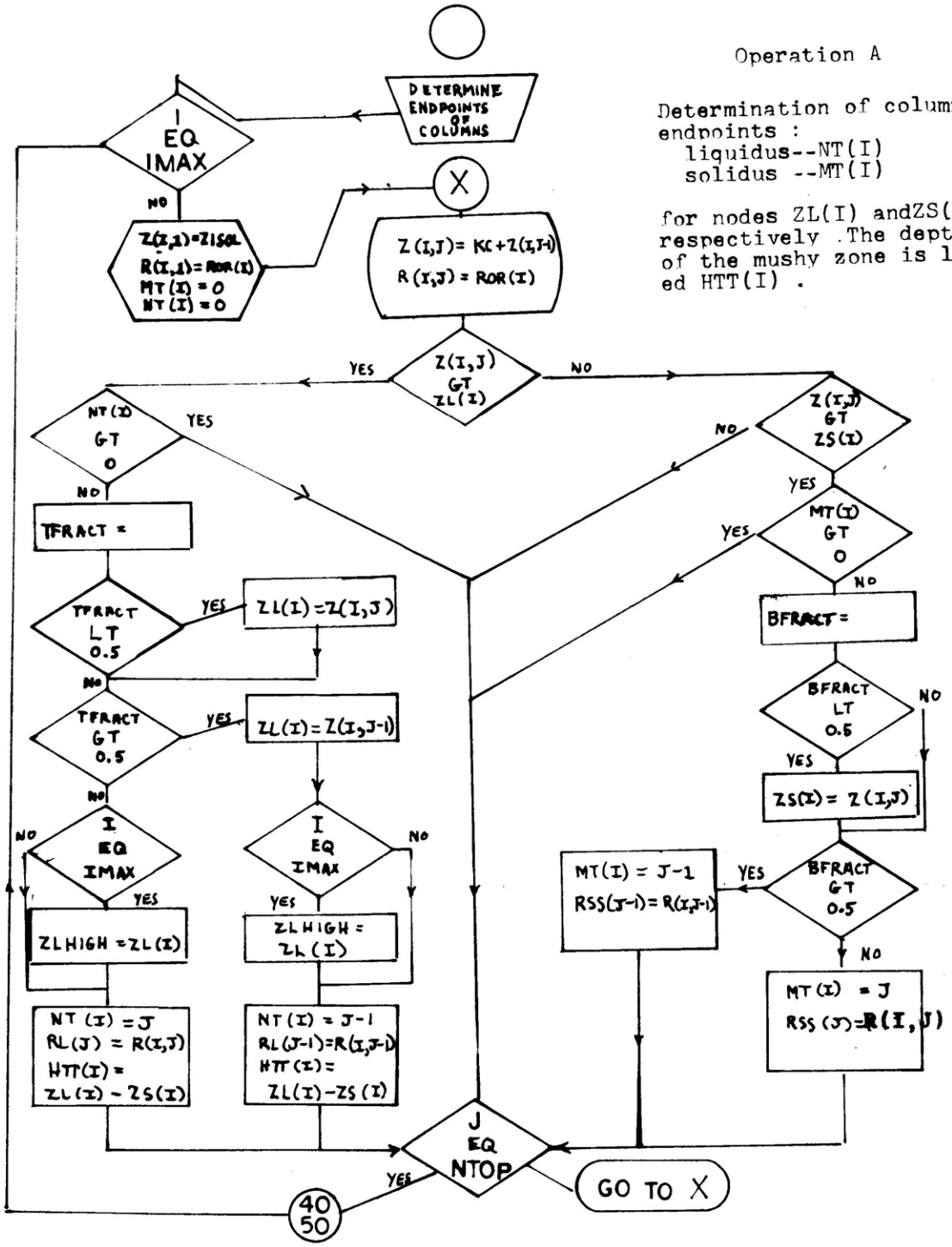

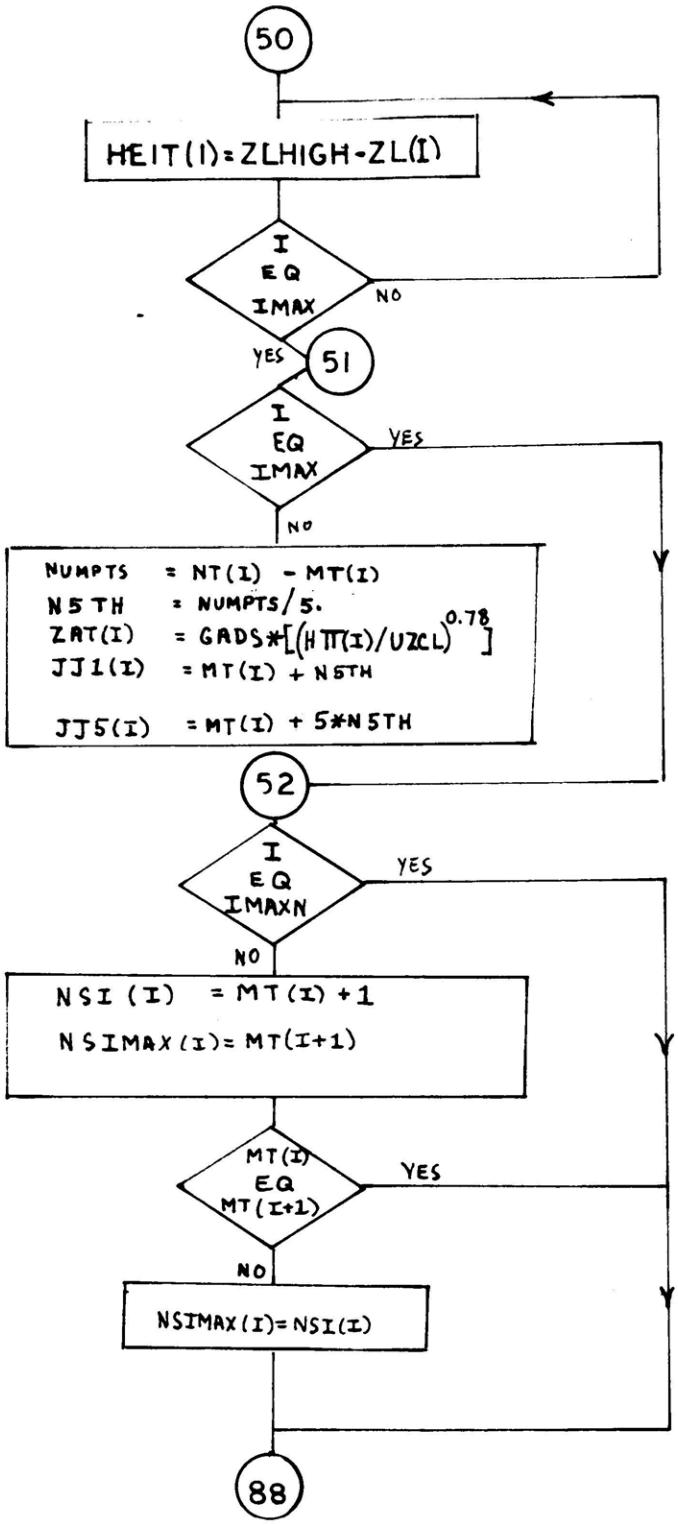

Sequence 2

The depth of the liquid metal pool above the 2-phase region is determined .

depth = HEIT(I)

Sequence 3

For formatting convenience each column is divided into 5 equally spaced segments . The secondary DAS term, ZAT(I) is evaluated for use in the specific permeability term , PERMI(I,J) .

Sequence 4

The pseudo-solidus boundary points are determined .

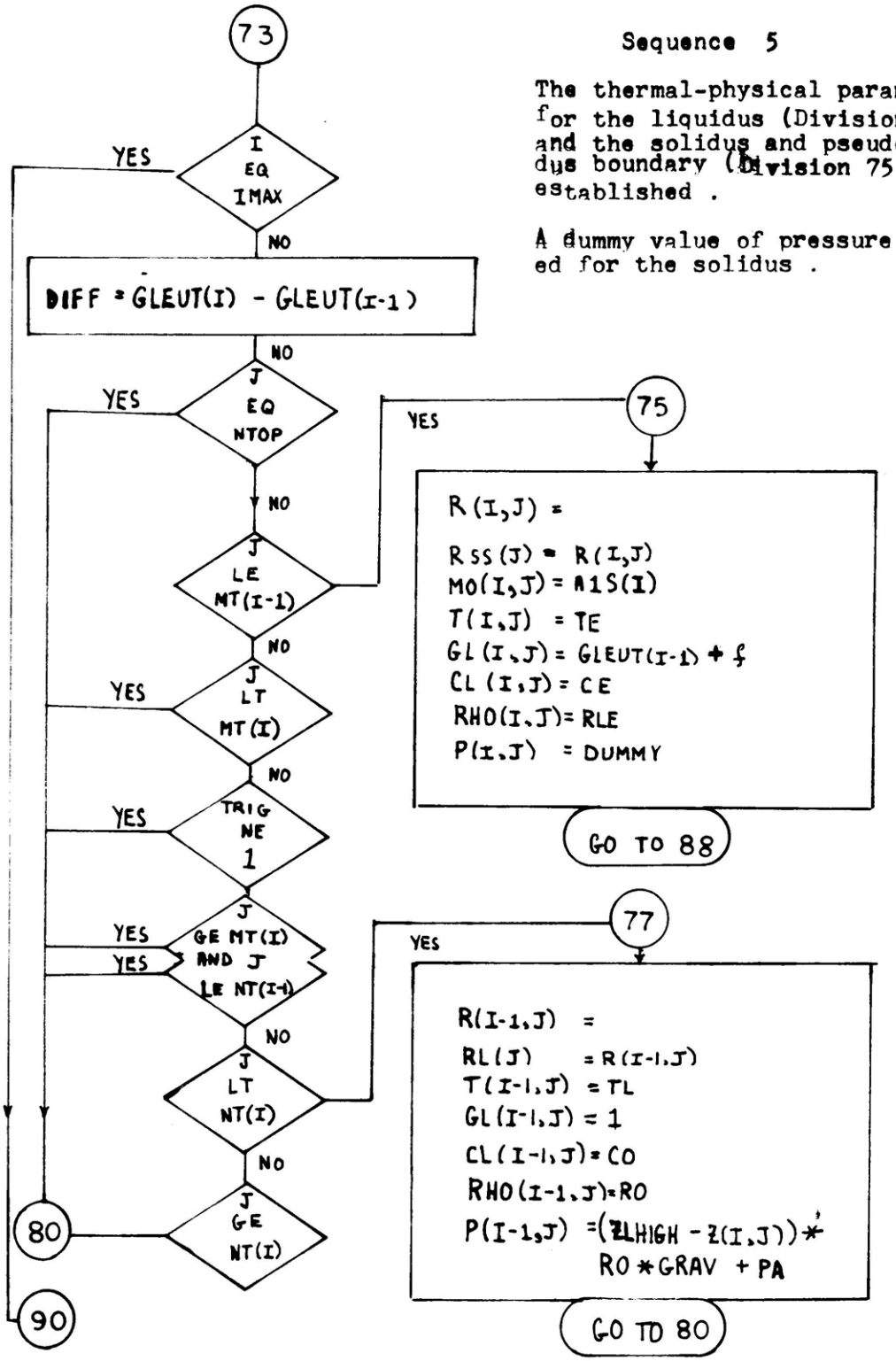

Sequence 5

The thermal-physical parameters for the liquidus (Division 77) and the solidus and pseudo-solidus boundary (Division 75) are established .

A dummy value of pressure is listed for the solidus .

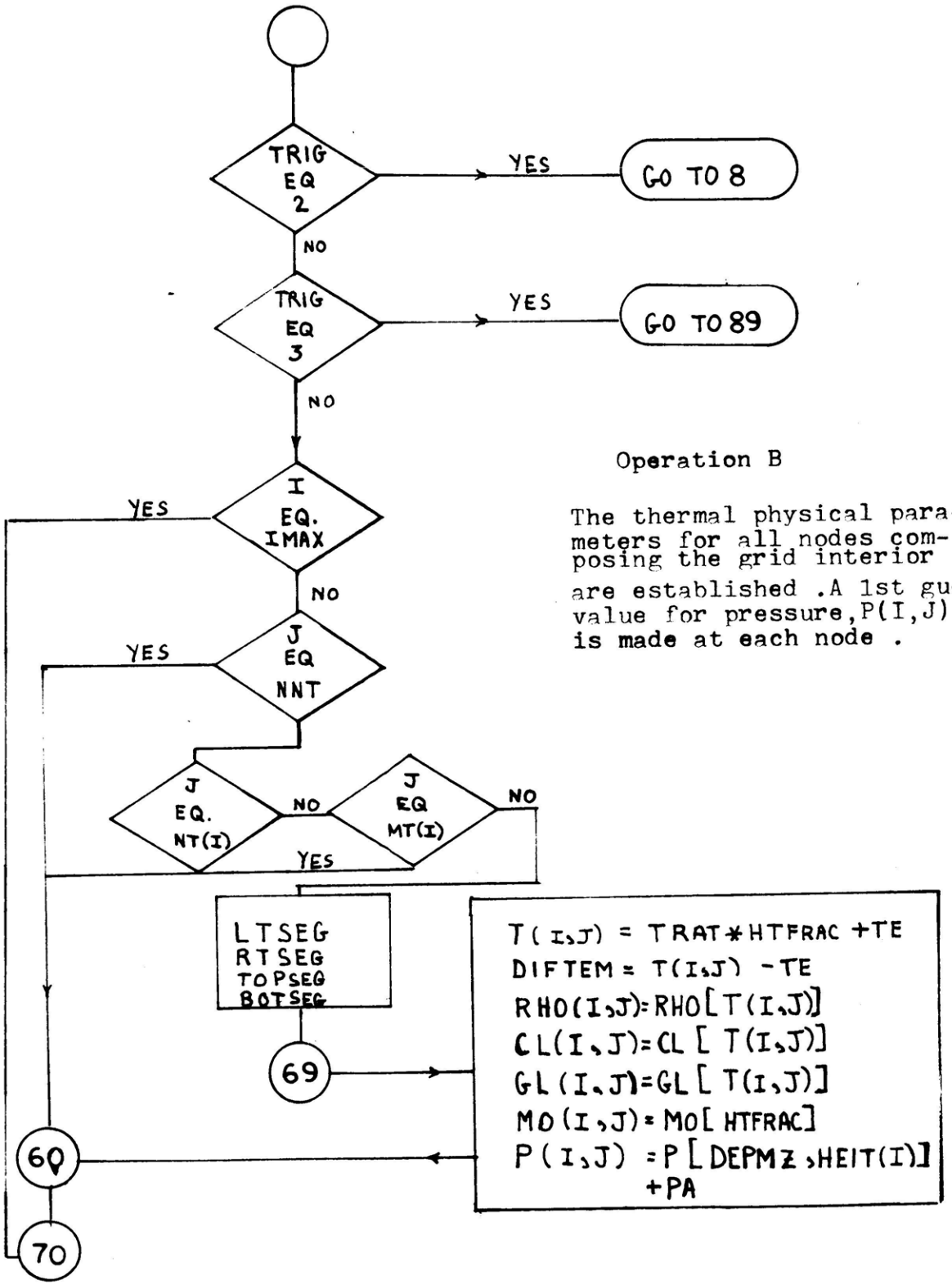

Operation B

The thermal physical parameters for all nodes composing the grid interior are established .A 1st guess value for pressure, P(I,J), is made at each node .

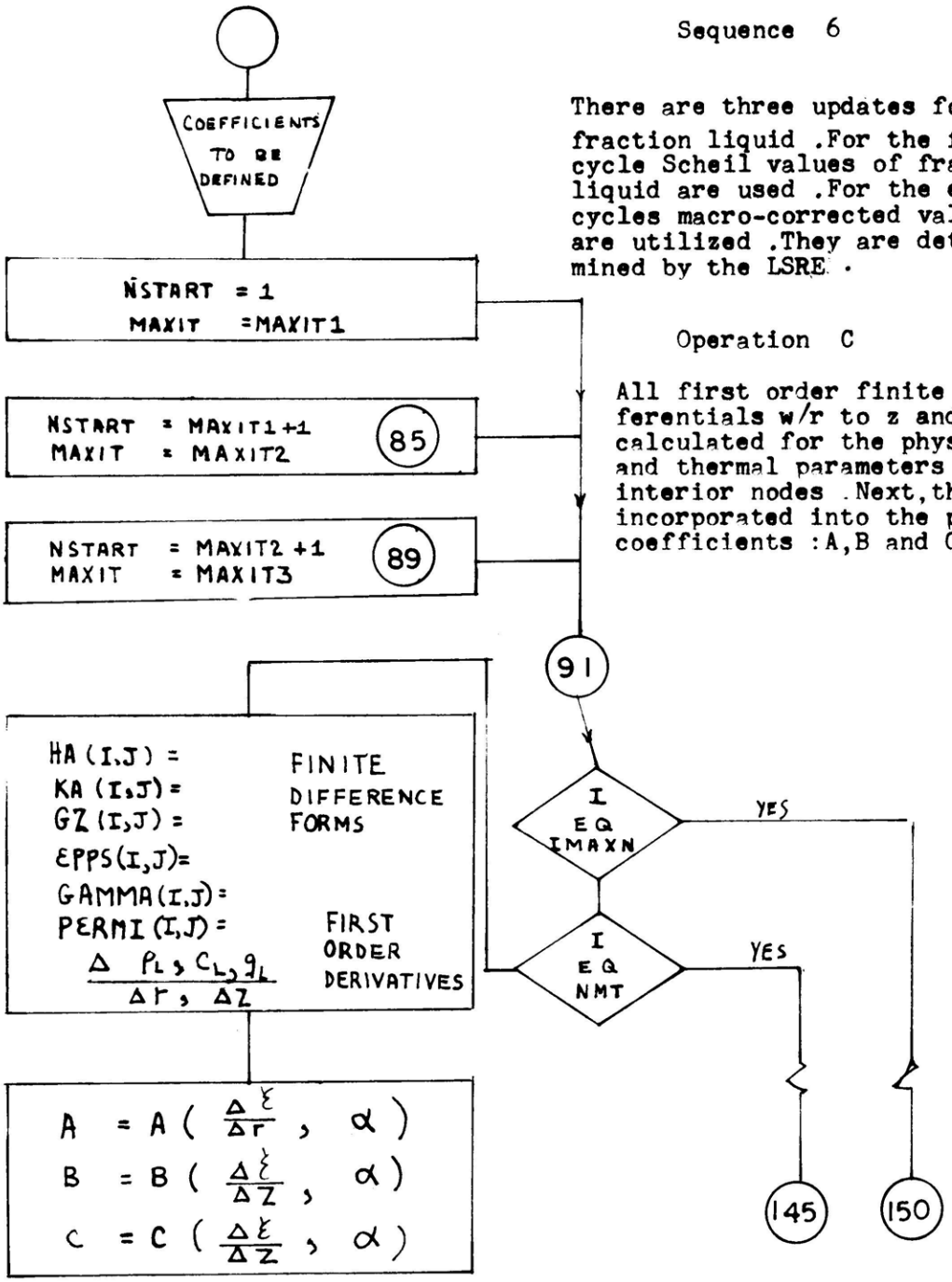

Sequence 6

There are three updates for fraction liquid .For the first cycle Scheil values of fraction liquid are used .For the ensueing cycles macro-corrected values are utilized .They are determined by the LSRE .

Operation C

All first order finite differentials w/r to z and r are calculated for the physical and thermal parameters at all interior nodes .Next,they are incorporated into the primary coefficients :A,B and C .

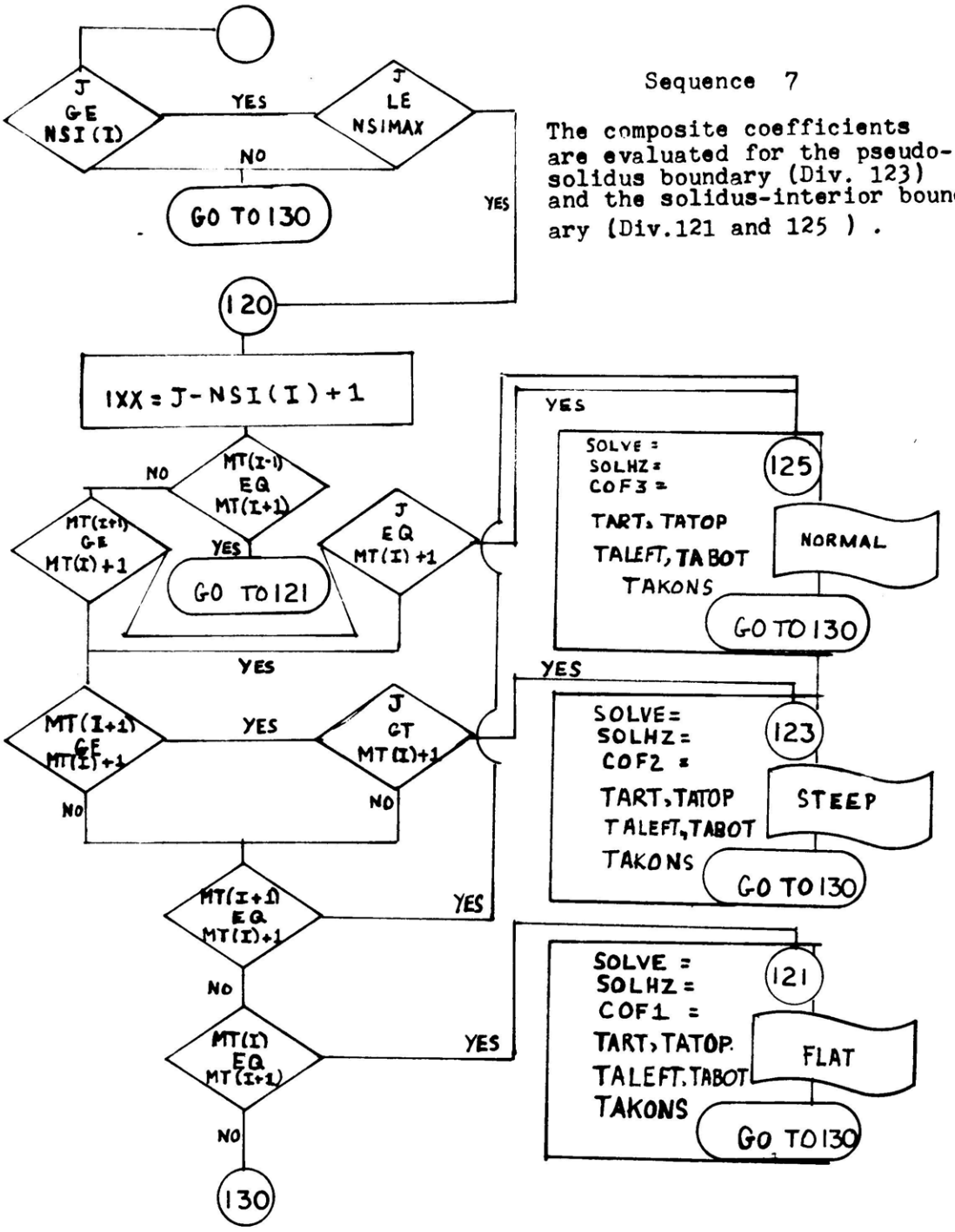

Sequence 7

The composite coefficients are evaluated for the pseudo-solidus boundary (Div. 123) and the solidus-interior boundary (Div.121 and 125) .

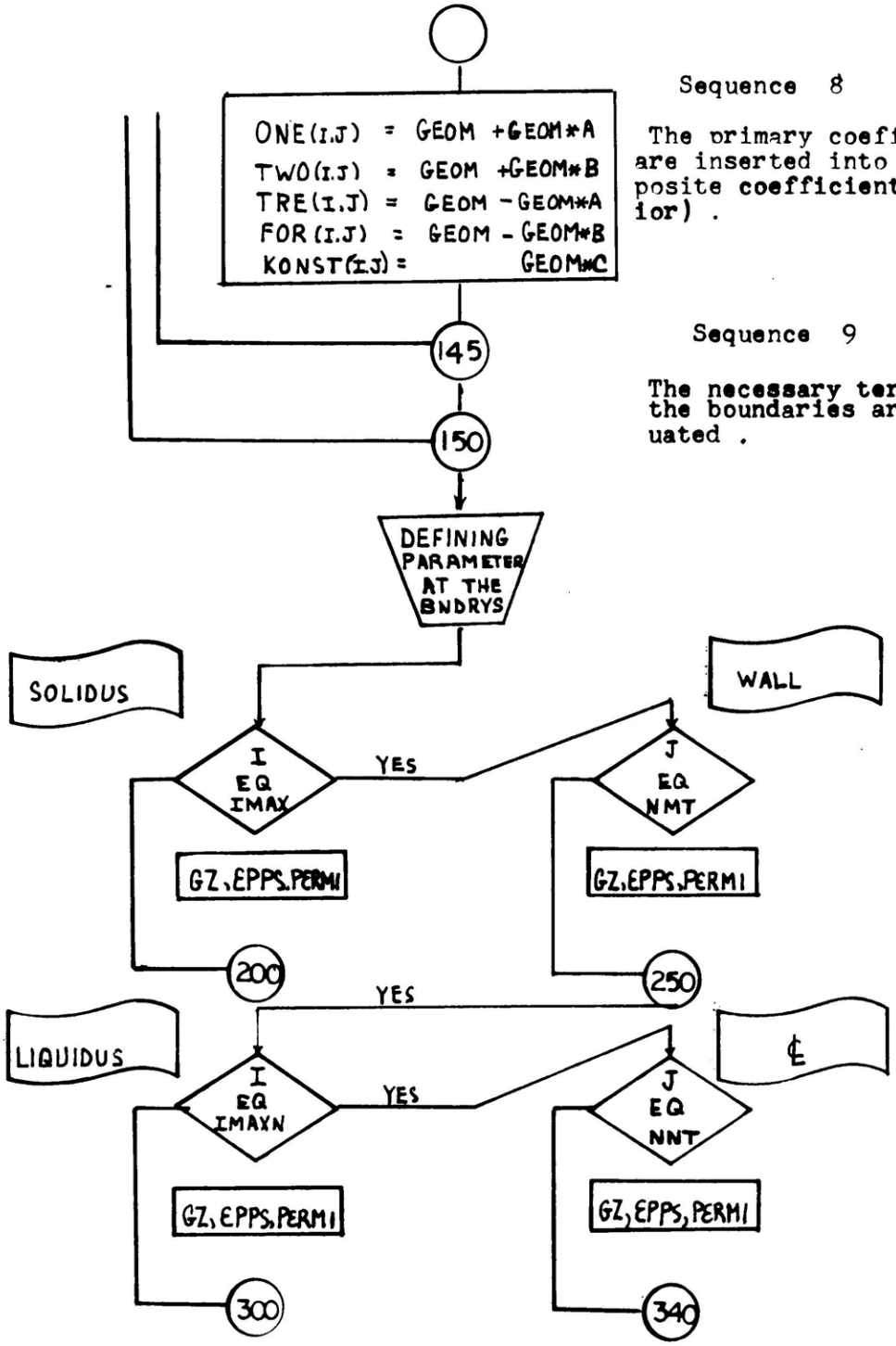

Sequence 8

The primary coefficients are inserted into the composite coefficients(Interior) .

Sequence 9

The necessary terms for the boundaries are evaluated .

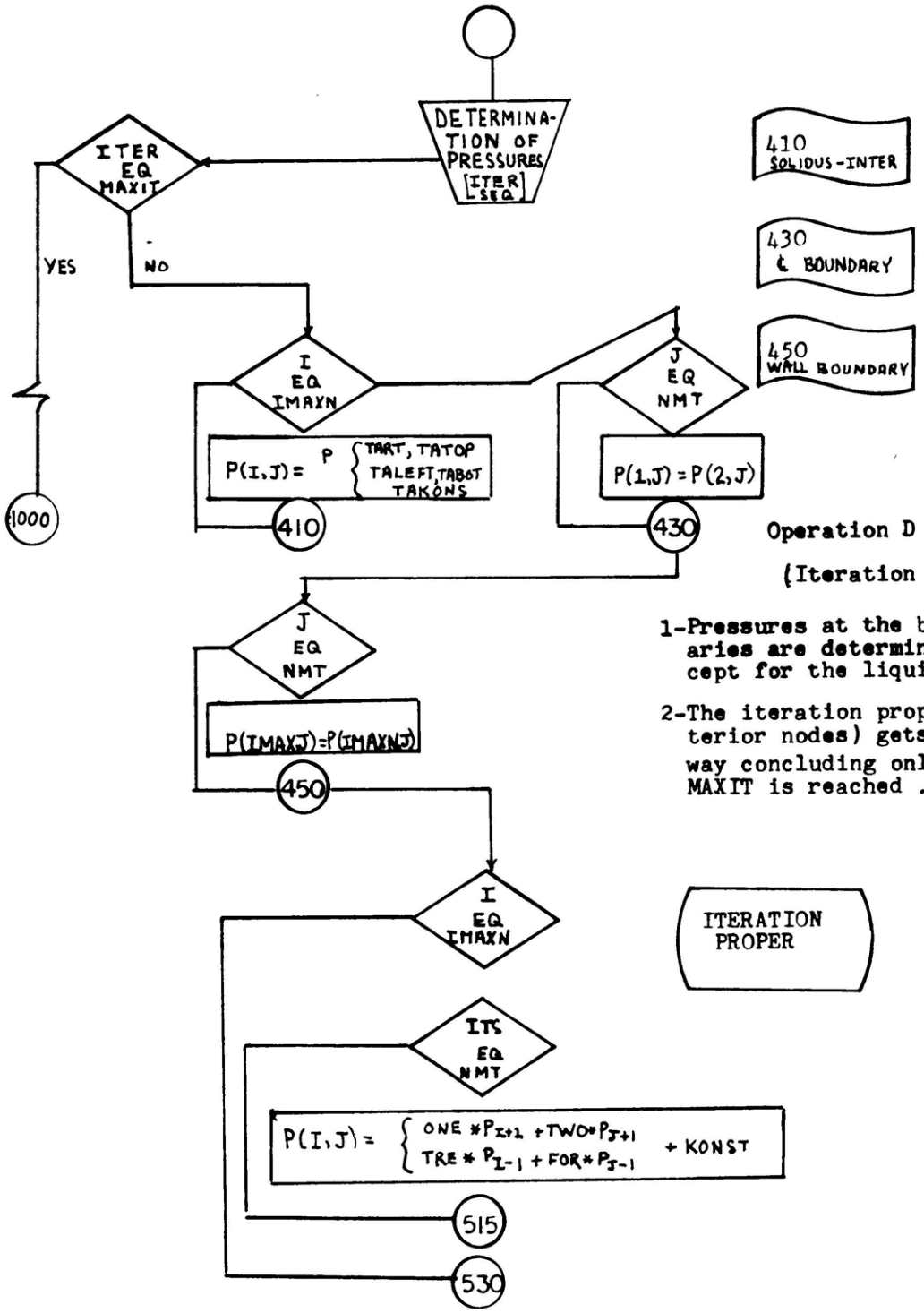

Operation D

(Iteration)

1-Pressures at the boundaries are determined(except for the liquidus)

2-The iteration proper(interior nodes) gets underway concluding only when MAXIT is reached .

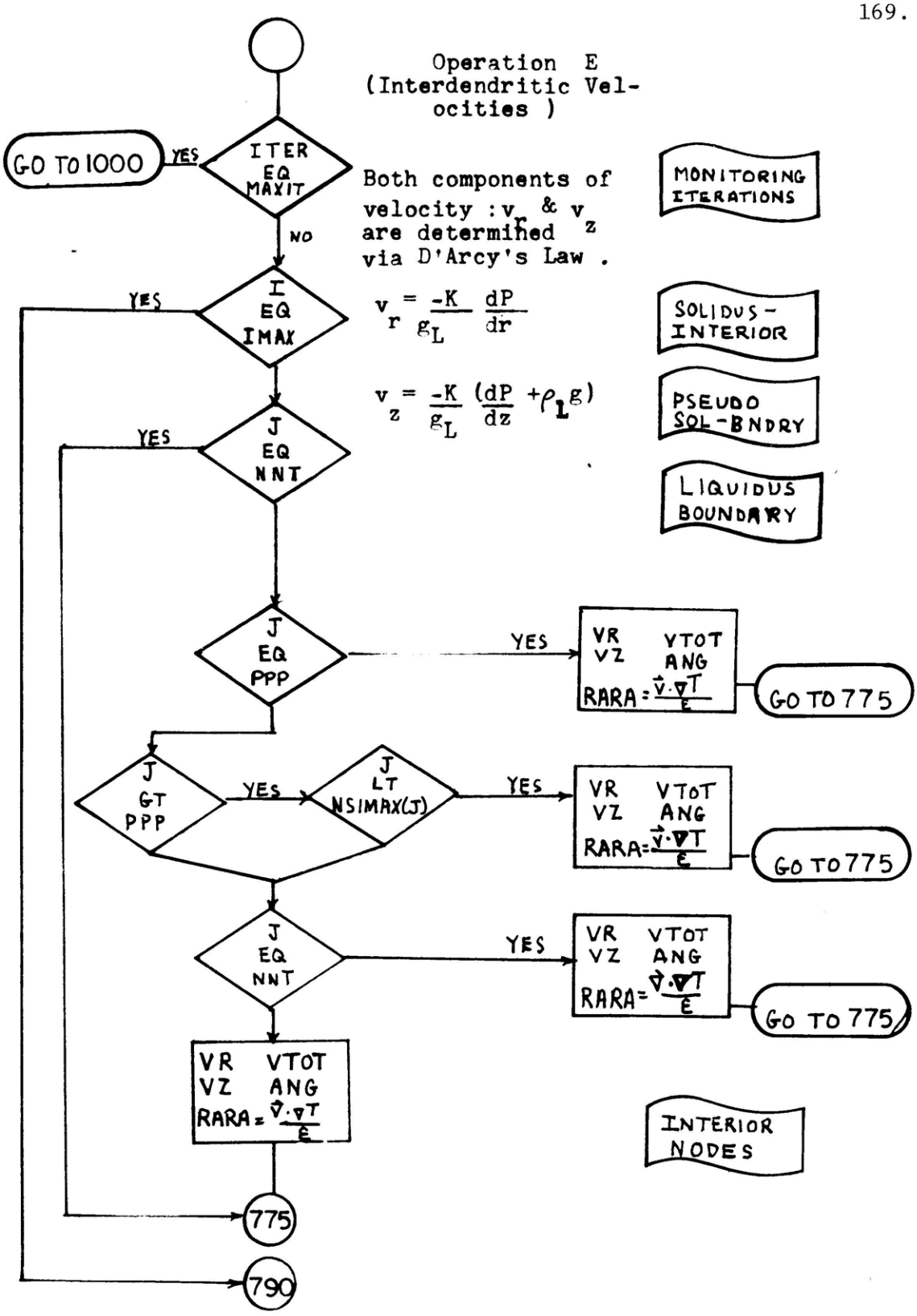
Operation E
(Interdendritic Velocities)
Both components of velocity : v_r & v_z are determined via D'Arcy's Law .
$v_r = \frac{-K}{g_L} \frac{dP}{dr}$
$v_z = \frac{-K}{g_L} (\frac{dP}{dz} + \rho_L g)$
MONITORING ITERATIONS
SOLIDUS - INTERIOR
PSEUDO SOL-BNDRY
LIQUIDUS BOUNDARY
INTERIOR NODES
GO TO 1000
YES
ITER EQ MAXIT
NO
I EQ IMAX
YES
J EQ NNT
YES
J EQ PPP
YES
VR VZ VTOT ANG
RARA = $\frac{\vec{v} \cdot \nabla T}{\epsilon}$
GO TO 775
J GT PPP
YES
J LT NSIMAX(J)
YES
VR VZ VTOT ANG
RARA = $\frac{\vec{v} \cdot \nabla T}{\epsilon}$
GO TO 775
J EQ NNT
YES
VR VZ VTOT ANG
RARA = $\frac{\vec{v} \cdot \nabla T}{\epsilon}$
GO TO 775
VR VZ VTOT ANG
RARA = $\frac{\vec{v} \cdot \nabla T}{\epsilon}$
775
790

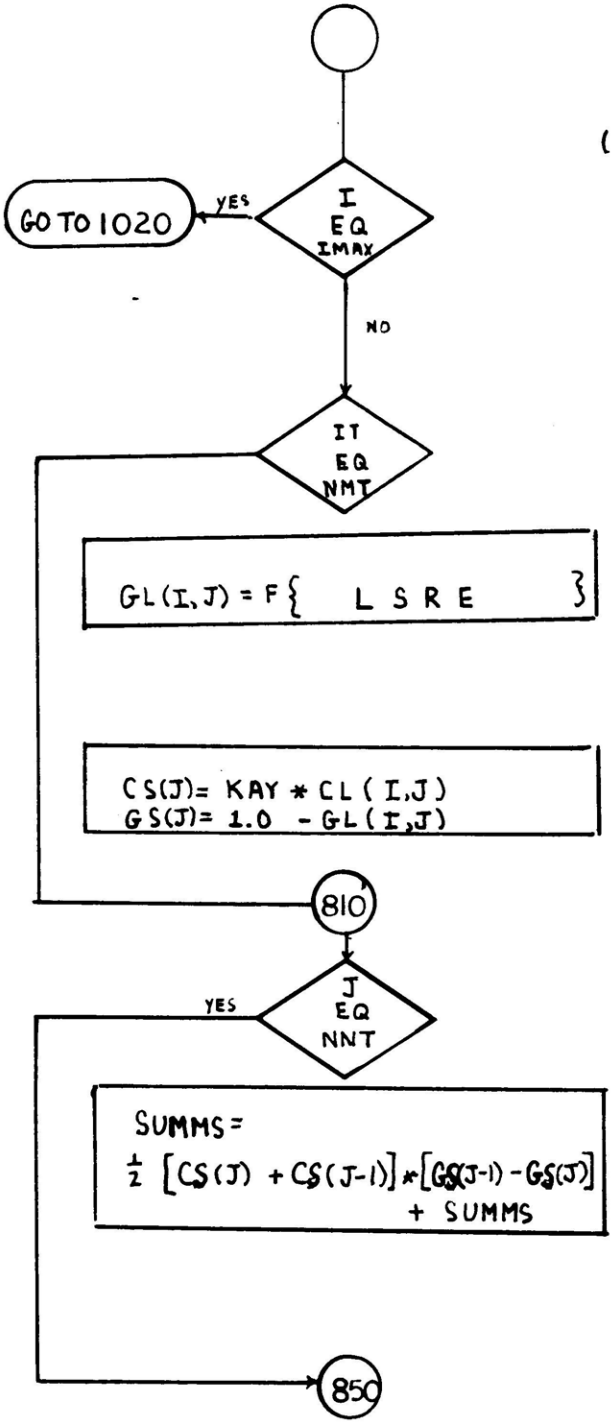

Operation F

(Local Solute Redistribution Eq.)

Updated values of the inter-dendritic velocities are now inserted into the LSRE .New values of the fraction liquid at each node are determined .

Sequence 10

(Segregation Discriminant)

If the area of this integral is greater than the Scheil value positive segregation results . If less than the type is negative .No segregation results if the two are equal .

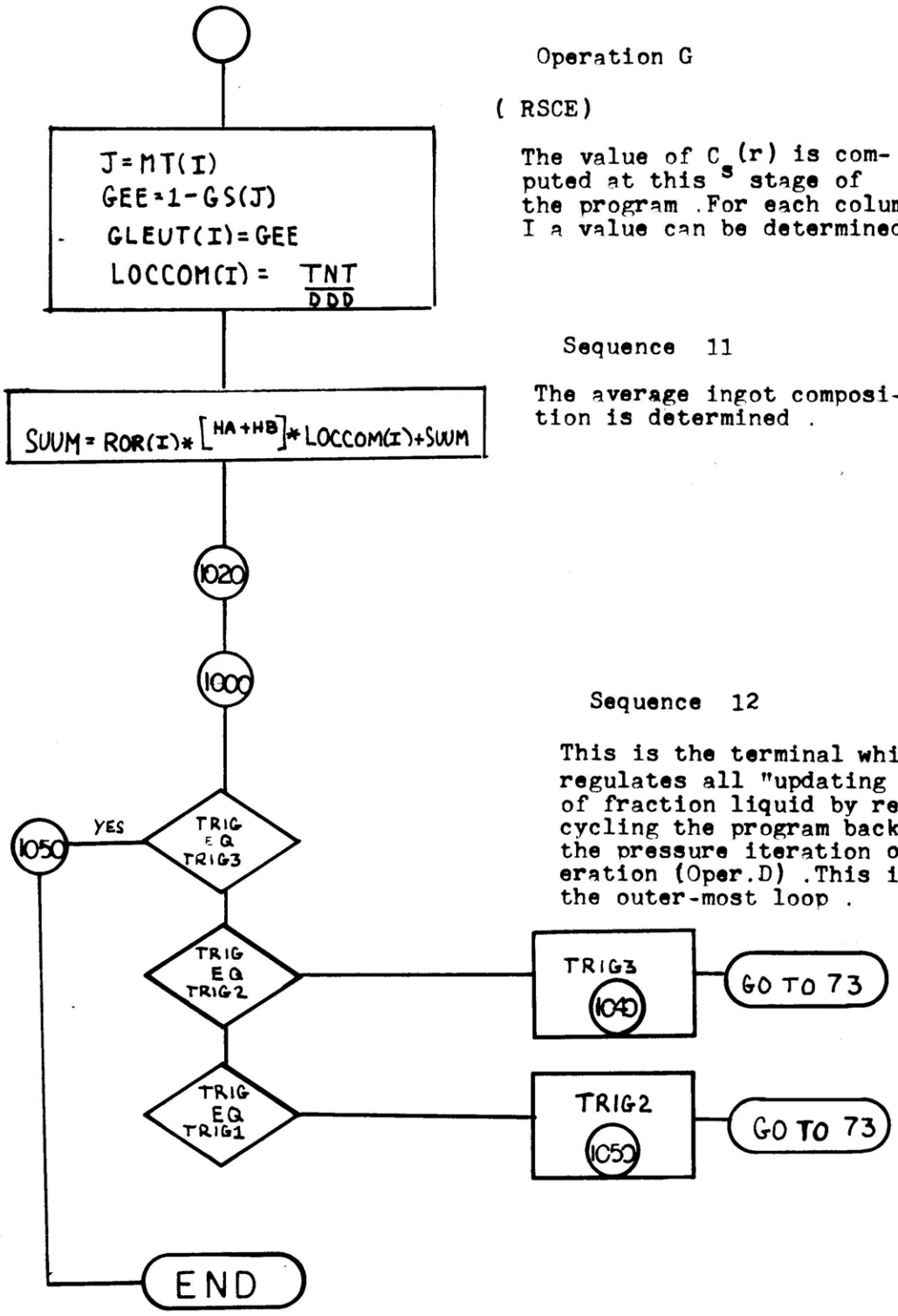

Operation G

(RSCE)

The value of $C_s(r)$ is computed at this stage of the program .For each column I a value can be determined .

Sequence 11

The average ingot composition is determined .

Sequence 12

This is the terminal which regulates all "updating " of fraction liquid by recycling the program back to the pressure iteration operation (Oper.D) .This is the outer-most loop .

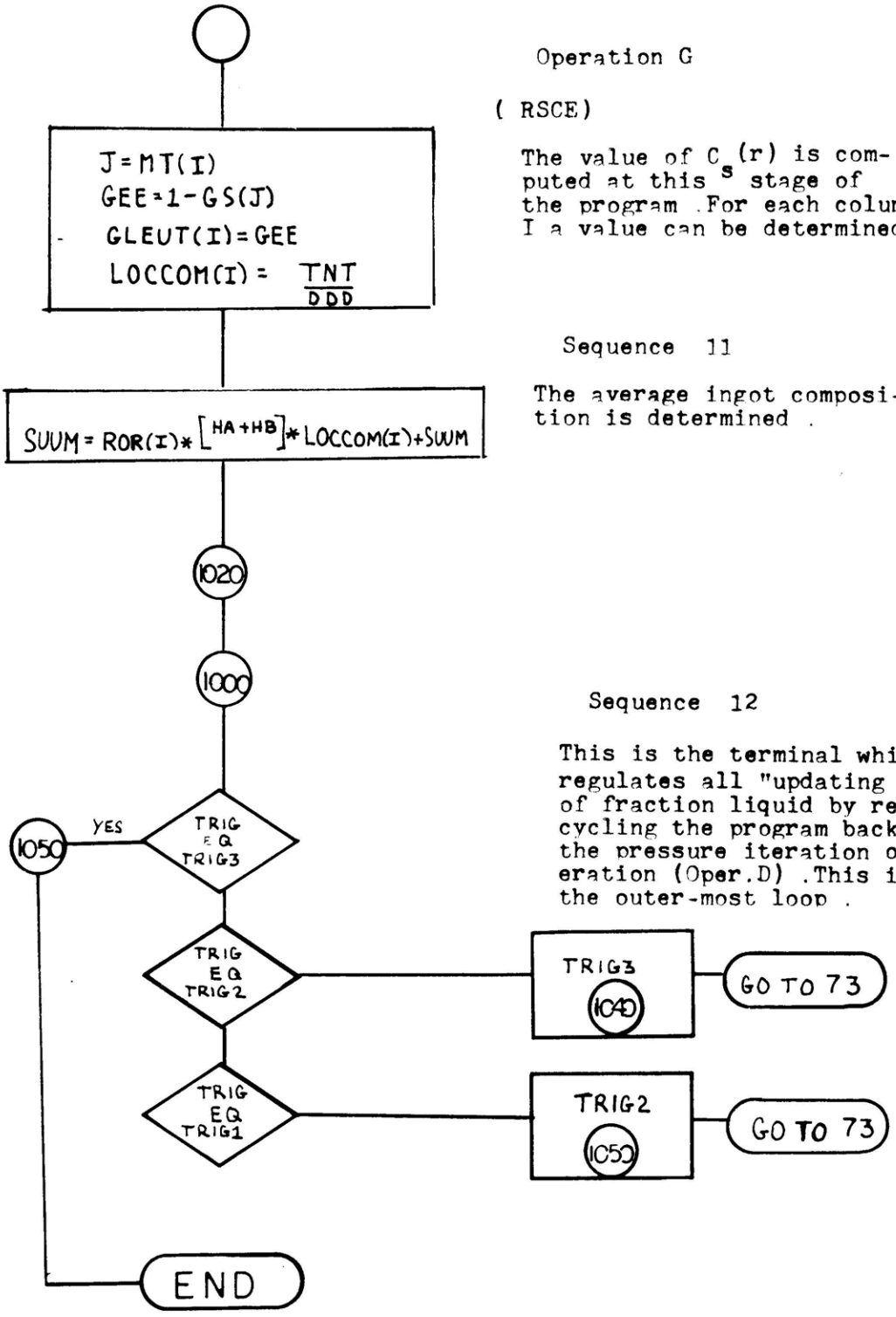

Operation G

(RSCE)

The value of $C_s(r)$ is computed at this stage of the program .For each column I a value can be determined .

Sequence 11

The average ingot composition is determined .

Sequence 12

This is the terminal which regulates all "updating " of fraction liquid by recycling the program back to the pressure iteration operation (Oper.D) .This is the outer-most loop .

APPENDIX D

SOLIDUS PRESSURE GRADIENTS

The effect of flow factor on the pressure gradients at the solidus is shown in Fig. (28). For each alloy there are two curves. One represents the radial component which is negative while the vertical component passes from positive to negative as γ increases.

At "free flow" conditions (no resistance due to dendrite obstructions) $\partial P/\partial Z$ approaches its Bernoulli limit asymptotically. $\partial P/\partial r$ tends to zero as γ increases. The other extreme is when γ produces the limiting gradient:

$$\frac{dP}{L} = 1 \text{ atmosphere}$$

where L = depth of mushy zone. For the Al-4.4% Cu alloy as γ approaches 10^{-9} cm^2 the limiting gradient is reached and pressure approaches the "negative pressure" region. This occurs at $\gamma = 10^{-11}$ cm^2 for the Sn-15% Pb binary. This violates the assumption that pore formation cannot exist within the mushy zone. Negative pressures are ficticious.

The value of such plots is that they give information about the magnitude of the limits of γ. It is easier to "scan" for the proper values of γ and confirm their validity if they concur with the range of γ dictated the solidus boundary conditions of Fig. (28). Computer instabilities result if γ is within the range of the "negative pressure" zone.

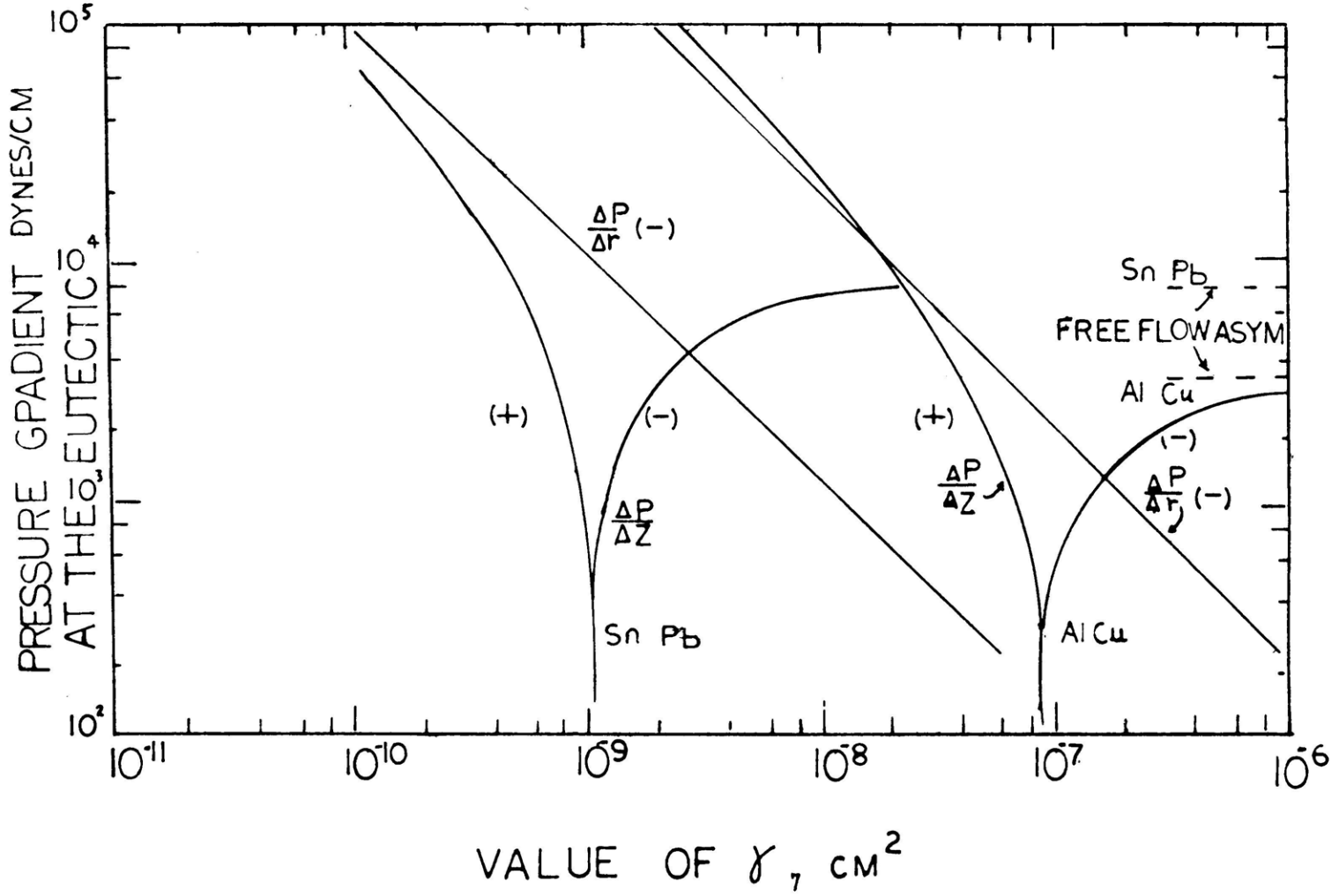

Fig. 28 - Influence of γ on the radial and vertical pressure gradients at the eutectic. dP/dr increases to zero and dP/dz approaches an asymptotic limit as γ increases.

APPENDIX E

Computer Program Printout

```
      INTEGER PT1                                                       0001
      INTEGER NPARAM                                                    0002
      INTEGER*4 N                                                       0003
      INTEGER PPPMAX                                                    0004
      INTEGER PPP                                                       0005
      INTEGER NSI(25),NSIMAX(25),MT(25),NT(25)                          0006
      INTEGER JJ1(25),JJ2(25),JJ3(25),JJ4(25)                           0007
      INTEGER JJ5(25),JJ6(25),JJ7(25),JJ8(25)                           0008
      REAL*8 KAB,KAC                                                    0009
      REAL*8 ANG                                                        0010
      REAL*8 GADS                                                       0011
      REAL*8 MSOL,MLIQ                                                  0012
      REAL*8 LEFT,KC,KAY,KAWALL                                         0013
      REAL*8 KSOL,KLIQ,K,KB,KM,KT                                       0014
      REAL*8 KON1,KON2,KON3,KON4                                        0015
      REAL*8 GAMO1,GAMO2,CONSTT                                         0016
      REAL*4 SLOLIQ,SLOSOL                                              0017
      REAL*4 LTSEG                                                      0018
      REAL*8 RSS(82),RL(82)                                             0019
      REAL*8 DELKA(82)                                                  0020
      REAL*8 HHA(25)                                                    0021
      REAL*8 HMM(25)                                                    0022
      REAL*4 ROR(25)                                                    0023
      REAL*8 HTT(25),HEIT(25),GRAV,EM,DTT                               0024
      REAL*8 HTE,TL,TE,HORAT,CRAT,TRAT,RADIUS                           0025
      REAL*8 RO,RLE,RSE,RS,GE,MU,CO,CE                                  0026
      REAL*8 H,HA,HB,HC,HM,HT                                           0027
      REAL*8 DABS                                                       0028
      REAL*8 UR,UZ(22,82),ZL(25),ZS(25)                                 0029
      REAL*8 PA                                                         0030
      REAL*8 SOLVE,SOLHZ                                                0031
      REAL*4 A1S(25),A1L(25),DELA1(25)                                  0032
      REAL*8 TABOT(22,15),TAKONS(22,15)                                 0033
      REAL*8 TART(22,15),TATOP(22,15),TALEFT(22,15)                     0034
      REAL*8 GOPS                                                       0035
      REAL*8 KMM(22,82),KA(22,82)                                       0036
```

```
REAL*8 T(22,82),RHO(22,82),MO(22,82)                                    0037
REAL*8 CL(22,82),GL(22,82),Z(22,82),R(22,82)                            0038
REAL*8 UZURRO,UZURCL,DERHOR,DERHOZ,DECLR,DECLZ,DEGLR,DEGLZ              0039
REAL*8 DENOM1,DENOM2,THETA                                              0040
REAL*8 ONE(22,82),TWO(22,82),TRE(22,82),FOR(22,82)                      0041
REAL*8 PERMI(22,82),GAMMA(22,82)                                        0042
REAL*8 GR(22,82),GZ(22,82),EPPS(22,82)                                  0043
REAL*8 A1,A2,A3,B1,B2,C1,C2,C3,C4                                       0044
REAL*8 AX,B,C                                                           0045
REAL*8 VR(22,82),VZ(22,82)                                              0046
REAL*4 OMEGAS,OMEGAL                                                    0047
REAL*4 NLGL(82),FN(82)                                                  0048
REAL*4 GS(82)                                                           0049
REAL*8 P(22,82),KONST(22,82)                                            0050
REAL*8 ZAT(22)                                                          0051
REAL*8 A(82),X1,X2                                                      0052
REAL*4 LOCCOM(22),CS(82)                                                0053
REAL*8 PDR,PDZ                                                          0054
REAL*8 GLEUT(25)                                                        0055
POWNUM=1.618                                                            0056
POWDEN=2.                                                               0057
CONSTT=0.022                                                            0058
GADSCL=1.0D-6                                                           0059
GADSWL=2.5D-7                                                           0060
GADS=5.0D-7                                                             0061
MAXIT1=150                                                              0062
MAXIT2=300                                                              0063
MAXIT3=450                                                              0064
MAXIT4=600                                                              0065
MAXIT5=750                                                              0066
UZCL=0.053                                                              0067
MU=.013                                                                 0068
PA=1.0D6                                                                0069
TRIG=1                                                                  0070
NTOP=70                                                                 0071
KC=0.15                                                                 0072
```

```
HC=0.2                                                          0073
RADIUS=3.4                                                      0074
IMAX=RADIUS/HC+.0001                                            0075
IMAX=IMAX+1                                                     0076
CO=4.40                                                         0077
ZISOL=0.0                                                       0078
W=0.0                                                           0079
ZILIQ=3.8                                                       0080
A0S=ZISOL                                                       0081
A0L=ZILIQ                                                       0082
A2S=0.0                                                         0083
A2L=0.0                                                         0084
DELA0=A0L-A0S                                                   0085
HTE=DELA0                                                       0086
DELA2=A2L-A2S                                                   0087
DTT=0.                                                          0088
GRAV=980.                                                       0089
RLE=3.2                                                         0090
RSE=3.38                                                        0091
RS=2.62                                                         0092
RO=2.45                                                         0093
PI=3.14156                                                      0094
CE=33.                                                          0095
CSE=5.65                                                        0096
TM=660.                                                         0097
TE=548.                                                         0098
KAY=CSE/CE                                                      0099
KON1=(1.0D0/CO)**(1./(KAY-1.))                                  0100
KON2=1.0D0/(KAY-1.0D0)                                          0101
KON3=KON2-1.0D0                                                 0102
KON4=-KON2                                                      0103
KAY=CSE/CE                                                      0104
GE=(CE/CO)**(1./(KAY-1.))                                       0105
EM=(TE-TM)/CE                                                   0106
TL=EM*(CO-CE)+TE                                                0107
CONTR=RSE/RLE-1.                                                0108
```

```
      CONTRL=(RS/RO-1.)                                                 0109
      HORAT=RO-RLE                                                      0110
      TRAT=TL-TE                                                        0111
      CRAT=CO-CE                                                        0112
      IMAXN=IMAX-1                                                      0113
      IMAXP=IMAX+1                                                      0114
      DO 8 I=1,IMAX                                                     0115
      GLEUT(I)=GE                                                       0116
    8 CONTINUE                                                          0117
      WRITE(6,8565)                                                     0118
 8565 FORMAT(8X,'LIQUIDUS TEMP',3X,'EUTEC FR LIQ',3X,'SLOPE OF LIQ'     0119
     1,2X,'PARTIT RATIO',2X,'COMP SOL EUT',2X,'EUT TEMP'///)            0120
      WRITE(6,8888) TL,GE,EM,KAY,CSE,TE                                 0121
 8888 FORMAT(5X,6E15.6///)                                              0122
      WRITE(6,9059)                                                     0123
 9059 FORMAT(6X,'PERMEABILITY',5X,'PERCENTAGE SOLUTE',5X,               0124
     1'CNTL ISOTHERM VELOCITY',5X,'HEIGHT OF MUSHY ZONE AT CNTL'//)     0125
      WRITE(6,8059) GADS,CO,UZCL,HTE                                    0126
 8059 FORMAT(4E23.6////)                                                0127
      WRITE(6,9000)                                                     0128
 9000 FORMAT(12X,'Z-SOLIDUS',10X,'Z-LIQUIDUS',12X,'I'///)               0129
      DO 10 I=1,IMAX                                                    0130
      H=HC                                                              0131
      IF(I.EQ.1) MSOL=0.0                                               0132
      IF(I.GT.1) MSOL=0.25                                              0133
      IF(I.EQ.1) MLIQ=0.0                                               0134
      IF(I.GT.1) MLIQ=0.25                                              0135
      IF(I.EQ.1) A1S(I)=0.0                                             0136
      IF(I.EQ.1) A1L(I)=0.0                                             0137
      A1S(I)=MSOL                                                       0138
      A1L(I)=MLIQ                                                       0139
      IF(I.EQ.1) GO TO 22                                               0140
      GO TO 23                                                          0141
   22 CONTINUE                                                          0142
      ROR(1)=0.0                                                        0143
      ZS(I)=A0S                                                         0144
```

```
      ZL(I)=A0L                                                          0145
      GO TO 19                                                           0146
   23 CONTINUE                                                           0147
      ROR(I)=ROR(I-1)+H                                                  0148
      ZL(I)=ZL(I-1)+A1L(I)*H                                             0149
      ZS(I)=ZS(I-1)+A1S(I)*H                                             0150
   19 CONTINUE                                                           0151
      WRITE(6,6000) ZS(I),ZL(I),I                                        0152
 6000 FORMAT(1X,2E20.6,I10//)                                            0153
   10 CONTINUE                                                           0154
      DO 25 I=1,IMAX                                                     0155
      DELA1(I)=A1L(I)-A1S(I)                                             0156
   25 CONTINUE                                                           0157
      DO 20 I=1,IMAX                                                     0158
      IF(I.EQ.IMAX) GO TO 20                                             0159
      HHA(I)=ROR(I+1)-ROR(I)                                             0160
   20 CONTINUE                                                           0161
      DO 24 J=1,NTOP                                                     0162
      DELKA(J)=KC                                                        0163
   24 CONTINUE                                                           0164
C                                                                        0165
C                  CONSTRUCTION OF THE GRID MESH***********            0166
C                                                                        0167
C          THIS PARTICULAR SECTION DEALS WITH THE SETTING UP OF THE GRID 0168
C          MESH FOR THE MUSHY ZONE .NOTICE THAT BOTH THE SPACING INCREME 0169
C          FOR BOTH THE VERTICAL AND RADIAL  DIRECTIONS ARE VARIABLE .   0170
C                                                                        0171
      DO 50 I=1,IMAX                                                     0172
      Z(I,1)=ZISOL                                                       0173
      R(I,1)=ROR(I)                                                      0174
      MT(I)=0.0                                                          0175
      NT(I)=0.0                                                          0176
      DO 40 J=2,NTOP                                                     0177
      Z(I,J)=DELKA(J-1)+Z(I,J-1)                                         0178
      R(I,J)=ROR(I)                                                      0179
      IF(Z(I,J).GT.ZL(I)) GO TO 37                                       0180
```

```
      IF(Z(I,J).GT.ZS(I)) GO TO 33                                      0181
      GO TO 40                                                          0182
   33 IF(MT(I).GT.0) GO TO 40                                           0183
      BFRACT=(Z(I,J)-ZS(I))/(Z(I,J)-Z(I,J-1))                          0184
      IF(BFRACT.LT.0.5) ZS(I)=Z(I,J)                                    0185
      IF(BFRACT .GT.0.5) GO TO 35                                       0186
      MT(I)=J                                                           0187
      RSS(J)=R(I,J)                                                     0188
      GO TO 40                                                          0189
   35 ZS(I)=Z(I,J-1)                                                    0190
      MT(I)=J-1                                                         0191
      RSS(J-1)=R(I,J-1)                                                 0192
      GO TO 40                                                          0193
   37 IF(NT(I).GT.0) GO TO 40                                           0194
C                                                                       0195
CC                                                                      0196
C              INTERPOLATION APPROXIMATIONS AT THE LIQUIDUS*****        0197
C                                                                       0198
C          THERE IS SOME INTERPOLATION APPROXIMATIONS BEING MADE AT THE  0199
C          LIQUIDUS DUE TO THE VARIABLE SPACING INCREMENTS (CARTESIAN) D 0200
C          CUSSED BEFORE .THE SMALLER THE VALUES OF THE SPACING THE GREA 0201
C         THE ACCURACY ATTAINED FOR VALUES OF THE GRADIENTS USED         0202
C          IN THE COEFFICIENTS SEQUENCE                                  0203
C                                                                       0204
      TFRACT=(Z(I,J)-ZL(I))/(Z(I,J)-Z(I,J-1))                          0205
      IF(TFRACT.LT.0.5) ZL(I)=Z(I,J)                                    0206
      IF(TFRACT.GT.0.5) GO TO 39                                        0207
      IF(I.EQ.IMAX) ZLHIGH=ZL(I)                                        0208
      NT(I)=J                                                           0209
      RL(J)=R(I,J)                                                      0210
      HTT(I)=ZL(I)-ZS(I)                                                0211
      GO TO 40                                                          0212
   39 ZL(I)=Z(I,J-1)                                                    0213
      IF(I.EQ.IMAX) ZLHIGH=ZL(I)                                        0214
      NT(I)=J-1                                                         0215
      RL(J-1)=R(I,J-1)                                                  0216
```

```
      HTT(I)=ZL(I)-ZS(I)                                                0217
   40 CONTINUE                                                          0218
   50 CONTINUE                                                          0219
      DO 51 I=1,IMAX                                                    0220
      HEIT(I)=ZLHIGH-ZL(I)                                              0221
      WRITE(6,5555) HTT(I),HEIT(I),ZS(I),ZL(I),I                        0222
 5555 FORMAT(3X,4E20.6,I10)                                             0223
   51 CONTINUE                                                          0224
      DO 52 I=1,IMAX                                                    0225
      NUMPTS=NT(I)-MT(I)                                                0226
      N8TH=NUMPTS/5.                                                    0227
      ZAT(I)=GADSCL-((GADSCL-GADSWL)/RADIUS)*ROR(I)                     0228
      ZAT(1)=1.0                                                        0229
      ZAT(2)=1.0                                                        0230
      ZAT(3)=1.0                                                        0231
      ZAT(4)=1.0                                                        0232
      ZAT(5)=1.0                                                        0233
      ZAT(6)=1.0                                                        0234
      ZAT(7)=1.0                                                        0235
      ZAT(8)=1.0                                                        0236
      ZAT(9)=1.0                                                        0237
      ZAT(10)=1.0                                                       0238
      ZAT(11)=1.0                                                       0239
      ZAT(12)=1.0                                                       0240
      ZAT(13)=1.0                                                       0241
      ZAT(14)=1.0                                                       0242
      ZAT(15)=1.0                                                       0243
      ZAT(16)=1.0                                                       0244
      ZAT(17)=1.0                                                       0245
      ZAT(18)=1.0                                                       0246
      JJ1(I)=MT(I)+N8TH                                                 0247
      JJ2(I)=MT(I)+2.*N8TH                                              0248
      JJ3(I)=MT(I)+3.*N8TH                                              0249
      JJ4(I)=MT(I)+4.*N8TH                                              0250
      JJ5(I)=MT(I)+5.*N8TH                                              0251
      WRITE(6,8125) JJ1(I),JJ2(I),JJ3(I),JJ4(I),JJ5(I),ZAT(I),I         0252
```

```
8125 FORMAT(10X,5I10,E20.6,I10/)                                                0253
  52 CONTINUE                                                                   0254
     WRITE(6,9010)                                                              0255
9010 FORMAT(10X,'VALUE OF NSI',4X,'NSIMAX',4X,                                  0256
    1'VALUE OF MT',4X,'VALUE OF NT',8X,'I'///)                                  0257
     DO 88 I=1,IMAXN                                                            0258
     NSI(I)=MT(I)+1                                                             0259
     NSIMAX(I)=MT(I+1)                                                          0260
     IF(MT(I).EQ.MT(I+1)) NSIMAX(I)=NSI(I)                                      0261
     WRITE(6,8010) NSI(I),NSIMAX(I),MT(I),NT(I),I                               0262
8010 FORMAT(1X,5I15/)                                                           0263
  88 CONTINUE                                                                   0264
  73 CONTINUE                                                                   0265
     DO 90 I=2,IMAX                                                             0266
     DIFF=GLEUT(I)-GLEUT(I-1)                                                   0267
     DO 80 J=1,NTOP                                                             0268
     IF(J.LE.MT(I-1)) GO TO 80                                                  0269
     IF(J.LT.MT(I)) GO TO 75                                                    0270
     IF(TRIG.NE.1) GO TO 80                                                     0271
     IF((J.GE.MT(I)).AND.(J.LE.NT(I-1))) GO TO 80                               0272
     IF(J.LT.NT(I)) GO TO 77                                                    0273
     IF(J.GE.NT(I)) GO TO 80                                                    0274
     GO TO 80                                                                   0275
  75 R(I,J)=R(I-1,J)+((Z(I,J)-ZS(I-1))/(ZS(I)-ZS(I-1)))*HHA(I-1)                0276
     RSS(J)=R(I,J)                                                              0277
     MO(I,J)=A1S(I)+A2S*2.0*R(I,J)                                              0278
     T(I,J)=TE                                                                  0279
     GL(I,J)=GLEUT(I-1)+((Z(I,J)-ZS(I-1))/(ZS(I)-ZS(I-1)))*DIFF                 0280
     CL(I,J)=CE                                                                 0281
     RHO(I,J)=RLE                                                               0282
     P(I,J)=10000.                                                              0283
     GO TO 80                                                                   0284
  77 R(I-1,J)=R(I-1,J)+((Z(I,J)-ZL(I-1))/(ZL(I)-ZL(I-1)))*HHA(I-1)              0285
     RL(J)=R(I-1,J)                                                             0286
     T(I-1,J)=TL                                                                0287
     GL(I-1,J)=1.                                                               0288
```

```
      CL(I-1,J)=CO                                                          0289
      RHO(I-1,J)=RO                                                         0290
      P(I-1,J)=(ZLHIGH-Z(I,J))*RO*GRAV+0.5*RO*(W**2)*(R(I-1,J)**2)          0291
      P(I-1,J)=P(I-1,J)+PA                                                  0292
   80 CONTINUE                                                              0293
   90 CONTINUE                                                              0294
      IF(TRIG.EQ.2) GO TO 85                                                0295
      IF(TRIG.EQ.3) GO TO 89                                                0296
      IF(TRIG.EQ.4)GO TO 93                                                 0297
      IF(TRIG.EQ.5)GO TO 95                                                 0298
C                                                                           0299
C              TEMPERATURE AND TEMP RELATED ITEMS  FOR EACH NODE            0300
C                                                                           0301
C          NOW WE BEGIN TO FILL-IN THE VALUES OF COMPOSITION ,DENSITY,AN    0302
C          FRACTION LIQUID(SCHEIL)  AS WELL AS THE INDEPENDENT VARIABLE     0303
C          TEMPERATURE FOR ALL NODES WITHIN THE NEWLY CONSTRUCTED GRID .    0304
C                                                                           0305
      NMT=NT(1)-1                                                           0306
      DO 55 J=2,NMT                                                         0307
      RL(J)=0.0                                                             0308
   55 CONTINUE                                                              0309
      I=IMAX                                                                0310
      PPP=MT(I)-1                                                           0311
      NMT=NT(I)-1                                                           0312
      JMAXUM=MT(I)                                                          0313
      DO 70 I=1,IMAX                                                        0314
      MNT=MT(I)                                                             0315
      NNT=NT(I)                                                             0316
      DO 60 J=MNT,NNT                                                       0317
      KA(I,J)=DELKA(J)                                                      0318
      DEPMZ=ZL(I)-Z(I,J)                                                    0319
      HTMZ=HTT(I)-DEPMZ                                                     0320
      HTFRAC=HTMZ/HTT(I)                                                    0321
      IF(J.EQ.NT(I)) HTFRAC=1.0                                             0322
      IF(J.EQ.MT(I)) HTFRAC=0.0                                             0323
      SLOLIQ=A1L(I)                                                         0324
```

```
      SLOSOL=A1S(I)                                                          0325
      IF((J.EQ.NT(I)).OR.(J.EQ.MT(I)))  SLOLIQ=A1L(I)+2.0*A2L*R(I,J)         0326
      IF((J.EQ.NT(I)).OR.(J.EQ.MT(I)))SLOSOL=A1S(I)+2.0*A2S*R(I,J)           0327
      MO(I,J)=SLOSOL+HTFRAC*(SLOLIQ-SLOSOL)                                  0328
      T(I,J)=TRAT*HTFRAC+TE                                                  0329
      DIFTEM=T(I,J)-TE                                                       0330
      RHO(I,J)=(HORAT/TRAT)*DIFTEM+RLE                                       0331
      CL(I,J)=(CRAT/TRAT)*DIFTEM+CE                                          0332
      GL(I,J)=KON1*(CL(I,J)**KON2)                                           0333
      GAMMA(I,J)=GADS*(ZAT(I))**2                                            0334
      IF(I.EQ.1)  MO(I,J)=0.0                                                0335
      P(I,J)=.5D0*(RHO(I,J)+RO)*GRAV*DEPMZ+GRAV*RO*HEIT(I)                   0336
      P(I,J)=P(I,J)+0.5*RO*(W**2)*(R(I,J)**2)                                0337
      P(I,J)=P(I,J)+PA                                                       0338
   60 CONTINUE                                                               0339
   70 CONTINUE                                                               0340
      NSTART=1                                                               0341
      MAXIT=MAXIT1                                                           0342
      GO TO 91                                                               0343
   85 CONTINUE                                                               0344
      NSTART=MAXIT1+1                                                        0345
      MAXIT=MAXIT2                                                           0346
      GO TO 91                                                               0347
   89 CONTINUE                                                               0348
      NSTART=MAXIT2+1                                                        0349
      MAXIT=MAXIT3                                                           0350
      GO TO 91                                                               0351
   93 CONTINUE                                                               0352
      NSTART=MAXIT3+1                                                        0353
      MAXIT=MAXIT4                                                           0354
      GO TO 91                                                               0355
   95 CONTINUE                                                               0356
      NSTART=MAXIT4+1                                                        0357
      MAXIT=MAXIT5                                                           0358
   91 CONTINUE                                                               0359
C                                                                            0360
```

```
C                THE COEFFICIENT SEQUENCE                                       0361
C                                                                               0362
C           THIS SECTION DEALS WITH THE DETERMINATION OF THE PARAMETERS         0363
C           DEALING WITH THE COEFFICIENTS OF THE SECOND ORDER PARTIAL           0364
C           DIFFERENTIAL EQUATION USED TO FIND THE VALUES OF PRESSURE           0365
C           AT ANY GIVEN NODE WITHIN THE MUSHY ZONE.                            0366
C                                                                               0367
      DO 150 I=2,IMAXN                                                          0368
      PPP=MT(I)+1                                                               0369
      NMT=NT(I)-1                                                               0370
      DO 145 J=PPP,NMT                                                          0371
      HA=R(I+1,J)-R(I,J)                                                        0372
      IF(MT(I).EQ.MT(I+1)) GO TO 100                                            0373
      IF(J.LT.MT(I+1)) HA=((Z(I,J)-ZS(I))/(ZS(I+1)-ZS(I)))*HHA(I)               0374
  100 CONTINUE                                                                  0375
      HB=R(I,J)-R(I-1,J)                                                        0376
      IF(NT(I).EQ.NT(I-1)) GO TO 101                                            0377
      IF(J.GT.NT(I-1)) HB=((ZL(I)-Z(I,J))/(ZL(I)-ZL(I-1)))*HHA(I-1)             0378
  101 CONTINUE                                                                  0379
      HM=(HA+HB)/2.                                                             0380
      HMM(I)=HM                                                                 0381
      HT=(HA*HB*HM)                                                             0382
      A1=1.0D0/R(I,J)                                                           0383
      KB=Z(I,J)-Z(I,J-1)                                                        0384
      KM=(KA(I,J)+KB)/2.                                                        0385
      KMM(I,J)=KM                                                               0386
      KT=(KA(I,J)*KB*KM)                                                        0387
      THETA=2.0D0*(HT*KM+KT*HM)                                                 0388
      GR(I,J)=(T(I+1,J)-T(I-1,J))/(2.0D0*HM)                                    0389
      GZ(I,J)=(T(I,J+1)-T(I,J-1))/(2.0D0*KM)                                    0390
      UZ(I,J)=UZCL/(1.+MO(I,J)**2)                                              0391
      UR=-MO(I,J)*UZ(I,J)                                                       0392
      EPPS(I,J)=-(UZ(I,J)*GZ(I,J)+UR*GR(I,J))                                   0393
      FACT1=1.0                                                                 0394
      FACT2=GL(I,J)**2                                                          0395
      PERMI(I,J)=GAMMA(I,J)*(GL(I,J)**2)                                        0396
```

```
      DERHOR=(RHO(I+1,J)-RHO(I-1,J))/(2.0D0*HM)                          0397
      DERHOZ=(RHO(I,J+1)-RHO(I,J-1))/(2.0D0*KM)                          0398
      DECLR=(CL(I+1,J)-CL(I-1,J))/(2.0D0*HM)                             0399
      DECLZ=(CL(I,J+1)-CL(I,J-1))/(2.0D0*KM)                             0400
      DEGLR=(GL(I+1,J)-GL(I-1,J))/(2.0D0*HM)                             0401
      DEGLZ=(GL(I,J+1)-GL(I,J-1))/(2.0D0*KM)                             0402
      UZURCL=UZ(I,J)*DECLZ+UR*DECLR                                      0403
      UZURRO=UZ(I,J)*DERHOZ+UR*DERHOR                                    0404
      ALFA=(RHO(I,J)/RS-1.)*KON2/CL(I,J)                                 0405
      A2=2.*DEGLR/GL(I,J)+DERHOR/RHO(I,J)                                0406
      A3=ALFA*DECLR                                                      0407
      B1=2.*DEGLZ/GL(I,J)+DERHOZ/RHO(I,J)                                0408
      B2=ALFA*DECLZ                                                      0409
      C1=2.*DEGLZ/GL(I,J)+2.*DERHOZ/RHO(I,J)                             0410
      C2=ALFA*(DECLZ-(W**2)*DECLR*R(I,J)/GRAV)                           0411
      C3=GRAV*RHO(I,J)*(C1+C2)                                           0412
      C4=(DERHOZ/DECLZ)/RHO(I,J)+ALFA                                    0413
      C5=EPPS(I,J)*MU/(EM*GAMMA(I,J)*GL(I,J))                            0414
      C6=(W**2)*(2.*RHO(I,J)+2.*RHO(I,J)*R(I,J)*DEGLR/GL(I,J)+2.*R(I,J)* 0415
     1DERHOR)                                                            0416
      AX=A1+A2+A3                                                        0417
      B=B1+B2                                                            0418
      C=C3-C4*C5-C6                                                      0419
      IF((J.GE.NSI(I)).AND.(J.LE.NSIMAX(I))) GO TO 120                   0420
      GO TO 130                                                          0421
  120 CONTINUE                                                           0422
      IXX=J-NSI(I)+1                                                     0423
      IF(MT(I-1).EQ.MT(I+1)) GO TO 121                                   0424
      IF((MT(I+1).GE.MT(I)+1).AND.(J.EQ.MT(I)+1)) GO TO 125              0425
      IF((MT(I+1).GE.MT(I)+1).AND.(J.GT.MT(I)+1)) GO TO 123              0426
      IF(MT(I+1).EQ.MT(I)+1) GO TO 125                                   0427
      IF(MT(I).EQ.MT(I+1)) GO TO 121                                     0428
      GO TO 130                                                          0429
  121 CONTINUE                                                           0430
      SOLVE=MU*CONTR*UZCL/(GAMMA(I,J)*GLEUT(I)*(1.+MO(I,J)**2))          0431
     1-RLE*GRAV                                                          0432
```

```
      SOLHZ=-MU*CONTR*UZCL*MO(I,J)/(GAMMA(I,J)*GLEUT(I)*                0433
     1(1.+MO(I,J)**2))+RLE*R(I,J)*(W**2)                                0434
      COF0=1./(KC**2)+2./(HA*(HA+HB))+2./(HB*(HA+HB))+B/(2.*KC)         0435
      COF0=COF0+AX*HB/(HA+HB)-AX*HA/(HA+HB)                             0436
      TART(I,IXX)=(1./COF0)*(2./(HA*(HA+HB))+HB*AX/(HA*(HA+HB)))        0437
      TATOP(I,IXX)=(1./COF0)*(1./(KC**2)+B/(2.*KC))                     0438
      TALEFT(I,IXX)=(1./COF0)*(2./(HB*(HA+HB))-HA*AX/(HB*(HA+HB)))      0439
      TABOT(I,IXX)=0.0                                                  0440
      TAKONS(I,IXX)=(1./COF0)*(SOLVE*(B/2.-1./KC)+C)                    0441
      GO TO 130                                                         0442
  123 CONTINUE                                                          0443
      SOLVE=MU*CONTR*UZCL/(GAMMA(I,J)*GLEUT(I)*(1.+MO(I,J)**2))         0444
     1-RLE*GRAV                                                         0445
      SOLHZ=-MU*CONTR*UZCL*MO(I,J)/(GAMMA(I,J)*GLEUT(I)*                0446
     1(1.+MO(I,J)**2))+RLE*R(I,J)*(W**2)                                0447
      COF1=2./(KC**2)+2./(HB*(HA+HB))-HA*AX/(HB*(HA+HB))                0448
      TART(I,IXX)=0.0                                                   0449
      TATOP(I,IXX)=(1./COF1)*(1./(KC**2)+B/(2.*KC))                     0450
      TALEFT(I,IXX)=(1./COF1)*(2./(HB*(HA+HB))-AX*HA/(HB*(HA+HB)))      0451
      TABOT(I,IXX)=(1./COF1)*(1./(KC**2)-B/2.*(1./KC))                  0452
      TAKONS(I,IXX)=(1./COF1)*(2.*SOLHZ/(HA+HB)+AX*HB/(HA+HB)+SOLHZ+C)  0453
      GO TO 130                                                         0454
  125 CONTINUE                                                          0455
      SOLVE=MU*CONTR*UZCL/(GAMMA(I,J)*GLEUT(I)*(1.+MO(I,J)**2))         0456
     1-RLE*GRAV                                                         0457
      SOLHZ=-MU*CONTR*UZCL*MO(I,J)/(GAMMA(I,J)*GLEUT(I)*                0458
     1(1.+MO(I,J)**2))+RLE*R(I,J)*(W**2)                                0459
      COF2=1./(KC**2)+2./(HB*(HA+HB))-AX*HA/(HB*(HA+HB))+B/(2.*KC)      0460
      TART(I,IXX)=0.0                                                   0461
      TATOP(I,IXX)=(1./COF2)*(1./(KC**2)+B/(2.*KC))                     0462
      TALEFT(I,IXX)=(1./COF2)*(2./(HB*(HA+HB))-AX*HA/(HB*(HA+HB)))      0463
      TABOT(I,IXX)=0.0                                                  0464
      TAKONS(I,IXX)=(1./COF2)*(SOLHZ*(2.+HB*AX)/(HA+HB)+C               0465
     1+SOLVE*(B/2.-1./KC))                                              0466
  130 CONTINUE                                                          0467
      DENOM1=2.0D0*KM*THETA                                             0468
```

```
      DENOM2=(HM/KM)*DENOM1                                                    0469
      ONE(I,J)=(KT*HB)/THETA+(KT*HT*AX)/DENOM2                                 0470
      TWO(I,J)=(HT*KB)/THETA+(KT*HT*B)/DENOM1                                  0471
      TRE(I,J)=(KT*HA)/THETA-(KT*HT*AX)/DENOM2                                 0472
      FOR(I,J)=(HT*KA(I,J))/THETA-(KT*HT*B)/DENOM1                             0473
      KONST(I,J)=(KT*HT*C)/THETA                                               0474
      IF(I.EQ.16) GO TO 141                                                    0475
      IF(I.EQ.11) GO TO 141                                                    0476
      IF(I.EQ.6) GO TO 141                                                     0477
      IF(I.EQ.3) GO TO 141                                                     0478
      GO TO 145                                                                0479
  141 CONTINUE                                                                 0480
      IF(J.EQ.JJ1(I)) GO TO 143                                                0481
      IF(J.EQ.JJ2(I)) GO TO 143                                                0482
      IF(J.EQ.JJ3(I)) GO TO 143                                                0483
      IF(J.EQ.JJ4(I)) GO TO 143                                                0484
      IF(J.EQ.JJ5(I)) GO TO 143                                                0485
      GO TO 145                                                                0486
  143 CONTINUE                                                                 0487
      WRITE(6,8001)                                                            0488
 8001 FORMAT(7X,'AX',11X,'B',10X,'HEIGHT',12X,'U-Z',7X,'ISO-T-SLOPE',          0489
     19X,'EPS',7X ,'I',3X,'J',8X,'PERMI',7X,'FRACT LIQ')                       0490
      WRITE(6,7001) T(I,J),CL(I,J),Z(I,J),UZ(I,J),MO(I,J),EPPS(I,J),I,J,      0491
     1PERMI(I,J),GL(I,J)                                                       0492
 7001 FORMAT(1X,6E14.5,2I5,2E14.5/)                                            0493
  145 CONTINUE                                                                 0494
  150 CONTINUE                                                                 0495
C                                                                              0496
C                NECESSARY PARAMETERS FOUND AT THE  GIVEN BOUNDARIES           0497
C                                                                              0498
C          SET-UP OF THE SOLIDUS FOR THE MACROSEGREGATION SEQUENCE             0499
C                                                                              0500
      DO 200 I=2,IMAX                                                          0501
      MNT=MT(I)                                                                0502
      J=MNT                                                                    0503
      GR(I,J)=(T(I,J)-T(I-1,J))/(HHA(I-1))                                     0504
```

```
      GZ(I,J)=(T(I,J+1)-T(I,J))/KA(I,J)                                 0505
      UZ(I,J)=UZCL/(1.+MO(I,J)**2)                                      0506
      UR=-MO(I,J)*UZ(I,J)                                               0507
      EPPS(I,J)=-(UZ(I,J)*GZ(I,J)+UR*GR(I,J))                          0508
      FACT1=1.0                                                         0509
      FACT2=GL(I,J)**2                                                  0510
      PERMI(I,J)=GAMMA(I,J)*(GL(I,J)**2)                                0511
      VR(I,J)=-UR*CONTR                                                 0512
      VZ(I,J)=-UZ(I,J)*CONTR                                            0513
  200 CONTINUE                                                          0514
C                                                                       0515
C          SET-UP OF THE WALL BOUNDARY FO THE M.Z. FOR THE MACRO-SEQUENC 0516
C                                                                       0517
      I=IMAX                                                            0518
      PPP=1+MT(I)                                                       0519
      NMT=NT(I)-1                                                       0520
      DO 250 J=PPP,NMT                                                  0521
      KMM(I,J)=(Z(I,J+1)-Z(I,J-1))/2.                                   0522
      GR(I,J)=(T(I,J)-T(I-1,J))/(HHA(I-1))                              0523
      GZ(I,J)=(T(I,J+1)-T(I,J-1))/KMM(I,J)                              0524
      UZ(I,J)=UZCL/(1.+MO(I,J)**2)                                      0525
      UR=-MO(I,J)*UZ(I,J)                                               0526
      EPPS(I,J)=-(UZ(I,J)*GZ(I,J)+UR*GR(I,J))                          0527
      FACT1=1.0                                                         0528
      FACT2=GL(I,J)**2                                                  0529
      PERMI(I,J)=GAMMA(I,J)*(GL(I,J)**2)                                0530
  250 CONTINUE                                                          0531
      I=IMAX                                                            0532
      NNT=NT(I)                                                         0533
      GZ(I,J)=(T(I,J)-T(I,J-1))/KA(I,J-1)                               0534
      GR(I,J)=-MO(I,J)*GZ(I,J)                                          0535
      UZ(I,J)=UZCL/(1.+MO(I,J)**2)                                      0536
      UR=-MO(I,J)*UZ(I,J)                                               0537
      EPPS(I,J)=-(UZ(I,J)*GZ(I,J)+UR*GR(I,J))                          0538
      FACT1=1.0                                                         0539
      FACT2=GL(I,J)**2                                                  0540
```

```
      PERMI(I,J)=GAMMA(I,J)*(GL(I,J)**2)                                0541
C                                                                       0542
C          SET-UP OF THE LIQUIDUS FOR THE MACROSEGREGATION SEQUENCE     0543
C                                                                       0544
      DO 300 I=2,IMAXN                                                  0545
      NNT=NT(I)                                                         0546
      J=NNT                                                             0547
      GR(I,J)=(T(I+1,J)-T(I,J))/HHA(I)                                  0548
      GZ(I,J)=(T(I,J)-T(I,J-1))/KA(I,J-1)                               0549
      UZ(I,J)=UZCL/(1.+MO(I,J)**2)                                      0550
      UR=-MO(I,J)*UZ(I,J)                                               0551
      EPPS(I,J)=-(UZ(I,J)*GZ(I,J)+UR*GR(I,J))                           0552
      FACT1=1.0                                                         0553
      FACT2=GL(I,J)**2                                                  0554
      PERMI(I,J)=GAMMA(I,J)*(GL(I,J)**2)                                0555
  300 CONTINUE                                                          0556
C                                                                       0557
C          SET-UP OF THE CENTER LINE REGION FOR THE MACRO-SEQUENCE      0558
C                                                                       0559
      I=1                                                               0560
      NNT=NT(I)                                                         0561
      DO 340 J=1,NNT                                                    0562
      GR(I,J)=0.0                                                       0563
      MO(I,J)=0.0                                                       0564
      GZ(I,J)=TRAT/HTT(I)                                               0565
      UZ(I,J)=UZCL                                                      0566
      UR=0.0                                                            0567
      EPPS(I,J)=-UZ(I,J)*GZ(I,J)                                        0568
      FACT1=1.0                                                         0569
      FACT2=GL(I,J)**2                                                  0570
      PERMI(I,J)=GAMMA(I,J)*(GL(I,J)**2)                                0571
      IF(J.EQ.NNT) GO TO 339                                            0572
      IF(J.EQ.I) GO TO 338                                              0573
      KM=(KA(I,J)+KA(I,J-1))/2.                                         0574
      KMM(I,J)=KM                                                       0575
      GO TO 340                                                         0576
```

```
  338 CONTINUE                                                          0577
      VR(I,J)=0.0                                                       0578
      VZ(I,J)=-UZ(I,J)*CONTR                                            0579
      GO TO 340                                                         0580
  339 CONTINUE                                                          0581
  340 CONTINUE                                                          0582
C                                                                       0583
C                THE ITERATION SEQUENCE                                 0584
C                                                                       0585
C          THE ITERATION SEQUENCE NOW IS INITIATED .....IT IS IMPORTANT 0586
C          TO REALIZE THAT THE SEQUENCE IS ACTUALLY EXECUTED TWICE      0587
C          DURING A GIVEN RUN---THE FIRST TIME IT,S EXECUTED FOR THE    0588
C          VALUES OF FRACTION LIQUID CORRESPONDING TO THE SCHEIL EQUATIO 0589
C          THE SECOND TIME IT IS RUN FOR FRACTION LIQUID AND THE CONCOMI 0590
C          GRADIENTS CORRESPONDING TO REVISED VALUES FOUND DURING THE   0591
C          MACROSEGREGATION SEQUENCE )                                  0592
C                                                                       0593
      DO 1000 ITER=NSTART,MAXIT                                         0594
C                                                                       0595
C          FIRSTLY,THE INDIVIDUAL BOUNDARIES ARE TAKEN CARE OF          0596
C                                                                       0597
      DO 410 I=2,IMAXN                                                  0598
      PPP=NSI(I)                                                        0599
      PPPMAX=NSIMAX(I)                                                  0600
      DO 408 J=PPP,PPPMAX                                               0601
      IXX=J-NSI(I)+1                                                    0602
      P(I,J)=TART(I,IXX)*P(I+1,J)+TATOP(I,IXX)*P(I,J+1)+TALEFT(I,IXX)   0603
     1*P(I-1,J)+TABOT(I,IXX)*P(I,J-1)+TAKONS(I,IXX)                     0604
      IF(P(I,J).LE.0)  P(I,J)=0.0                                       0605
  408 CONTINUE                                                          0606
  410 CONTINUE                                                          0607
      NNT=NT(1)                                                         0608
      NMT=NNT-1                                                         0609
      I=1                                                               0610
      DO 430 J=3,NMT                                                    0611
      P(1,J)=P(2,J)                                                     0612
```

```
      IF(P(I,J).LE.0)  P(I,J)=0.0                                          0613
  430 CONTINUE                                                             0614
      P(1,2)=(Z(1,3)-Z(1,2))*(RLE*GRAV-CONTR*MU*UZCL/(GAMMA(1,2)           0615
     1*GE))+P(1,3)                                                         0616
      I=1                                                                  0617
      J=2                                                                  0618
      IF(P(I,J).LE.0)  P(I,J)=0.0                                          0619
      I=IMAX                                                               0620
      NMT=NT(I)-1                                                          0621
      MNT=MT(I)                                                            0622
      DO 450 J=MNT,NMT                                                     0623
      P(I,J)=P(I-1,J)+RHO(I,J)*(W**2)*RADIUS*HC                            0624
      IF(P(I,J).LE.0)  P(I,J)=0.0                                          0625
  450 CONTINUE                                                             0626
C                                                                          0627
C          SECONDLY,THE INTERIOR NODES ARE ATTENDED TO IN A COLUMN-WISE    0628
C          FASHION.(WE ,R GOING FROM SOLIDUS TO LIQUIDUS AND FROM          0629
C          CENTERLINE TO WALL)                                             0630
C                                                                          0631
      DO 530 I=2,IMAXN                                                     0632
      III=NSIMAX(I)+1                                                      0633
      NMT=NT(I)-1                                                          0634
      CCC=NMT+III                                                          0635
      DO 515 ITS=III,NMT                                                   0636
      J=CCC-ITS                                                            0637
      RIGHT=ONE(I,J)*P(I+1,J)                                              0638
      TOP=TWO(I,J)*P(I,J+1)                                                0639
      LEFT=TRE(I,J)*P(I-1,J)                                               0640
      BOTTOM=FOR(I,J)*P(I,J-1)                                             0641
      P(I,J)=RIGHT+TOP+LEFT+BOTTOM+KONST(I,J)                              0642
      IF(P(I,J).LE.0)  P(I,J)=0.0                                          0643
  515 CONTINUE                                                             0644
  530 CONTINUE                                                             0645
C                                                                          0646
C          SELECTION SEQUENCE---WHICH ITERATIONS DO WE WANT TO             0647
C          MONITOR FOR LATER EXAMINATION                                   0648
```

```
      IF(ITER.EQ.MAXIT) GO TO 600                                       0649
      GO TO 1000                                                        0650
  600 CONTINUE                                                          0651
C                                                                       0652
C          INTERDENDRITIC VELOCITIES ARE DETERMINED AT EACH NODE        0653
C          IN THE MUSHY ZONE OF TH E INGOT                              0654
C                                                                       0655
C                                                                       0656
      DO 790 I=1,IMAX                                                   0657
      NNT=NT(I)                                                         0658
      PPP=MT(I)+1                                                       0659
      DO 775 J=PPP,NNT                                                  0660
      PDR=1.0                                                           0661
      IF(J.EQ.PPP) GO TO 710                                            0662
      IF(I.EQ.IMAX) GO TO 709                                           0663
      IF((J.GT.PPP).AND.(J.LE.NSIMAX(I))) GO TO 723                     0664
  709 CONTINUE                                                          0665
      IF(J.EQ.NNT) GO TO 720                                            0666
      GO TO 730                                                         0667
  710 PDZ=(P(I,J+1)-P(I,J))/KA(I,J)                                     0668
      VZ(I,J)=-PERMI(I,J)/(MU*GL(I,J))*(PDZ+GRAV*RHO(I,J))              0669
      YW=(W**2)*R(I,J)*RHO(I,J)                                         0670
      IF(I.EQ.1.OR.I.EQ.IMAX) PDR=YW                                    0671
      IF(PDR.EQ.YW) GO TO 711                                           0672
      PDR=(P(I,J)-P(I-1,J))/HHA(I-1)                                    0673
  711 CONTINUE                                                          0674
      VR(I,J)=-PERMI(I,J)/(MU*GL(I,J))*(PDR-RHO(I,J)*(W**2)*R(I,J))     0675
      VTOT=(VR(I,J)**2+VZ(I,J)**2)**0.5                                 0676
      IF(VR(I,J).EQ.0.0)  VR(I,J)=1.0D-6                                0677
      ANG=VZ(I,J)/VR(I,J)                                               0678
      TTHETA=(180.0/PI)*DATAN(ANG)                                      0679
      RARA=(VR(I,J)*GR(I,J)+VZ(I,J)*GZ(I,J))/EPPS(I,J)                  0680
      WRITE(6,9400)                                                     0681
 9400 FORMAT(3X,'RAD-TEMP GRAD',3X,'THE PRESSURE',4X,'VELOCITY-Z',      0682
     16X,'THE VEL-R',5X,'VEL-TOT',8X,'THETA',8X,'RATE-RATIO',           0683
     17X,'I   J')                                                       0684
```

```
      WRITE(6,7400) GR(I,J),P(I,J),VZ(I,J),VR(I,J),VTOT,TTHETA,RARA,I,J          0685
 7400 FORMAT(1X,7E15.6,2I5)                                                      0686
      GO TO 775                                                                  0687
  720 PDZ=(P(I,J)-P(I,J-1))/KA(I,J-1)                                            0688
      VZ(I,J)=-PERMI(I,J)/(MU*GL(I,J))*(PDZ+GRAV*RHO(I,J))                       0689
      YW=(W**2)*R(I,J)*RHO(I,J)                                                  0690
      IF(I.EQ.1.OR.I.EQ.IMAX) PDR=YW                                             0691
      IF(PDR.EQ.YW) GO TO 721                                                    0692
      PDR=(P(I+1,J)-P(I,J))/HHA(I)                                               0693
  721 CONTINUE                                                                   0694
      VR(I,J)=-PERMI(I,J)/(MU*GL(I,J))*(PDR-RHO(I,J)*(W**2)*R(I,J))              0695
      VTOT=(VR(I,J)**2+VZ(I,J)**2)**0.5                                          0696
      IF(VR(I,J).EQ.0.0) VR(I,J)=1.0D-6                                          0697
      ANG=VZ(I,J)/VR(I,J)                                                        0698
      TTHETA=(180.0/PI)*DATAN(ANG)                                               0699
      RARA=(VR(I,J)*GR(I,J)+VZ(I,J)*GZ(I,J))/EPPS(I,J)                          0700
      WRITE(6,7500) GR(I,J),P(I,J),VZ(I,J),VR(I,J),VTOT,TTHETA,RARA,I,J          0701
 7500 FORMAT(1X,7E15.6,2I5//)                                                    0702
      GO TO 775                                                                  0703
  723 PDZ=(P(I,J+1)-P(I,J-1))/(2.0D0*KMM(I,J))                                   0704
      VZ(I,J)=-PERMI(I,J)/(MU*GL(I,J))*(PDZ+GRAV*RHO(I,J))                       0705
      YW=(W**2)*R(I,J)*RHO(I,J)                                                  0706
      IF(I.EQ.1.OR.I.EQ.IMAX) PDR=YW                                             0707
      IF(PDR.EQ.YW) GO TO 725                                                    0708
      PDR=(P(I,J)-P(I-1,J))/HHA(I-1)                                             0709
  725 CONTINUE                                                                   0710
      VR(I,J)=-PERMI(I,J)/(MU*GL(I,J))*(PDR-RHO(I,J)*(W**2)*R(I,J))              0711
      VTOT=(VR(I,J)**2+VZ(I,J)**2)**0.5                                          0712
      IF(VR(I,J).EQ.0.0) VR(I,J)=1.0D-6                                          0713
      ANG=VZ(I,J)/VR(I,J)                                                        0714
      TTHETA=(180.0/PI)*DATAN(ANG)                                               0715
      RARA=(VR(I,J)*GR(I,J)+VZ(I,J)*GZ(I,J))/EPPS(I,J)                          0716
      GO TO 775                                                                  0717
  730 PDZ=(P(I,J+1)-P(I,J-1))/(2.0D0*KMM(I,J))                                   0718
      VZ(I,J)=-PERMI(I,J)/(MU*GL(I,J))*(PDZ+GRAV*RHO(I,J))                       0719
      YW=(W**2)*R(I,J)*RHO(I,J)                                                  0720
```

```
      IF(I.EQ.1.OR.I.EQ.IMAX) PDR=YW                                          0721
      IF(PDR.EQ.YW) GO TO 731                                                 0722
      PDR=(P(I+1,J)-P(I-1,J))/(2.0D0*HMM(I))                                  0723
  731 CONTINUE                                                                0724
      VR(I,J)=-PERMI(I,J)/(MU*GL(I,J))*(PDR-RHO(I,J)*(W**2)*R(I,J))           0725
C                                                                             0726
C                     HEIGHT SELECTION***                                     0727
C                                                                             0728
      IF(J.EQ.JJ1(I)) GO TO 735                                               0729
      IF(J.EQ.JJ2(I)) GO TO 735                                               0730
      IF(J.EQ.JJ3(I)) GO TO 735                                               0731
      IF(J.EQ.JJ4(I)) GO TO 735                                               0732
      IF(J.EQ.JJ5(I)) GO TO 735                                               0733
      GO TO 775                                                               0734
  735 CONTINUE                                                                0735
C                                                                             0736
C                       COLUMN SELECTION**                                    0737
C                                                                             0738
      IF(I.EQ.16) GO TO 740                                                   0739
      IF(I.EQ.14) GO TO 740                                                   0740
      IF(I.EQ.11) GO TO 740                                                   0741
      IF(I.EQ.9) GO TO 740                                                    0742
      IF(I.EQ.6) GO TO 740                                                    0743
      IF(I.EQ.3) GO TO 740                                                    0744
      IF(I.EQ.1) GO TO 740                                                    0745
      GO TO 775                                                               0746
  740 CONTINUE                                                                0747
      VTOT=(VR(I,J)**2+VZ(I,J)**2)**0.5                                       0748
      IF(VR(I,J).EQ.0.0) VR(I,J)=1.0D-6                                       0749
      ANG=VZ(I,J)/VR(I,J)                                                     0750
      TTHETA=(180.0/PI)*DATAN(ANG)                                            0751
      RARA=(VR(I,J)*GR(I,J)+VZ(I,J)*GZ(I,J))/EPPS(I,J)                        0752
      WRITE(6,7300) GR(I,J),P(I,J),VZ(I,J),VR(I,J),VTOT,TTHETA,RARA,I,J       0753
 7300 FORMAT(1X,7E15.6,2I5/)                                                  0754
  775 CONTINUE                                                                0755
  790 CONTINUE                                                                0756
```

```
  805 CONTINUE                                                          0757
C                                                                       0758
C          MACROSEGREGATION SEQUENCE                                    0759
C                                                                       0760
C          INTEGRATION OF THE LOCAL SOLUTE DISTRIBUTION EQUATION IS     0761
C          FOLLOWED-THROUGH COLUMN-WISE STARTING FROM THE LIQUIDUS.     0762
C                                                                       0763
      VOLCFD=0.                                                         0764
      SUUM=0.0                                                          0765
      DO 1020 I=1,IMAX                                                  0766
      NMT=NT(I)-1                                                       0767
      SUM=0.                                                            0768
      MNT=MT(I)                                                         0769
      DO 810 IT=MNT,NMT                                                 0770
      NN=NMT-IT                                                         0771
      J=NN+MNT                                                          0772
      IF(J.EQ.NMT) NLGL(J+1)=0.0                                        0773
      COEFT1=-KON4*RHO(I,J)/(CL(I,J)*RS)                                0774
      COEFT2=-KON4*RHO(I,J+1)/(CL(I,J+1)*RS)                            0775
      RATER1=VR(I,J)*GR(I,J)+VZ(I,J)*GZ(I,J)                            0776
      RATER2=VR(I,J+1)*GR(I,J+1)+VZ(I,J+1)*GZ(I,J+1)                    0777
      FN(J)=COEFT1*(1.+RATER1/EPPS(I,J))                                0778
      FN(J+1)=COEFT2*(1.+RATER2/EPPS(I,J+1))                            0779
      NLGL(J)=.5*(CL(I,J)-CL(I,J+1))*(FN(J)+FN(J+1))+SUM                0780
      SUM=NLGL(J)                                                       0781
      GL(I,J)=EXP(NLGL(J))                                              0782
      GS(J)=1.0-GL(I,J)                                                 0783
      CS(J)=KAY*CL(I,J)                                                 0784
      GO TO 810                                                         0785
  809 CONTINUE                                                          0786
  810 CONTINUE                                                          0787
C                                                                       0788
C          LOCAL SCLUTE COMPOSITION FOR DESIGNATED RADII WITHIN         0789
C          THE INGOT IS INITIATED.                                      0790
C                                                                       0791
      SUMMS=0.                                                          0792
```

```
      NNT=NT(I)                                                          0793
      J=NNT                                                              0794
      GS(J)=0.0                                                          0795
      CS(J)=KAY*CL(I,J)                                                  0796
      PPP=MT(I)+1                                                        0797
      DO 850 J=PPP,NNT                                                   0798
      SUMMS=.5*(CS(J)+CS(J-1))*(GS(J-1)-GS(J))+SUMMS                     0799
  850 CONTINUE                                                           0800
      J=MT(I)                                                            0801
      GEE=1.-GS(J)                                                       0802
      GLEUT(I)=GEE                                                       0803
      TNT=RS*SUMMS+RSE*CE*GEE                                            0804
      DDD=RS*(1.-GEE)+RSE*GEE                                            0805
      LOCCOM(I)=TNT/DDD                                                  0806
C                                                                        0807
C          FINALLY, WE TAKE A READING ON THE AVERAGE COMPOSITION OF THE  0808
C          INGOT FOR A GIVEN INGOT HEIGHT.HOWEVER,SINCE WE,RE ASSUMING   0809
C          STEADY STATE WE NEGLECT TRANSIENT ZONES-INGOT BOTTOM AND TOP   0810
C                                                                        0811
      IF(I.EQ.1) GO TO 880                                               0812
      IF(I.EQ.IMAX) GO TO 885                                            0813
      DELRAD=(HHA(I)+HHA(I-1))/2.                                        0814
      GO TO 890                                                          0815
  880 DELRAD=HHA(I)/2.0                                                  0816
      GO TO 890                                                          0817
  885 DELRAD=HHA(I-1)/2.0                                                0818
  890 CONTINUE                                                           0819
      SUUM=2.0*ROR(I)*DELRAD*LOCCOM(I)+SUUM                              0820
      CSINGT=SUUM/(RADIUS**2)                                            0821
      WRITE(6,9900)                                                      0822
 9900 FORMAT(5X,'LOCAL SOLUTE COMP',4X,'ESTIMATE ON INGOT COM',4X,'FRACT 0823
     1 LIQUID EUTECTIC',4X,'RADIUS OFINGOT',2X,'COLUMN NO',8X,'ITERAT')  0824
      WRITE(6,7900) LOCCOM(I),CSINGT,GEE,ROR(I),I,ITER                   0825
 7900 FORMAT(1X,4E23.6,2I10//)                                           0826
 1020 CONTINUE                                                           0827
 1000 CONTINUE                                                           0828
```

```
      IF(TRIG.EQ.5)GO TO 1070                                           0829
      IF(TRIG.EQ.4)GO TO 1060                                           0830
      IF(TRIG.EQ.3) GO TO 1050                                          0831
      IF(TRIG.EQ.2) GO TO 1040                                          0832
      IF(TRIG.EQ.1) GO TO 1030                                          0833
 1030 CONTINUE                                                          0834
      TRIG=2                                                            0835
      GO TO 73                                                          0836
 1040 CONTINUE                                                          0837
      TRIG=3                                                            0838
      GO TO 73                                                          0839
 1050 CONTINUE                                                          0840
      TRIG=4                                                            0841
      GO TO 73                                                          0842
 1060 CONTINUE                                                          0843
      TRIG=5                                                            0844
      GO TO 73                                                          0845
 1070 CONTINUE                                                          0846
      STOP                                                              0847
      END                                                               0848
$ENTRY                                                                  0849
$STOP                                                                   0850
```

APPENDIX F

STABILITY CRITERIA

Fluid flow through the interdendritic network is fundamental to studies on segregation. When flow is from hotter to cooler regions flow is "stable". However, "unstable" flow can result in highly segregated channels called "freckles". It occurs when the interdendritic fluid travels from cooler to hotter regions of the mushy zone. The equation:

$$\frac{\partial g_L}{\partial T} = -\left[\frac{1-\beta}{1-K}\,\frac{g_L}{c_L}\,\frac{\partial c_L}{\partial T}\right]\left(1 + \vec{v}\,\frac{\nabla T}{\varepsilon}\right)$$

in which the quantity within brackets is always negative is simplified to the proportionality:

$$\frac{\partial g_L}{\partial T} \propto (1 + \vec{v}\nabla T/\varepsilon)$$

The three cases are:

case (1) $\partial g_L/\partial T > 0$ if $\vec{v}\nabla T/\varepsilon > -1$

case (2) $\partial g_L/\partial T = 0$ if $\vec{v}\nabla T/\varepsilon = -1$ and

case (3) $\partial g_L/\partial T < 0$ if $\vec{v}\cdot\nabla T/\varepsilon < -1$

Several subclasses of case (1) are:

class (a) $\vec{v}\cdot\nabla T/\varepsilon > 0$

class (b) $\vec{v}\nabla T/\varepsilon = 0$ and

class (c) $-1 < \vec{v}\nabla T/\varepsilon < 0$

Case (1) is the stable situation stating that upon traversing the volume element towards warmer regions the tendency is "to see" more liquid. Class (b) is a condition of the Scheil Equation. Perturbations

of passage diameter within the volume element occur such that a single passage may become slightly larger than surrounding passageways. In class (b) the flow has no effect on this localized passage and it returns to normal size.

For class (a) less liquid "is seen" relative to class (b) though $\partial g_L/\partial T>0$ still holds. Fluid flow has therefore caused an enhancement of solidification rate. The localized passageway has shrunk in diameter relative to surrounding passages. In class (c) the flow has retarded the solidification rate relative to (b). More liquid "is seen" meaning that localized passageways are swollen.

Case (2) states that flow within a perturbed interdendritic passage is great enough to completely retard solidification. This can result in severe channeling since the perturbation remains throughout solidification.

Case (3) is the extreme case. The solidification rate within the perturbed passage is negative. Remelting is occurring causing the passage to evolve into a severely localized channel called a "freckle". This channel actually grows during solidification of the volume element. The enlarged channel is optically visible.